Conversion of CO_2 to Fuels using Supported Cu Catalysts

Anisa Tariq

Cardiff University

School of Chemistry

2022

Thesis submitted in accordance with the requirements of Cardiff University for the degree of Doctor of Philosophy

Summary

Amid global warming concerns and skyrocketing CO_2 emissions in the atmosphere, mainly associated with the combustion of fossil fuels to produce energy, the research community has gained a large interest in CO_2 capture and reutilization to produce renewable fuels such as methanol (MeOH), dimethylether (DME) and additional hydrocarbons. MeOH is currently produced from syngas (H_2 + CO + CO_2) over a Cu/ZnO/Al_2O_3 (CZA) catalyst at mild temperature (200 - 270 °C) and high pressure (50 - 100 bar) and has a global demand exceeding 98 Mt/annum. Syngas is produced from the steam reforming of hydrocarbons, predominantly methane, and consequently the overall process has a great environmental cost (ca. 88 Mt GHG eq). Therefore, a more effective approach such as CO_2 hydrogenation to MeOH is required to enable the synthesis of CO_2-neutral fuels whilst mitigating anthropogenic emissions. The catalytic conversion of CO_2 into methanol and DME bears a strong potential to transform large amounts of CO_2 in a short span of time due to the commonly reported high reaction rates. In order for the process to be sustainable in the light of the carbon cycle, H_2 should be produced in a greener way, e.g., photocatalytic water splitting and water electrolysis sourced by natural/renewable energy sources.

The literature surrounding the synthesis of methanol from CO_2 hydrogenation has predominately been based on Cu catalysts and this is due to its remarkable hydrogenation activity and abundance. Although many new active catalyst formulations have been developed, they still carry the problem of incorporating harmful/expensive elements, making them less valuable for commercial use. As such this thesis explores the use of various supported Cu catalysts; Chapter 3 investigates the effect of various supported Cu catalysts prepared via the oxalate gel synthesis method, with a particular focus on Cu/ZrO_2, towards the conversion of CO_2 to MeOH. The role of various promoters (Pd, Pt, Ce, Ni and Ag) and the stability of these catalysts is also investigated. Chapter 4 explores the impact of varying the calcination temperature and reduction temperature of the Cu/ZrO_2 catalysts prepared via oxalate gel, towards their hydrogenation of carbon dioxide to methanol. The deposition of Cu onto the ZrO_2 polymorphs by oxalate gel and wet impregnation is also investigated to understand the effects of preparation method and support phase on catalytic activity. Finally, Chapter 5 investigates the synthesis of MeOH, DME and higher chain hydrocarbon between various CuZn or CuZr Zeolite integrated catalysts prepared *via* chemical vapour impregnation (CVI) and oxalate gel precipitation. Physical mixtures of the catalysts, as well as changes to the catalyst bed, are also explored in order to compare the catalyst activity.

Acknowledgements

I would like to offer my heartfelt gratitude to all the people who have helped, guided and supported me both academically and non-academically throughout my studies. This journey has been incredibly challenging, especially during the COVID-19 pandemic, however I am grateful for the number of opportunities I have been given and skills gained during this experience.

First and foremost, I would like to thank my supervisors, Prof. Graham Hutchings and Prof. Stuart Taylor for allowing me the opportunity to undertake this project and be part of such a vibrant research group. I would especially like to thank my academic supervisor Prof. Michael Bowker, for his enthusiasm, guidance and support particularly during the early stages of my PhD.

I offer my sincerest gratitude to my postdoctoral supervisors, Dr Robert Armstrong, who is incredibly knowledgeable and helpful, and to Dr Jonathan Ruiz Esquius, who has been very patient and insightful. I would also like to give thanks to Dr James Hayward for his advice during my project.

I would like to thank the members of the CCI's external advisory board, as well as the wonderful group members at the University of Liverpool and Imperial College London with whom I had the opportunity to collaborate and learn from.

I am incredibly grateful to Dr Greg Shaw who was always on hand to address any issues and provided fantastic training to many of us at the CCI. I would like to also extend a special thanks to Dr. David J. Morgan for help with XPS analysis, Dr. Thomas Davies for the TEM analysis, and the technical CCI staff Dr. Chris Morgan, Christopher Court Wallace and to Dr. Michal Perdjon for their help along the way and I must thank the amazing Steve Morris, Lee Wescombe and Julian Young from the workshop for the work they do not only for me, but the entire group. Without them, we would cease to function. Their contributions cannot be overstated.

I would like to offer thanks to all the wonderful colleagues and researchers at the CCI, who have made this experience more enjoyable, particularly Tak Bere, Rhodri Maunder and Karl Mugford who have been on this rollercoaster with me since the start of our Master's in catalysis.

I would also like to give special thanks to the PGR admin team who go above and beyond, especially Caru Shanahan, at times when I felt alone and lost she provided me with the comfort and confidence I needed and for this I will be forever be grateful.

Finally, my biggest thanks and love go to God and my wonderful family, their support throughout this journey have been crucial, especially during the last phases of this PhD.

Abbreviations and Units

At.%	Atomic percentage
Atm	Atmospheres
a.u.	Arbitrary units
BET	Brunauer-Emmett-Teller
cm	Centimetre
CP	Coprecipitation
CVI	Chemical vapour impregnation
DFT	Density functional theory
e-	Electron
Eq.	Equation
eV	Electron volts
FID	Flame ionisation detector
FTIR	Fourier-transform infrared
g	Gram
GC	Gas chromatography
GHG	Greenhouse gas
h	Hours
K	Kelvin
kg	Kilo gram
kJ	Kilo joule
L	Litre
mg	Milligram
MFC	Mass flow controller
min	Minute
ml	Millilitre
mmol	Millimoles
MPa	Megapascal

MS	Mass spectrometer
nm	Nanometre
OGP	Oxalate gel precipitation
PM	Physical mixing
RWG	Reverse water gas
TCD	Thermal conductivity detector
TEM	Transmission electron microscopy
TPR	Temperature programmed reduction
WI	Wet impregnation
wt %	Weight percent
XPS	X-ray photoelectron spectroscopy
XRD	X-ray powder diffraction
ΔG	Change in Gibbs energy
ΔH	Change in enthalpy
ΔS	Change in entropy
°C	Degrees celsius
µl	Microliter
µm	Micrometre

Table of Contents

Chapter 1

Introduction.

1.1 – CO_2 Emissions and Utilisation

The combustion of carbon-based fossil fuels (oil, coal, and natural gas) for energy generation is accompanied by an enormous emission of anthropogenic greenhouse gases (GHGs) to the atmosphere, mostly in the form of CO_2.[1] The impact of global warming and continued public and industrial interest globally has led to the drive in mitigation actions to reduce the global temperature rise and encourage the use of more sustainable and greener alternatives in the production of chemicals and the reduction of fossil fuel resources to reach the energy demand.[2-5] The annual global CO_2 emission in 2014 was recorded to be 39.25 Gt, of which fossil fuel emissions (including cement production) accounted for about 91% of the emissions from human sources. The distribution of the total emission comes from coal (42%), oil (33%), gas (19%), cement (6%), and gas flaring (1%). Consequently, the atmospheric CO_2 concentration increased from ∼270 ppm in the pre-industrialization era to ∼410 ppm in 2017, leading to serious climate change issues and detrimental ocean acidification.[6] As a result, various global initiatives like the Intergovernmental Panel on Climate Change and the United Nations Climate Change Conference (COP26, Glasgow, 2021; and COP21, Paris, 2015) have emphasized the urgency to mitigate CO_2 emissions by at least one-half of the current value by 2050, to limit the average global temperature increase to a maximum of 2 °C.[7, 8]

In the past decade, an immense amount of work has been done to reduce the impact of global warming and decrease GHG emissions, focusing on CO_2 sequestration and CO_2 utilization to synthesise valuable end products i.e. methanol, DME, formic acid, lower olefins, etc.[9] Carbon capture and storage (CCS), just as carbon capture and utilization (CCU), are believed to play a significant role in reducing the amount of released CO_2 in the atmosphere.[10, 11] In Europe the aim is for a 40% decrease in GHG emissions by 2030, compared to emission levels recorded in 1990.[12, 13] The technologies available for CCS and CCU continue to be developed every year, and there is an urgency to introduce a shift in the global energy base from fossil to renewable energy and greener fuels like hydrogen. These alternatives are considered important solutions to help reduce CO_2 emissions, but they do have a number of disadvantages: mainly the extensive changes that would need to be implemented in the energy infrastructure of the transportation sector, which could prove difficult and costly, as well as the political dilemma of introducing these changes in less developed geographic areas that rely on their abundant

fossil fuel deposits. The storage of CO_2 is also incredibly expensive and has high intensive energy requirements for separation and pumping, issues over the longevity and location of stored CO_2 in various sites, and an enlarged use of fossil C (from 20% to 60%) in the process.[14] For these reasons carbon utilization through CO_2 conversion is considered a more viable and practical option, as it is 20–40 times more efficient than sequestration over a span of 20 years.[15]

The catalytic conversion of CO_2 into methanol and DME bears a strong potential to transform large amounts of CO_2 in a short span of time, due to the commonly reported high reaction rates. In order for the process to be sustainable in the light of the carbon cycle (the process in which carbon atoms continually travel from the atmosphere to the Earth and then back into the atmosphere), H_2 should be produced in a greener way, e.g., photocatalytic water splitting and water electrolysis sourced by natural/renewable energy sources.

The production of methanol and its derivatives by alternative routes, and their use as fuels and chemicals, is the core of the methanol economy, a concept earlier proposed by Olah and co-workers.[16] In this conception, CO_2 is captured from any natural or industrial source, human activities or air by absorption and chemically transformed into methanol, dimethyl ether and varied products including synthetic hydrocarbons. According to Olah, methanol production from CO_2 is advantageous owing to the usage of non-fossil fuel sources (unlike syngas), avoidance of CO_2 sequestration (which is expensive) and the opportunity for mitigation of the greenhouse effect (by effective recycling of CO_2).[17] Olah *et al.* emphasized that the chemical recycling of CO_2 to methanol (and dimethyl ether) provides a renewable, carbon-neutral, unlimited source for efficient transportation fuels, for storing and transporting energy, as well as convenient feedstock for producing ethylene and propylene and from them, synthetic hydrocarbons and their products. Thus, it essentially substitutes petroleum oil and natural gas. It allows the lasting use of carbon-containing fuels and materials and avoids excessive CO_2 emissions causing global warming.[18]

Recently, trends of R&D in methanol synthesis are shifting toward a greener process, where CO_2 is reduced by H_2 generated from the technology sourced by natural/renewable energies. Mitsui Chemicals and Carbon Recycling International (CRI) Inc. are the two well-known companies, among others, that have demonstrated such processes for production of methanol. The plant of the latter, CRI, located in Iceland, has a production capacity of around 5 million litres of methanol per year (4 kta). The H_2 for this reaction is produced by water electrolysis using energy produced from natural sources, mainly geothermal, hydro, and wind.[19]

1.2 – Methanol Synthesis from Catalytic Hydrogenation of CO_2

1.2.1 – Methanol Production in Industry

MeOH is currently produced from syngas (H_2 + CO + CO_2) over a Cu/ZnO/Al_2O_3 (CZA) catalyst at mild temperature (200 - 270 °C) and high pressure (50 - 100 bar) and has a global demand exceeding 98 Mt/annum.[20, 21] Syngas is produced from the steam reforming of hydrocarbons, predominantly methane,[22] and consequently the overall process has a great environmental cost, (ca. 88 Mt GHG eq).[23] Small amounts of CO_2 (about 2–8%) are typically added to the CO/H_2 stream to balance the H/C ratio to the desired stoichiometry and to accelerate the reaction rate. Syngas production is not ideal if the aim is to prevent any further increases in CO_2 levels, therefore a more effective approach, such as CO_2 hydrogenation to MeOH, is required to enable the synthesis of CO_2-neutral fuels whilst mitigating anthropogenic emissions.

(Eq. 1) $CO_2 + 3H_2 \rightleftharpoons CH_3OH + H_2O$ $\Delta H_{25°C} = -49.5$ kJ mol^{-1}

(Eq. 2) $CO_2 + H_2 \rightleftharpoons CO + H_2O$ $\Delta H_{25°C} = 41.2$ kJ mol^{-1}

(Eq. 3) $CO + 2H_2 \rightleftharpoons CH_3OH$ $\Delta H_{25°C} = -90.6$ kJ mol^{-1}

The standard method adopted commercially to produce methanol via syngas is shown in Eq. 3; comparing this to methanol formation from CO_2 (Eq. 1), it can be seen that more hydrogen is required in order to remove the extra oxygen from CO_2 and subsequently form water as a by-product. Furthermore, methanol production from CO_2 is less thermodynamically favourable compared to CO, thus the one-pass methanol yield of the CO_2 based process is lower than that of the syngas based process.[24] Le Châtelier's principle states that if a dynamic equilibrium is disturbed by changing temperature, pressure, or concentrations of reactants in a system the position of equilibrium shifts in the opposite direction to offset the change.[25] According to Le Châtelier's principle, a combination of high pressure and low temperature is thermodynamically more favourable for the conversion of CO_2 to MeOH due to its exothermic nature and decrease in the number of molecules as the reaction proceeds forward; however, temperatures above 240 °C are utilised in order to activate CO_2 and provide a sufficient reaction rate.[26] As a consequence of the increased temperatures other unwanted side reactions occur, such as the reverse water gas shift (RWGS) shown in Eq.2, or formation of other hydrogenated products such as higher alcohols and hydrocarbons, resulting in reduced methanol yields.

Thermodynamic studies from Álvarez *et al.* showed that at 270 °C and H_2: CO_2 ratios of 3:1, the equilibrium conversion (the highest conversion that can be achieved in a reversible reaction) increases from 18%, to 23% to 38% as the pressure is increased from 10, 30 and 100 bar respectively. The selectivity is also found to be influenced by the temperatures and pressures; the equilibrium methanol selectivity at 270 °C are 5%, 20%, and 80% at the same pressures listed above. Thus, promising methanol catalysts must be not only be active at relatively low temperatures (less than 270 °C) but they should also be stable and highly selective.[27]

As discussed, the maximum methanol yield is limited by the thermodynamic equilibrium; however, the equilibrium limitation on methanol yield can be overcome by a several methods including the optimization of reaction conditions, the reactor designs, and innovations such as the recycling of the unconverted feed gas after product separation by condensation, and the *in situ* product removal (e.g. continuous water removal via distillation or membranes).[28]

1.2.2 – Mechanism of Industrial Catalyst ($Cu/ZnO/Al_2O_3$)

Several researchers have probed into the mechanism of CO_2 hydrogenation to methanol over the years, in order to improve the process; despite this the mechanism on the molecular level is still widely debated. The importance of the active site during the reaction is well-understood, but the exact nature of this active site still remains unclear. Early literature has concluded that metallic copper (Cu^0) is the major active site for the reaction, and have correlated the increased activity of the catalyst with an increase in copper surface area.[29-32]

Although a large emphasis has been placed on the active metal, it is important not to forget the role of the metal oxides present and their promoting effect. Indeed ZnO has shown to influence the chemical, structural, and electronic effects of Cu and hence improve the catalyst reactivity.[33] The Cu-Zn synergy is very unique and has shown to be essential towards explaining the catalyst activity; Arena and co-workers proposed that ZnO could act as a reservoir for atomic hydrogen and thus increase the rate of hydrogenation of the key intermediates. They also proposed that either ZnO could confer a peculiar morphology to the Cu particles, or ZnO was able to create additional active sites on the Cu surface.[9] These findings are in good agreement with Studt *et al*., who showed how the presence or absence of the Zn drastically altered not only the activity but also the reaction mechanism. Based on DFT calculations, they concluded that the intermediates in CO_2 hydrogenation are bound to the surface through an oxygen atom and the addition of Zn acted as a promoter. In the case of the CO

hydrogenation, in contrast, the intermediates are bound to the surface though C atoms, and a full layer of Zn blocked these sites and hindered CO hydrogenation.[34]

There are mainly two models proposed to describe the Cu–Zn active site. The first one assumes the active site to be a fully Zn-decorated surface step of Cu,[34, 35] and the second one is an electron-deficient $Cu^{\delta+}$ species dissolved across the ZnO promoter as the active site.[36-38] This first Zn-decorated model site was based on the experiments and theoretical studies, where the surface enrichment of Zn on the Cu particles was observed by XPS and HRTEM.[39] Kuld *et al.* found metallic Zn on the surface of reduced Cu–ZnO catalyst by Auger emission spectroscopy,[40] and Lunkenbein *et al.* showed clear evidence of the formation of metastable ZnO layer during reductive activation.[41] On the other hand, the electron-deficient $Cu^{\delta+}$ species has been widely used to explain the differences in catalytic activity of the Cu–ZnO–ZrO_2 systems.[33, 42-45] This hypothesis has been supported by chemisorption and FTIR studies and proved that the interaction of Cu particles with ZnO and ZrO_2 phases leads to the stabilization of $Cu^{\delta+}$ sites at the metal oxide interface.[46, 47]

Besides the open discussion about the nature of the active site, the second point described above on the reaction pathway is also still a matter of active debate. The initial adsorption of CO_2 has been reported to occur in several ways. Some researchers claim that CO_2 can dissociatively adsorb over bare Cu^0,[48, 49] while others report that pre-adsorbed H species are crucial to ensure CO_2 adsorption on Cu^0.[50, 51] In addition, the type of species that are formed after the successful adsorption of CO_2 is also widely debated. Some researchers support the formation of formate species (HCOO*) as the first hydrogenated species in the mechanism, whereas others propose the formation of hydrocarboxyl (COOH*).

The very first studies supported the formate route via transformation to dioxymethylene (CH_2O_2*), formaldehyde (CH_2O*), and then to methoxy. However, the only observable intermediates were formate and methoxy species.[52, 53] Grabow and Mavrikakis proposed a mean-field microkinetic model that fitted the experimental results obtained under realistic conditions on commercial Cu–ZnO–Al_2O_3. In their proposed mechanism, besides the formate (HCOO*) and methoxy species, they also considered intermediates such as formic acid HCOOH* and CH_3O_2*. The DFT calculations showed that CO_2 hydrogenation goes though the formate route, where formate (HCOO*) preferentially leads to the formation of formic acid rather than dioxymethylene (CH_2O_2*). This formic acid would be further hydrogenated to CH_3O_2*, which is subsequently transformed to CH_2O* by splitting off its OH group. In the final step, the hydrogenation of CH_2O* would yield methoxy.[53] As a favourable support of the formate route, Tabatabaei *et al.* reported the presence of formate species in the CO_2 hydrogenation by pulses and desorption analysis. They noted that the bidentate formate was an intermediate for the

RWGS reaction while a monodentate formate was the intermediate for CH_3OH synthesis on ZnO from CO_2/H_2 feeds.[54] Yang *et al.* showed that methanol synthesis on Cu surfaces proceeds through a formate intermediate to formaldehyde, but in this case via a dioxomethylene intermediate.[50] The overall reaction rate was found limited by both formate and dioxomethylene hydrogenation. In a recent study, Kattel *et al.* reported the synergy of Cu–ZnO and the transformation of formate to methanol via *HCOOH, *H_2COOH, and *CH_3O intermediates.[55]

Furthermore, the synergistic effects of Cu–ZrO_2 were evidently reported recently by Larmier *et al.* using a tailored catalyst with highly dispersed Cu on ZrO_2. They have shown by NMR, DRIFTS, and DFT calculations that formate is an intermediate and its transformation to methanol is highly favoured at the interface of Cu and ZrO_2 owing to lowered activation barrier by the interface. Interestingly, the unique interface of Cu and ZrO_2 facilitated transformation of formate to an acetal-like species ($H_2C(O)_2$*), which is further hydrogenated to methoxy and finally to methanol.[56]

Contrary to the formate route, Zhao *et al.* reported that formation of methanol from direct hydrogenation of formate (HCOO*) on Cu(111) is not feasible due to the high activation barriers in some of the elementary steps. Instead, CO_2 hydrogenation to hydrocarboxyl (*trans*-COOH) is kinetically more favourable than formate in the presence of water via a unique hydrogen transfer mechanism.[57] In agreement with Zhao *et al*., Yang *et al*. concluded that the direct hydrogenation of bidentate formate (HCOO*) on metallic Cu does not produce methanol. Interestingly, they found that a significant amount of methanol is formed if the Cu catalyst is pre-treated by N_2O or O_2, which implies that surface oxygen or possibly water-derived species may play a critical role in the reaction mechanism.[58] Figure 1.1 illustrates the different possible reaction intermediates and steps during the hydrogenation of CO and CO_2 into CH_3OH over Cu.

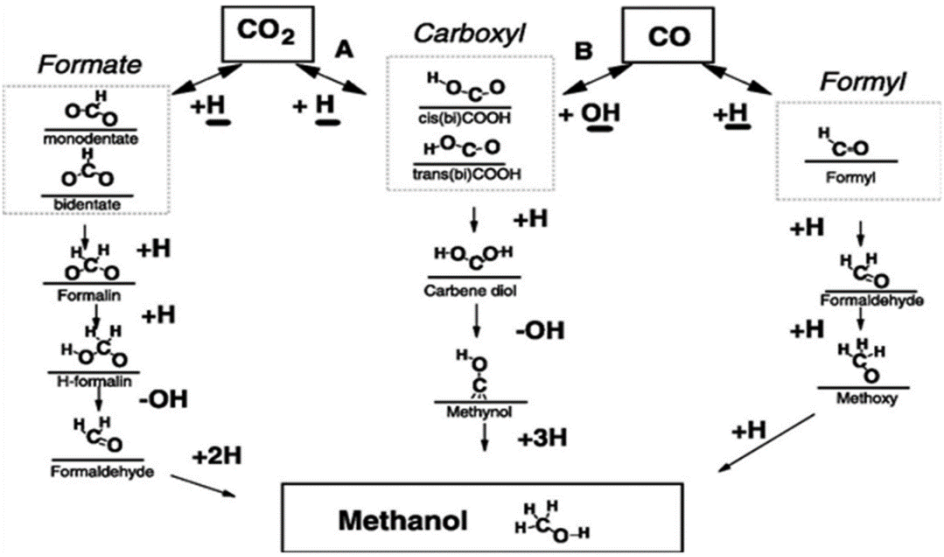

Figure 1.1 - Mechanistic pathways for conversion of CO and CO_2 to CH_3OH over Cu.[32]

1.2.3 – Cu Catalysts for CO_2 hydrogenation to MeOH

The literature surrounding the synthesis of methanol from CO_2 hydrogenation has predominately been based on Cu catalysts and this is due to its remarkable hydrogenation activity and abundance.[59-61] CO_2 hydrogenation to methanol over Cu catalysts is generally known as a structure-sensitive reaction, in which the catalytic properties are closely associated with (i) metal dispersion and surface Cu metallic area, (ii) dimension, composition, and electronic properties of the Cu–ZnO interface, and (iii) capability of adsorption of reagents and mass transfer. Generally, these factors are tunable by means of promoter effect, support effect, preparation methods, and the incorporation of core-shell structure and hydrotalcite-like compounds.[53]

Although $Cu/ZnO/Al_2O_3$ catalysts have dominated in industry, their catalytic performance remains unsatisfactory. The poor performance is due to several factors including the formation of water as a by-product, which facilitates ZnO agglomeration and oxidation of active Cu species as a strong oxidant, leading to the serious deactivation of $Cu/ZnO/Al_2O_3$ catalysts.[62] Therefore, by considering the catalytic kinetics, the development of highly effective Cu-based catalysts in terms of activity, selectivity, water tolerance, and stability are feasible for the hydrogenation of CO_2 to methanol. A selection of Cu based catalysts are shown in Table 1.1.

Table 1.1: *Summary of Cu based catalysts for the hydrogenation of CO_2 to MeOH from literature.*

Catalyst	Preparation	H_2/CO_2 ratio	Temperature (°C)	Pressure (MPa)	Con. (*63*)	Sel. (*63*)	STY (g_{MeOH} kg_{cat}^{-1})
Cu/Ga/ZnO[64]	Co-impregnation	3:1	270	2	6.0	88	378
Cu@ZnO_x (core-shell)[65]	Surface modification precipitation	3:1	250	3	2.3	100	147.2
Cu/Zn/ZrO_2[66]	Reverse coprecipitation	3:1	240	3	17.5	48.4	N/A
Cu/ Zn/ZrO_2[67]	Urea-nitrate combustion	3:1	240	3	17.0	56.2	N/A
Cu/ ZnO/ZrO_2/Ga_2O_3[68]	coprecipitation	3:1	250	8	N/A	75	324
Cu/ ZnO/ZrO_2/Ga_2O_3[68]	Citric complexing	3:1	250	8	N/A	70	382
Cu-ZnO/ZrO_2[69]	Oxalate coprecipitation	3:1	240	3	9.0	N/A	1200
Cu/ ZrO_2[70]	Deposition precipitation	3:1	240	2	6.3	48.8	360

For CO_2 hydrogenation to methanol over Cu-based catalysts, formate (*HCOO) produced by the reaction between CO_2 and dissociative H and CO generated from the RWGS are considered to be two major intermediates. For all catalysts, methanol selectivity is governed by the competition of the simultaneously catalyzed methanol synthesis and RWGS reactions. In both pathways, methanol is generated from the methoxy (*CH_3O) intermediate. In situ diffuse reflectance FT-IR studies reveals that CO_2 can be transformed into carbonate or bicarbonate, formate and methoxy, upon adsorption and hydrogenation on Cu/ZrO_2 particles. [71] The formate species is considered to be the most important reaction intermediate and that the Cu/ZrO_2 interface is crucial for the conversion of this intermediate to methanol. The rate-determining step for methanol synthesis is proposed to be the conversion of formate into formaldehyde or methoxy. [72] The ZrO_2 support is found to facilitate the conversion of adsorbed CO_2 to surface formate or hydroxycarbonyl entities. [73] DFT and kinetic Monte Carlo (KMC) simulations suggest that, on the oxygen-rich Cu/m-ZrO_2 interface, both methanol and CO are produced dominantly via the formate pathway, while the RWGS channel has only a minor contribution.[74]

In addition, the synthesis of methanol from CO_2 over Cu/ZrO_2 involves the spillover of H atoms formed on Cu to the surface of ZrO_2, and the atomic H then participates in the hydrogenation of carbon-containing species (i.e., HCOO and HCO_3) to methanol. [75] In general, a complete process of hydrogen spillover includes several steps, namely: (1) H_2 adsorption and dissociation on metal sites, (2) H atoms transfer from one surface to the other, (3) H atoms diffuse rapidly across the oxide surface and (4) H atoms react or exchange with other intermediates. [76] It should be highlighted that the –OH species on ZrO_2 is also involved in the spillover, because the exchange of atomically adsorbed H atoms and OH groups on the catalysts occurs, which would affect the spillover efficiency.

By combining DFT calculations, KMC simulations and in situ diffuse reflectance infrared Fourier transform spectroscopy (DRIFTS), Kattel et al. propose that the production of CH_3OH via the formate pathway does not seem to be efficient over time due to the formate species being likely spectators and poison the active sites on the surface. [77] The CO_2 conversion is facilitated due to the fine-tuning capability of ZrO_2 (reduced Zr^{3+} at the interface), being strong enough to stabilize *CO_2, *CO, *HCO, and *H_2CO at the Cu/ZrO_2 interface and therefore to promote its hydrogenation to CH_3OH via the RWGS + CO-Hydro pathway. This pathway is summarised in Figure 1.2.

Figure 1.2 - Possible reaction pathways and active sites of CO_2 hydrogenation to CH_3OH over the Cu/ZrO_2.[78]

1.3 – Indirect Conversion of CO_2 into Hydrocarbons

1.3.1 – Direct Vs Indirect Route

Replacement of part of the fossil fuel consumption by renewable energy sources (solar, wind, biomass and so on) is a central strategy for resource and energy efficiency. When hydrogen originates directly from renewable energy, CO_2 hydrogenation can also provide an important approach for dealing with the intermittence of renewable sources by storing energy in chemicals and fuels. As such, methanol is an important raw material for the production of fuels. The Methanol to Gasoline (MTG)[79] process (C_5–C_{11}) was first commercialized in the 1980's and was soon adopted to produce lower olefins (ethylene, propylene and butylene, $C_2^=$–$C_4^=$) via the Methanol to Olefin (MTO)[80, 81] process, due to the higher added value of the olefins when compared with gasoline. These light olefins are important chemical building blocks for a variety of useful derivatives in the petrochemical industries.[82, 83] In particular, ethylene and propylene production in the petrochemical industries has shown significant growth in the global market during the past decades.[84] The global market demand for ethylene and propylene is predicted to reach 184 and 127 Mton, respectively, by 2022, corresponding to a 20% and 25% increase over 2017.[85] Conventionally, C_2-C_4 hydrocarbons have primarily been produced using oil fractions from petroleum refineries and natural gas processing plants.[86-88] With the rapid depletion of petroleum sources,[89] many alternative feedstock (e.g. biomass-based)[90] and technological pathways (e.g. methanol-to-olefin[91] or coal-to-olefin routes[92, 93] have been investigated to satisfy the demand growth of C_2-C_4 hydrocarbons.

There are different possible routes to produce hydrocarbons from CO_2 hydrogenation. Two parallel reactions, the synthesis of methanol and reverse water-gas shift, RWGS), are typically present in the CO_2 hydrogenation process. The hydrocarbons could be directly produced from syngas ($CO + H_2$) based on Fischer–Tropsch synthesis [86, 94] or indirectly via industrial methanol synthesis and then converting methanol to a range of hydrocarbons using the methanol-to-hydrocarbon process, including the methanol-to-olefin (MTO), methanol-to-propene [91], and methanol-to-gasoline (MTG) processes. It had also been reported that aromatic or lower paraffin (LPG) hydrocarbons were synthesized from methanol or dimethyl ether (DME).[95-97] In addition, various hydrocarbons could be indirectly produced from CO_2 hydrogenation via CO_2 hydrogenation to methanol and methanol-to-hydrocarbon (MTH) reactions. Recently, the direct route of converting CO_2 into hydrocarbons has been developed based on Fischer-Tropsch synthesis (CO_2-FTS), via a two-step process with an initial reduction of CO_2 to CO via the RWGS reaction followed by the conversion of CO to hydrocarbons via FTS.[98-101] The catalyst

used should be active in both RWGS and FTS reactions. The issue, however, with the direct approach is the maximum C_5–C_{11} hydrocarbon fraction is limited by the Anderson–Schulz–Flory distribution to ∼48%, with an undesirable CH_4 fraction of ∼6%.[102, 103] Furthermore, the heat of adsorption of CO_2 is lower than that of CO because of the thermodynamic stability of CO_2, which leads to a much lower coverage of CO_2 over the catalyst, and thus a low CO_2 reactivity and high CH_4 selectivity. As an alternative it is possible to combine the catalysts for methanol and the zeolites for MTH to have a direct one-step formation of hydrocarbons from CO_2 hydrogenation.[104]

Dimethyl ether (DME), the dehydration product of methanol, can be used as a feed to produce several different classes of hydrocarbons, including lower olefins, gasoline-range hydrocarbons, branched alkanes, and aromatics. The selectivity to any of these classes of compounds is determined both by the zeolite topology and the operating conditions used. Direct transformation of CO_2 to DME involves a bifunctional catalyst capable of performing two reactions, methanol synthesis and methanol dehydration, simultaneously. These are known as hybrid catalysts; the active elements of these bifunctional catalysts inherently include a component active in the methanol synthesis, which is the preceding reaction in this process, while the methanol dehydration functionality of this hybrid catalyst relies on the solid acid catalyst component such as γ-Al_2O_3 and H-ZSM-5. The use of hybrid catalysts was initially investigated and practiced for direct conversion of syngas to DME. Similar to the methanol synthesis reaction, the hybrid catalysts developed for the syngas-to-DME/gasoline conversion are also known to be active for CO_2 hydrogenation to DME.[63, 105, 106]

There has been rapid development in DME synthesis from CO_2 hydrogenation using CH_3OH synthesis catalysts hybridized with CH_3OH coupling catalysts.[107] The effect of promoters, supports, and synthesis conditions have been explored.[108-110] For example, the acidic sites on γ-alumina surfaces and the $CuAl_2O_4$ spinel phase can be regulated by promoters like gallium or zinc oxides, resulting in higher stability for Cu NPs during CO_2-to-DME.[110] To date, CO_2 conversion and DME selectivity mostly vary between 35–80% and 5–50%, respectively,[107] but CO_2 conversion can reach up to 97% at 280 °C over a Cu–Zn–Al/HZSM-5 catalyst by drastically increasing the reaction pressure (to 36 MPa).[111] In addition, interesting results have been reported on core–shell structured hybrid catalysts with the MeOH synthesis catalysts at the core and the MeOH dehydration catalysts forming the shell.[112, 113] Compared with traditional hybrid catalysts prepared by physically mixing the components, these novel core–shell catalysts have received much attention in the literature due to their unique structures and ability to valorise CO_2 by improving conversion and DME selectivity.

Selective synthesis of lower olefins from a CO_2 + H_2 mixture by one-pass conversion, via methanol synthesis, was investigated by Inui *et al.* The authors considered that, for the selective synthesis of

olefin, a weakly acidic and narrow pore microporous crystalline catalyst such as SAPO-34 was required. A bifunctional catalyst containing In_2O_3 and SAPO-34 could realize the direct production of lower olefins from CO_2 hydrogenation with excellent selectivity and high activity. The selectivity of C_2–C_4 olefin reached up to around 76.9% with a much lower CH_4 selectivity of 4.4%, and CO_2 conversion was above 34%.[114]

Currently the indirect route is more developed and economical compared to the direct route; however, through optimisation of the catalyst, reactor designs, and reaction conditions, the product selectivity can be controlled and improvements to the catalytic stability can be made. Recently, the catalytic materials, mechanism, active intermediates and deactivation and commercial projects of MTH have been reviewed in detail.

1.3.2 – Proposed Reaction Pathway

The methanol (MeOH) mediated route to form hydrocarbons consists of two consecutive processes, i.e., CO_2-to-MeOH (Equation (1)) and a subsequent MeOH-to-olefins process (MTO) (Equation (4)). Additional competing reactions (i.e., Equation (5)) are also witnessed with the formation of light olefins. The control of the selectivity of the CO_2 hydrogenation to the desired olefin product requires the design of catalysts for reaction pathways that are compatible with favourable thermodynamics and a good understanding of the reaction kinetics.[115] The thermodynamic values in the equations indicate that lower temperatures favour methanol (Equation (1)), and methane synthesis (Equation (5)), while higher temperatures are needed to activate CO_2 for rapid reaction rates.[116]

Methanol to Olefins (MTO):

(Eq. 4) $nCH_3OH \rightarrow (CH_2)_n + nH_2O$ (n = 2) $\Delta H_{25°C} = -29.3$ KJ mol^{-1}

CO_2 methanation:

(Eq. 5) $CO_2 + 4H_2 \rightarrow CH_4 + 2H_2O$ $\Delta H_{25°C} = -165.0$ kJ mol^{-1}

In reviewing the mechanistic details of light olefin formation, it is clear that controlling the active H to C ratio is of primary importance. The presence of too much H* on the surface will result in excessive hydrogenation, and therefore methanation, while too little H* on the surface will restrict the hydrogenation ability of the catalyst and therefore reduce the CO_2 conversion activity. At its most fundamental, the pivotal steps of CO_2 conversion to light olefins are the cleavage of the C–O bonds and the formation of C–C bonds.[117]

The reaction mechanism of the MTH process is highly complex. Researchers have reported multiple pathways since its discovery.[118, 119] Of the reaction pathways proposed, the most dominant are the oxonium ylide, carbene, carbocationic, free radical, and the hydrocarbon pool mechanism.

According to Li *et al.*, the mechanism of the first C–C bond formation over SAPO-34 occurs through the formation of the methoxymethyl cation intermediate ($^{+}CH_2OCH_3$). The cation intermediate is formed from surface methoxy species and dimethyl ether. The methoxymethyl cation then reacts with another molecule of dimethyl ether or methanol to form 1,2-dimethoxyethane and 2-methoxyethanol, respectively, the compounds containing the first C–C bonds. The formation of the methyl cation was both theoretically and experimentally verified.[120]

Chowdhury *et al.* presented experimental magic-angle spinning nuclear magnetic resonance (MAS NMR) evidence for the involvement of acetate species in the first C–C bond formation over the SAPO-34 catalyst. In the proposed mechanism, the surface methoxy species undergo carbonylation (CO being derived via the decomposition of methanol) to form a surface-bound acetate species that, upon addition of a methanol molecule, generates a surface adsorbed methyl acetate species.[121]

The dual cycle mechanism deals with the formation of reaction products (selectivity) after the first C–C bond formation. According to Dessau *et al.*, various aliphatic and aromatic hydrocarbons in the MTH reaction can be considered to generate through the consecutive methylation by methanol (Figure 1.2). In principle, ethylene is methylated to form propylene. Further methylation of propylene yields butylene and the process carries on generating higher hydrocarbons. Cyclization of the C_6 alkenes and further methylation produces various substituted aromatics.[122]

Dahl et al. used ^{13}C labeled methanol and ^{12}C labeled ethene over a SAPO-34 catalyst to verify the probable routes to higher hydrocarbon formation. The authors considered two mechanistic pathways; the first one was the previously suggested consecutive methylation path, and the second one was the "hydrocarbon pool" (HCP) type mechanism. The HCP is a pool of adsorbates having many characteristics similar to ordinary coke, represented as $(CH_x)_n$ with $0 < x < 2$. In the latter mechanism, methanol is continuously added to the pool of $(CH_x)_n$ species, causing their growth. The $(CH_x)_n$ species also undergo splitting/cracking to generate the product molecules. According to the experimental results (^{13}C and ^{12}C), only a minor part of propylene was formed from ethene and methanol, indicating that the HCP mechanism is more prevalent than the consecutive mechanism.[123]

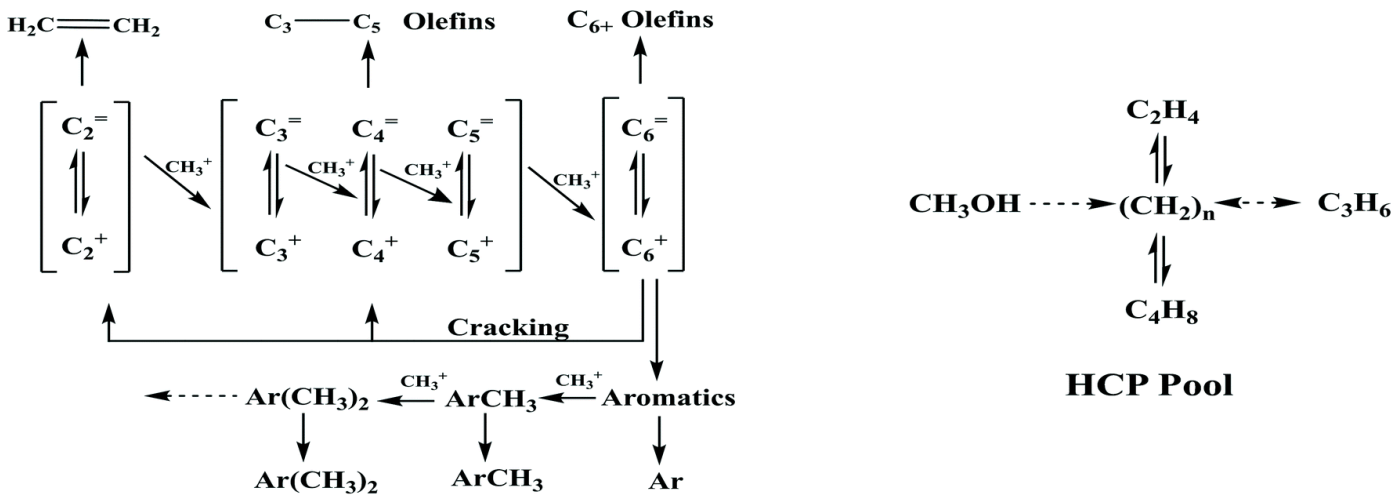

Figure 1.3 - Consecutive methylation scheme for higher hydrocarbons and hydrocarbon pool (HCP) pathway.[115]

1.4 – Aims and Objectives

The work presented in this thesis is part of a larger project (Flexible Routes to Liquid Fuels from CO_2). The aims and vision of the wider project are to determine if routes to CO_2 valorisation with sustainable H_2 are potentially viable, with emphasis on upgrading solar hydrogen by reaction with CO_2 to afford drop-in replacements for current hydrocarbon fuels using existing distribution and FTS infrastructure; next-generation candidate fuel DME; and fuel vector methanol, which is a versatile precursor to DME and gasoline via established processes, a fuel additive, and in some scenarios a candidate fuel. The stored solar energy can also be used as a power source for remote locations, in closed cycle space heating and manufacturing applications and also as a supplement to the power grid.

One of the main themes of this project was the thermocatalytic conversion of CO_2 to fuels, and in this study the main focus was on the production of methanol and DME via thermocatalytic routes from CO_2 and H_2, following this the catalyst design was adapted in order to produce additional hydrocarbons. The main aims of the project are summarised below:

- Identify catalysts that can operate under low temperatures (< 250 °C) for MeOH synthesis from CO_2.
- Identify and develop active catalysts composed of earth-abundant materials for the hydrogenation of CO_2 to MeOH and DME.
- Investigate the formation of hydrocarbons via methanol formation using integrated catalysts (MeOH synthesis + zeolite).

Chapter 1 has given a brief insight into the impact of increasing CO_2 levels globally and the importance of alternative routes that are less environmentally damaging. Emphasis is placed on CO_2 hydrogenation to methanol, DME and hydrocarbons, with a particular focus on Cu based catalysts and their proposed mechanisms. Chapter 2 will give all the experimental details for the catalyst preparation techniques, characterisation techniques, reaction procedures, and the data analysis used throughout this thesis. A detailed investigation into the promotion of Cu catalysts supported on ZrO_2 is given in chapter 3. Chapter 4 explores the phase composition of Cu/ZrO_2 catalysts and their impact on the hydrogenation of CO_2 to MeOH. Finally, in chapter 5 the indirect conversion of CO_2 to hydrocarbons is explored using Cu/Zn and Cu/Zr zeolite catalysts. As indicated above this thesis initially looks into a variety of supported Cu catalysts, before attempting the catalyst optimisation through the addition of promoters and investigating the catalyst structure to understand its performance. Finally, this information is then used to help develop catalysts for the formation of hydrocarbons.

1.5 – References

1. IEA, "Global Energy & CO_2 Status Report 2019, IEA, Paris," (2019).
2. C. Song, Global challenges and strategies for control, conversion and utilization of CO_2 for sustainable development involving energy, catalysis, adsorption and chemical processing. *Catalysis Today* **115**, 2-32 (2006).
3. M. Broumand, S. Albert-Green, S. Yun, Z. Hong, M. J. Thomson, Spray combustion of fast pyrolysis bio-oils: Applications, challenges, and potential solutions. *Progress in Energy and Combustion Science* **79**, 100834 (2020).
4. F. Fazlollahi, S. Saeidi, M.-S. Safdari, M. Sarkari, J. J. Klemes, L. L. Baxter, Effect of Operating Conditions on Cryogenic Carbon Dioxide Removal. *Energy Technology* **5**, 1588-1598 (2017).
5. S. Perathoner, G. Centi, Green Carbon Dioxide: Advances in CO_2 Utilization. (Wiley, 2014).
6. E. Catizzone, G. Bonura, M. Migliori, F. Frusteri, G. Giordano, CO_2 Recycling to Dimethyl Ether: State-of-the-Art and Perspectives. *Molecules* **23**, (2018).
7. CCC, "COP26: Key outcomes and next steps for the UK," (London, 2021).
8. R. K. Pachauri, M. R. Allen, V. R. Barros, J. Broome, W. Cramer, R. Christ, J. A. Church, L. Clarke, Q. Dahe, P. Dasgupta, *Climate change 2014: synthesis report. Contribution of Working Groups I, II and III to the fifth assessment report of the Intergovernmental Panel on Climate Change*. (Ipcc, 2014).
9. F. Arena, G. Mezzatesta, L. Spadaro, G. Trunfio, *Latest Advances in the Catalytic Hydrogenation of Carbon Dioxide to Methanol/Dimethylether.* (Springer, Berlin, Heidelberg, 2014), pp. 28.
10. D. Y. C. Leung, G. Caramanna, M. M. Maroto-Valer, An overview of current status of carbon dioxide capture and storage technologies. *Renewable and Sustainable Energy Reviews* **39**, 426-443 (2014).
11. E. S. Sanz-Pérez, C. R. Murdock, S. A. Didas, C. W. Jones, Direct Capture of CO_2 from Ambient Air. *Chemical Reviews* **116**, 11840 (2016).
12. F. deLlano-Paz, P. Martínez Fernandez, I. Soares, Addressing 2030 EU policy framework for energy and climate: Cost, risk and energy security issues. *Energy* **115**, 1347-1360 (2016).
13. A. Jäger-Waldau, I. Kougias, N. Taylor, C. Thiel, How photovoltaics can contribute to GHG emission reductions of 55% in the EU by 2030. *Renewable and Sustainable Energy Reviews* **126**, 109836 (2020).
14. M. Aresta, A. Dibenedetto, A. Angelini, Catalysis for the Valorization of Exhaust Carbon: from CO_2 to Chemicals, Materials, and Fuels. Technological Use of CO_2. *Chemical Reviews* **114**, 1709-1742 (2014).
15. S. C. Peter, Reduction of CO_2 to Chemicals and Fuels: A Solution to Global Warming and Energy Crisis. *ACS Energy Letters* **3**, 1557-1561 (2018).
16. G. A. Olah, Beyond Oil and Gas: The Methanol Economy. *Angewandte Chemie International Edition* **44**, 2636-2639 (2005).
17. G. A. Olah, A. Goeppert, G. K. S. Prakash, Chemical Recycling of Carbon Dioxide to Methanol and Dimethyl Ether: From Greenhouse Gas to Renewable, Environmentally Carbon Neutral Fuels and Synthetic Hydrocarbons. *The Journal of Organic Chemistry* **74**, 487-498 (2009).
18. G. A. Olah, G. K. S. Prakash, A. Goeppert, Anthropogenic Chemical Carbon Cycle for a Sustainable Future. *Journal of the American Chemical Society* **133**, 12881-12898 (2011).

19. I. Ganesh, Conversion of Carbon Dioxide into Methanol – a Potential Liquid Fuel: Fundamental Challenges and Opportunities (a Review). *Renewable Sustainable Energy Rev.* **31**, 221 (2014).
20. S. Lee, J. G. Speight, S. K. Loyalka, *Handbook of Alternative Fuel Technologies, Second Edition*. Green Chemistry and Chemical Engineering (Taylor & Francis, 2014).
21. C. Jaggai, Z. Imkaraaz, K. Samm, A. Pounder, N. Koylass, D. P. Chakrabarti, P. Dhurjati, M. Guo, K. Ward, Towards greater sustainable development within current Mega-Methanol (MM) production. *Green Chemistry* **22**, 4279-4294 (2020).
22. J. Rostrup-Nielsen, in *Studies in Surface Science and Catalysis,* X. Bao, Y. Xu, Eds. (Elsevier, 2004), vol. 147, pp. 121-126.
23. DECHEMA, Technology Roadmap "Energy and GHG Reductions in the Chemical Industry via Catalytic Processes". (2013), vol. 2021.
24. A. González-Garay, M. S. Frei, A. Al-Qahtani, C. Mondelli, G. Guillen-Gosalbez, J. Perez-Ramirez, Plant-to-planet analysis of CO_2-based methanol processes. *Energy & Environmental Science* **12**, 3425-3436 (2019).
25. H. Arakawa, Advances in Chemical Conversions for Mitigating Carbon Dioxide. **114**, p. 19-p. 19 (1998).
26. M. Aresta, A. Dibenedetto, E. Quaranta, State of the art and perspectives in catalytic processes for CO_2 conversion into chemicals and fuels: The distinctive contribution of chemical catalysis and biotechnology. *Journal of Catalysis* **343**, 2-45 (2016).
27. A. Álvarez, A. Bansode, A. Urakawa, A. V. Bavykina, T. A. Wezendonk, M. Makkee, J. Gascon, F. Kapteijn, Challenges in the Greener Production of Formates/Formic Acid, Methanol, and DME by Heterogeneously Catalyzed CO_2 Hydrogenation Processes. *Chemical Reviews* **117**, 9804-9838 (2017).
28. E. Kunkes, M. Behrens, R. Schlögl, Chemical Energy Storage, 5.3 Methanol Chemistry, Ed. (De Gruyter, 2012), pp. 413-442.
29. G. C. Chinchen, P. J. Denny, J. R. Jennings, M. S. Spencer, K. C. Waugh, Synthesis of Methanol: Part 1. Catalysts and Kinetics. *Applied Catalysis* **36**, 1-65 (1988).
30. J. Nakamura, T. Uchijima, Y. Kanai, T. Fujitani, The role of ZnO in Cu/ZnO methanol synthesis catalysts. *Catalysis Today* **28**, 223-230 (1996).
31. V. E. Ostrovskii, Mechanisms of Methanol Synthesis from Hydrogen and Carbon Oxides at Cu–Zn-Containing Catalysts in the Context of some Fundamental Problems of Heterogeneous Catalysis. *Catalysis Today* **77**, 141 (2002).
32. Y. Yang, C. A. Mims, D. H. Mei, C. H. F. Peden, C. T. Campbell, Mechanistic Studies of Methanol Synthesis over Cu from $CO/CO_2/H_2/H_2O$ Mixtures: The Source of C in Methanol and the Role of Water. *Journal of Catalysis,* **298**, 10 (2013).
33. F. Arena, G. Mezzatesta, G. Zafarana, L. Spadaro, G. Trunfio, F. Frusteri, How Oxide Carriers Control the Catalytic Functionality of the Cu–ZnO System in the Hydrogenation of CO_2 to Methanol. *Catalysis Today* **210**, 39 (2013).
34. E. L. Kunkes, F. Studt, F. Abild-Pedersen, R. Schlögl, M. Behrens, Hydrogenation of CO_2 to methanol and CO on $Cu/ZnO/Al_2O_3$: Is there a common intermediate or not? *Journal of Catalysis* **328**, 43-48 (2015).
35. M. Behrens, F.Studt, I. Kasatkin, S. Kuhl, M. Havecker, F. Ablid-Pedersen, S. Zander, F. Girgsdies, P. Kurr, B. L. Kniep, M. Tovar, R. W. Fischer, J. K. Norskov, R. Schlogl, The Active Site of Methanol Synthesis over $Cu/ZnO/Al_2O_3$ Industrial Catalysts. *Science* **336**, 893 (2012).
36. X. M. Liu, G. Q. Lu, Z. F. Yan, J. Beltramini, Recent Advances in Catalyst for Methanol Synthesis via Hydrogenation od CO and CO_2. *Industrial and Engineering Chemistry Research* **42**, 6518 (2003).

37. K. Klier, in *Advances in Catalysis,* D. D. Eley, H. Pines, P. B. Weisz, Eds. (Academic Press, 1982), vol. 31, pp. 243-313.
38. B. Bems, M. Schur, A. Dassenoy, H. Junkes, D. Herein, R. Schlogl, Relations between Synthesis and Microstructural Properties of Copper/Zinc Hydroxycarbonates. *Chemistry – A European Journal* **9**, 2039-2052 (2003).
39. M. Behrens, F.Studt, I. Kasatkin, S. Kuhl, M. Havecker, F. Ablid-Pedersen, S. Zander, F. Girgsdies, P. Kurr, B. L. Kniep, M. Tovar, R. W. Fischer, J. K. Norskov, R. Schlogl, The Active Site of Methanol Synthesis over Cu/ZnO/Al_2O_3 Industrial Catalysts. *Science* **336**, 893 (2012).
40. S. Kuld, C. Conradsen, P. G. Moses, I. Chorkendorff, J. Sehested, Quantification of Zinc Atoms in a Surface Alloy on Copper in an Industrial-Type Methanol Synthesis Catalyst. *Angewandte Chemie International Edition* **53**, 5941 (2014).
41. T. Lunkenbein, J. Schumann, M. Behrens, R. Schlögl, M. G. Willinger, Formation of a ZnO Overlayer in Industrial Cu/ZnO/Al_2O_3 Catalysts Induced by Strong Metal–Support Interactions. *Angewandte Chemie International Edition* **54**, 4544 (2015).
42. F. Arena, G. Mezzatesta, L. Spadaro, G. Trunfio, B.M. Bhanage, M. Arai, *Transformation and utilization of Carbon Dioxide*. (2014), pp. 103.
43. F. Arena, K. Barbera, G. Italiano, G. Bonura, L. Spadaro, F. Fruster, Synthesis, Characterization and Activity Pattern of Cu–ZnO/ZrO_2 Catalysts in the Hydrogenation of Carbon Dioxide to Methanol. *Journal of Catalysis* **249**, 185 (2007).
44. K. Klier, Methanol Synthesis. *Advances in Catalysis* **31**, 243 (1982).
45. L. C. Grabow, M. Mavrikakis, Mechanism of Methanol Synthesis on Cu through CO_2 and CO Hydrogenation. *American Chemical Society Catalysis.* **1**, 365 (2011).
46. F. Arena, G. Italiano, K. Barbera, G. Bonura, L. Spadaro, F. Frusteri, Basic Evidences for Methanol-Synthesis Catalyst Design. *Catalysis Today* **143**, 80 (2009).
47. F. Arena, G. Italiano, K. Barbera, S. Bordiga, G. Bonura, L. Spadaro, F. Frusteri, Solid-state Interactions, Adsorption Sites and Functionality of Cu-ZnO/ZrO_2 Catalysts in the CO_2 Hydrogenation to CH_3OH. *Applied Catalysis, A* **350**, 16 (2008).
48. B. Eren, R. S. Weatherup, N. Liakakos, G. A. Somorjai, M. Salmeron, Dissociative Carbon Dioxide Adsorption and Morphological Changes on Cu(100) and Cu(111) at Ambient Pressures. *Journal of American Chemical Society* **138**, 8207 (2016).
49. I. E. Wachs, R. J. Madix, The Selective Oxidation of CH_3OH to H_2CO on a copper(110) Catalyst. *Journal of Catalysis.* **53**, 208 (1978).
50. Y. Yang, J. Evans, J. A. Rodriguez, M. G. White, P. Liu, Fundamental Studies of Methanol Synthesis from $CO(_2)$ Hydrogenation on Cu(111), Cu Clusters, and Cu/ZnO(0001). *Physical Chemistry Chemical Physics* **12**, 9909 (2010).
51. Y. Kim, T. S. B. Trung, S. Yang, S. Kim, H. Lee, Mechanism of the Surface Hydrogen Induced Conversion of CO_2 to Methanol at Cu(111) Step Sites. *American Chemical Society Catalysis* **6**, 1037 (2016).
52. G. C. Chinchen, P. J. Denny, J. R. Jennings, M. S. Spencer, K. C. Waugh, Synthesis of Methanol- Part 1. Catalysts and Kinetics. *Applied Catalysis* **36**, 1 (1988).
53. L. C. Grabow, M. Mavrikakis, Mechanism of Methanol Synthesis on Cu through CO_2 and CO Hydrogenation. *ACS Catalysis* **1**, 365-384 (2011).
54. J. Tabatabaei, B. H. Sakakini, K. C. Waugh, On the mechanism of Methanol Synthesis and the Water-gas Shift Reaction on ZnO. *Catalysis Letters.* **110**, 77 (2006).
55. S. Kattel, P. J. Ramírez, J. G. Chen, J. A. Rodriguez, P. Liu, Active sites for CO_2 hydrogenation to methanol on Cu/ZnO catalysts. *Science* **355**, 1296-1299 (2017).
56. K. Larmier, W.C. Liao, S. Tada, E. Lam, R. Verel, A. Bansode, A. Urakawa, A. Comas-Vives, C. Coperet, CO_2-to-Methanol Hydrogenation on Zirconia-Supported Copper Nanoparticles:

Reaction Intermediates and the Role of the Metal–Support Interface. *Angewandte Chemie International Edition* **56**, 2318-2323 (2017).

57. Y. F. Zhao, Y. Yang, C. Mims, C. H. F. Peden, J. Li, D. Mei, Insight into Methanol Synthesis from CO_2 Hydrogenation on Cu(111): Complex Reaction Network and the Effects of H_2O. *Journal of Catalysis.* **281**, 199 (2011).
58. M. Yang, J. Yu, X. Tong, X. Sun, H. Xu, J. Sun, Flame-made Cu/ZrO_2 catalysts with metastable phase and strengthened interactions for CO_2 hydrogenation to methanol. *Chemical Communications* **57**, 7509-7512 (2021).
59. S. Li, Y. Wang, B. Yang, L. Guo, A highly active and selective mesostructured Cu/AlCeO catalyst for CO_2 hydrogenation to methanol. *Applied Catalysis A: General* **571**, 51-60 (2019).
60. H. Ahouari, A. Soualah, A. Le Valant, L. Pinard, P. Magnoux, Methanol synthesis from CO_2 hydrogenation over copper based catalysts. *Reaction kinetics, mechanisms and catalysis* **110**, 131-145 (2013).
61. Y.-M. Liu, J. T. Liu, S. Z. Liu, J. Li, Z. H. Gao, Z. J. Zuo, W. Huang, Reaction mechanisms of methanol synthesis from CO/CO_2 hydrogenation on Cu_2O(111): Comparison with Cu(111). *Journal of CO_2 Utilization* **20**, 59-65 (2017).
62. B. Liang, J. Ma, X. Su, C. Yang, H. Duan, H. Zhou, S. Deng, L. Li, Y. Huang, Investigation on Deactivation of Cu/ZnO/Al_2O_3 Catalyst for CO_2 Hydrogenation to Methanol. *Industrial & Engineering Chemistry Research* **58**, 9030-9037 (2019).
63. G. Bonura, S. Todaro, L. Frusteri, I. Majchrzak-Kuceba, D. Wawrzynczak, Z. Paszti, E. Talas, A. Tompos, L. Ferenc, H. Solt, C. Cannilla, F. Frusteri, Inside the reaction mechanism of direct CO_2 conversion to DME over zeolite-based hybrid catalysts. *Applied Catalysis B: Environmental* **294**, 120255 (2021).
64. J. Toyir, P. Ramírez de la Piscina, J. L. G. Fierro, N. s. Homs, Catalytic performance for CO_2 conversion to methanol of gallium-promoted copper-based catalysts: influence of metallic precursors. *Applied Catalysis B: Environmental* **34**, 255-266 (2001).
65. A. Le Valant, C. Comminges, C. Canaff, L. Pinard, Y. Pouilloux, The Cu–ZnO Synergy in Methanol Synthesis from CO_2, Part 1: Origin of Active Site Explained by Experimental Studies and a Sphere Contact Quantification Model on Cu+ZnO Mechanical Mixtures. *Journal of Catalysis* **324**, 41 (2015).
66. F. Arena *et al.*, Synthesis, characterization and activity pattern of Cu–ZnO/ZrO_2 catalysts in the hydrogenation of carbon dioxide to methanol. *Journal of Catalysis* **249**, 185-194 (2007).
67. X. Guo, D. Mao, S. Wang, G. Wu, G. Lu, Combustion synthesis of CuO–ZnO–ZrO_2 catalysts for the hydrogenation of carbon dioxide to methanol. *Catalysis Communications* **10**, 1661-1664 (2009).
68. J. Słoczyński, R. Grabowski, P. Olszewski, A. Kozlowska, J. Stoch, M. Lachowska, J. Skrzypek, Effect of metal oxide additives on the activity and stability of Cu/ZnO/ZrO_2 catalysts in the synthesis of methanol from CO_2 and H_2. *Applied Catalysis A: General* **310**, 127-137 (2006).
69. G. Bonura, M. Cordaro, C. Cannilla, F. Arena, F. Frusteri, The changing nature of the active site of Cu-Zn-Zr catalysts for the CO_2 hydrogenation reaction to methanol. *Applied Catalysis B: Environmental* **152-153**, 152-161 (2014).
70. J. Liu, J. Shi, D. He, Q. Zhang, X. Wu, Y. Liang, Q. Zhu, Surface active structure of ultra-fine Cu/ZrO_2 catalysts used for the CO_2+H_2 to methanol reaction. *Applied Catalysis A: General* **218**, 113-119 (2001).
71. K. Larmier *et al.*, CO2-to-Methanol Hydrogenation on Zirconia-Supported Copper Nanoparticles: Reaction Intermediates and the Role of the Metal-Support Interface. *Angew. Chem., Int. Ed.* **56**, 2318 (2017).

72. S.-K. Ihm, Y.-K. Park, J.-K. Jeon, K.-C. Park, D.-K. Lee, in *Studies in Surface Science and Catalysis,* T. Inui, M. Anpo, K. Izui, S. Yanagida, T. Yamaguchi, Eds. (Elsevier, 1998), vol. 114, pp. 505-508.
73. B. Denise, R. P. A. Sneeden, Oxide-supported copper catalysts prepared from copper formate: Differences in behavior in methanol synthesis from CO/H2 and CO2/H2 mixtures. *Applied Catalysis* **28**, 235-239 (1986).
74. Q.-J. Hong, Z.-P. Liu, Mechanism of CO2 hydrogenation over Cu/ZrO2(Z̄12) interface from first-principles kinetics Monte Carlo simulations. *Surface Science* **604**, 1869-1876 (2010).
75. K.-D. Jung, A. T. Bell, Role of Hydrogen Spillover in Methanol Synthesis over Cu/ZrO2. *Journal of Catalysis* **193**, 207-223 (2000).
76. E. L. Fornero, A. L. Bonivardi, M. A. Baltanás, Isotopic study of the rates of hydrogen provision vs. methanol synthesis from CO2 over Cu–Ga–Zr catalysts. *Journal of Catalysis* **330**, 302-310 (2015).
77. S. Kattel, B. Yan, Y. Yang, J. G. Chen, P. Liu, Optimizing Binding Energies of Key Intermediates for CO2 Hydrogenation to Methanol over Oxide-Supported Copper. *Journal of the American Chemical Society* **138**, 12440-12450 (2016).
78. K. Li, J. G. Chen, CO2 Hydrogenation to Methanol over ZrO2-Containing Catalysts: Insights into ZrO2 Induced Synergy. *ACS Catalysis* **9**, 7840-7861 (2019).
79. S. A. Tabak, F. J. Krambeck, W. E. Garwood, Conversion of propylene and butylene over ZSM-5 catalyst. *The American Institute of Chemical Engineers Journal* **32**, 1526-1531 (1986).
80. F. J. Keil, Methanol-to-hydrocarbons: process technology. *Microporous and Mesoporous Materials* **29**, 49-66 (1999).
81. M. Stöcker, Methanol-to-hydrocarbons: Catalytic Materials and their Behavior. *Microporous Mesoporous Materials.* **29**, 3 (1999).
82. M. Fakhroleslam, S. M. Sadrameli, Thermal/catalytic cracking of hydrocarbons for the production of olefins; a state-of-the-art review III: Process modeling and simulation. *Fuel* **252**, 553-566 (2019).
83. V. Arutyunov, N. Pogosyan, M. Pogosyan, L. Tavadyan, O. Shapovalova, L. Strekova, Production of olefins by the conjugated oxidation of light hydrocarbons. *Chemical Engineering Journal* **329**, 231-237 (2017).
84. M. Al-Samhan, J. Al-Fadhli, A. M. Al-Otaibi, F. Al-Attar, R. Bouresli, M. S. Rana, Prospects of refinery switching from conventional to integrated: An opportunity for sustainable investment in the petrochemical industry. *Fuel* **310**, 122161 (2022).
85. B. Eskew., US Petrochemicals-The Growing Importance of Export Markets, EI Energy Conference (2018).
86. I. Amghizar, L. A. Vandewalle, K. M. Van Geem, G. B. Marin, New Trends in Olefin Production. *Engineering* **3**, 171-178 (2017).
87. S. Seifzadeh Haghighi, M. R. Rahimpour, S. Raeissi, O. Dehghani, Investigation of ethylene production in naphtha thermal cracking plant in presence of steam and carbon dioxide. *Chemical Engineering Journal* **228**, 1158-1167 (2013).
88. J. Sundberg, S. Standl, T. Von Aretin, M. Tonigold, S. Rehfeldt, O. Hinrichsen, H. Klein, Optimal process for catalytic cracking of higher olefins on ZSM-5. *Chemical Engineering Journal* **348**, 84-94 (2018).
89. M. Höök, X. Tang, Depletion of fossil fuels and anthropogenic climate change—A review. *Energy Policy* **52**, 797-809 (2013).
90. Y. Xiang, J. Zhou, B. Lin, X. Xue, X. Tian, Z. LuO, Exergetic evaluation of renewable light olefins production from biomass via synthetic methanol. *Applied Energy* **157**, 499-507 (2015).

91. S. Jasper, M. M. El-Halwagi, A Techno-Economic Comparison between Two Methanol-to-Propylene Processes. *Processes* **3**, (2015).
92. D. Xiang, Y. Qian, Y. Man, S. Yang, Techno-economic analysis of the coal-to-olefins process in comparison with the oil-to-olefins process. *Applied Energy* **113**, 639-647 (2014).
93. D. Xiang, S. Yang, X. Liu, Z. Mai, Y. Qian, Techno-economic performance of the coal-to-olefins process with CCS. *Chemical Engineering Journal* **240**, 45-54 (2014).
94. C. Yang, M. Qiu, S. Hu, X. Chen, G. Zeng, Z. Liu, Y. Sun, Stable and efficient aromatic yield from methanol over alkali treated hierarchical Zn-containing HZSM-5 zeolites. *Microporous and Mesoporous Materials* **231**, 110-116 (2016).
95. U. Olsbye, S. Svelle, M. Bjorgen, P. Beato, T. V. W. Janssens, F. Joensen, S. Bordiga, K. P. Lillerud, Conversion of Methanol to Hydrocarbons: How Zeolite Cavity and Pore Size Controls Product Selectivity. *Angewandte Chemie International Edition* **51**, 5810-5831 (2012).
96. K. Asami, Q. Zhang, X. Li, S. Asaoka, K. Fujimoto, Semi-indirect synthesis of LPG from syngas: Conversion of DME into LPG. *Catalysis Today* **106**, 247-251 (2005).
97. S. Ilias, A. Bhan, Mechanism of the Catalytic Conversion of Methanol to Hydrocarbons. *ACS Catalysis* **3**, 18-31 (2013).
98. T. A. Atsbha, T. Yoon, B.-H. Yoo, C.-J. Lee, Techno-Economic and Environmental Analysis for Direct Catalytic Conversion of CO2 to Methanol and Liquid/High-Calorie-SNG Fuels. *Catalysts* **11**, (2021).
99. A. Álvarez, O. H. Laguna, S. Murcia-López, in *Heterogeneous Catalysis for Energy Applications*. (The Royal Society of Chemistry, 2020), pp. 397-430.
100. R. E. Owen, P. Plucinski, D. Mattia, L. Torrente-Murciano, V. P. Ting, M. D. Jones, Effect of support of Co-Na-Mo catalysts on the direct conversion of CO_2 to hydrocarbons. *Journal of CO_2 Utilization* **16**, 97-103 (2016).
101. M. P. Rohde, D. Unruh, G. Schaub, Membrane Application in Fischer−Tropsch Synthesis to Enhance CO_2 Hydrogenation. *Industrial & Engineering Chemistry Research* **44**, 9653-9658 (2005).
102. U. Rodemerck, M. Holena, E. Wagner, Q. Smejkal, A. Barkschat, M. Baems, Catalyst Development for CO_2 Hydrogenation to Fuels. *ChemCatChem* **5**, 1948-1955 (2013).
103. R. W. S. Ghosh, L. Olsson, D. Creaser, Methanol mediated direct CO_2 hydrogenation to hydrocarbons: Experimental and kinetic modeling study. *Chemical Engineering Journal* **435**, 135090 (2022).
104. R. W. Dorner, D. R. Hardy, F. W. Williams, H. D. Willauer, Heterogeneous catalytic CO_2 conversion to value-added hydrocarbons. *Energy & Environmental Science* **3**, 884-890 (2010).
105. G. Bonura, C. Cannilla, L. Frusteri, E. Catizzone, S. Todaro, M. Migliori, G. Giordano, F. Frusteri, Interaction effects between CuO-ZnO-ZrO_2 methanol phase and zeolite surface affecting stability of hybrid systems during one-step CO_2 hydrogenation to DME. *Catalysis Today* **345**, 175-182 (2020).
106. F. Arena, L. Spadaro, O. Di Blasi, G. Bonura, F. Frusteri, in *Studies in Surface Science and Catalysis,* X. Bao, Y. Xu, Eds. (Elsevier, 2004), vol. 147, pp. 385-390.
107. K. Saravanan, H. Ham, N. Tsubaki, J. W. Bae, Recent progress for direct synthesis of dimethyl ether from syngas on the heterogeneous bifunctional hybrid catalysts. *Applied Catalysis B: Environmental* **217**, 494-522 (2017).
108. X. Nie, X. Jiang, H. Wang, W. Luo, M. J. Janik, Y. Chen, X. Guo, C. Song, Mechanistic Understanding of Alloy Effect and Water Promotion for Pd-Cu Bimetallic Catalysts in CO_2 Hydrogenation to Methanol. *ACS Catalysis* **8**, 4873-4892 (2018).

109. Y. Yin, B. Hu, X. Li, X. Zhou, X. Hong, G. Liu, Pd@zeolitic imidazolate framework-8 derived PdZn alloy catalysts for efficient hydrogenation of CO_2 to methanol. *Applied Catalysis B: Environmental* **234**, 143-152 (2018).
110. H. Ham, S. W. Baek, C.-H. Shin, J. W. Bae, Roles of Structural Promoters for Direct CO_2 Hydrogenation to Dimethyl Ether over Ordered Mesoporous Bifunctional Cu/M–Al_2O_3 (M = Ga or Zn). *ACS Catalysis* **9**, 679-690 (2019).
111. A. Bansode, A. Urakawa, Towards full one-pass conversion of carbon dioxide to methanol and methanol-derived products. *Journal of Catalysis* **309**, 66-70 (2014).
112. G. Yang, N. Tsubaki, J. Shamoto, Y. Yoneyama, Y. Zhang, Confinement Effect and Synergistic Function of H-ZSM-5/Cu-ZnO-Al_2O_3 Capsule Catalyst for One-Step Controlled Synthesis. *Journal of the American Chemical Society* **132**, 8129-8136 (2010).
113. R. Phienluphon, K. Pinkaew, G. Yang, J. Li, Q. Wei, Y. Yoneyama, T. Vitidsant, N. Tsubaki, Designing core (Cu/ZnO/Al_2O_3)–shell (SAPO-11) zeolite capsule catalyst with a facile physical way for dimethyl ether direct synthesis from syngas. *Chemical Engineering Journal* **270**, 605-611 (2015).
114. T. Inui, Highly effective conversion of carbon dioxide to valuable compounds on composite catalysts. *Catalysis Today* **29**, 329-337 (1996).
115. M. D. Porosoff, B. Yan, J. G. Chen, Catalytic reduction of CO_2 by H_2 for synthesis of CO, methanol and hydrocarbons: challenges and opportunities. *Energy & Environmental Science* **9**, 62-73 (2016).
116. D. Wang, Z. Xie, M. D. Porosoff, J. G. Chen, Recent advances in carbon dioxide hydrogenation to produce olefins and aromatics. *Chem* **7**, 2277-2311 (2021).
117. W. Li, H. Wang, X. Jiang, J. Zhu, Z. Liu, X. Guo, C. Song, A short review of recent advances in CO_2 hydrogenation to hydrocarbons over heterogeneous catalysts. *RSC Advances* **8**, 7651-7669 (2018).
118. I. Yarulina, A. D. Chowdhury, F. Meirer, B. M. Weckhuysen, J. Gascon, Recent trends and fundamental insights in the methanol-to-hydrocarbons process. *Nature Catalysis* **1**, 398-411 (2018).
119. J. Li, Z. Wei, Y. Chen, B. Jing, Y. He, M. Dong, H. Jiao, X. Li, Z. Qin, J. Wang, W.Fan, A route to form initial hydrocarbon pool species in methanol conversion to olefins over zeolites. *Journal of Catalysis* **317**, 277-283 (2014).
120. A. D. Chowdhury, K. Houben, G. J. Whiting, M. Mokhtar, A. M. Asiri, S. A. Al-Thabaiti, S. N. Basahel, M. Baldus, B. M. Weckhuysen, Initial Carbon–Carbon Bond Formation during the Early Stages of the Methanol-to-Olefin Process Proven by Zeolite-Trapped Acetate and Methyl Acetate. *Angewandte Chemie International Edition* **55**, 15840-15845 (2016).
121. R. M. Dessau, R. B. LaPierre, On the mechanism of methanol conversion to hydrocarbons over HZSM-5. *Journal of Catalysis* **78**, 136-141 (1982).
122. I. M. Dahl, S. Kolboe, On the Reaction Mechanism for Hydrocarbon Formation from Methanol over SAPO-34: I. Isotopic Labeling Studies of the Co-Reaction of Ethene and Methanol. *Journal of Catalysis* **149**, 458-464 (1994).
123. Y. Ono, T. Mori, Mechanism of methanol conversion into hydrocarbons over ZSM-5 zeolite. *Journal of the Chemical Society, Faraday Transactions 1: Physical Chemistry in Condensed Phases* **77**, 2209-2221 (1981).

Chapter 2

Experimental.

2.1 – Materials

The chemicals, used throughout this work, including their supplier and purity, are presented in Table 2.1.

Table 2.1: *List of all the materials and gases used throughout this thesis and their suppliers.*

Material	Supplier
Copper (II) nitrate trihydrate - $Cu(NO_3)_2 \cdot 3H_2O$	Merck
Zirconyl (IV) nitrate hydrate - $ZrO(NO_3)_2{\cdot}xH_2O$	Acros Organics
Oxalic Acid - HO_2CCO_2H	Sigma Aldrich
Palladium (II) nitrate dihydrate - $Pd(NO_3)_2{\cdot}2H_2O$	Sigma Alrdich
Platinum (IV) nitrate solution, Pt 15% w/w - $Pt(NO_3)_4$	Alfa Aesar
Cerium (III) nitrate hexahydrate - $Ce(NO_3)_3{\cdot}6H_2O$	Sigma Aldrich
Silver nitrate - $Ag(NO_3)_2$	Sigma Aldrich
Nickel (II) nitrate hexahydrate - $Ni(NO_3)_2.6H_2O$	Sigma Aldrich
Cerium (III) nitrate hexahydrate - $Ce(NO_3)_3{\cdot}6H_2O$	Sigma Aldrich
Magnesium nitrate hexahydrate - $Mg(NO_3)_3{\cdot}6H_2O$	Sigma Aldrich
Lanthanum (III) nitrate hexahydrate - $La(NO_3)_3{\cdot}6H_2O$	Sigma Aldrich
Manganese (II) nitrate tetrahydrate - $Mn(NO_3)_2{\cdot}4H_2O$	Sigma Aldrich
Aluminium nitrate nonahydrate - $Al(NO_3)_3{\cdot}9H_2O$	Sigma Aldrich

Copper (II) acetylacetonate - $Cu(C_5H_7O_2)_2$	Sigma Aldrich
Zinc acetylacetonate hydrate - $Zn(C_5H_7O_2)_2 \cdot xH_2O$	Sigma Aldrich
ZSM-5 (Si:Al 23; 30; 50 and 80)	Alfa Aesar
Mordenite (20:1)	Alfa Aesar
Zeolite Y	Alfa Aesar
Sodium carbonate - Na_2CO_3	Fischer
Absolute Ethanol	Sigma Aldrich
20 % CO_2 / 60 % H_2 / 20 % N_2	BOC
5% H_2 / Ar (99.99 %)	BOC
Helium, He (99.99 %)	BOC

2.2 – Catalyst Preparation

2.2.1 – Wet impregnation (WI)

Wet impregnation (WI) is the simplest method for catalyst preparation. In this method, a solution of the metal salt precursor is added to the support material and mixed so that the metal is distributed throughout the pores of the support.[1] The material is then dried in order to remove the solvent, but care must be taken that the drying is carried out in a way that the metal component does not migrate to the surface from the pores. After drying, calcination or elevated heat treatment may be carried out to decompose metal salt precursors or prepare the catalytic sites. Reduction treatment may also be employed. Incipient wetness impregnation is a variation of WI where the volume of the metal salt solution is equal to or smaller than the pore volume of the support. This process is simple, quick, reproducible, and ensures that all the metal is directly deposited onto the surface thereby reducing waste, which is especially important when expensive precious metals are used. Industries frequently use WI for the preparation of heterogeneous metal catalysts for these reasons.

Wet impregnation was used a method for Cu deposition onto ZrO_2 in Chapter 4. The Cu loading for all catalyst were fixed at 31 wt. %. The copper metal precursor was dissolved in deionised water (excess) and added dropwise to the ZrO_2 support with vigorous stirring until a paste was formed. The resulting wet solid was dried in the oven at 110 °C for 4 hours before calcining at under static air at 500 °C, 2 °C/min for 2 hours.

2.2.2 – Co-precipitation (CP)

Co-precipitation (CP) is a common catalyst preparation technique that involves the simultaneous precipitation of two or more metal components using a precipitant under a constant or a varied pH. There are many factors to consider in the synthesis of catalysts by CP including temperature, pH, flow rate of precipitating agent, ageing time, and washing. All of the preparation parameters must be controlled carefully in order to ensure that the catalysts are prepared reproducibly. Because catalysts can be prepared reproducibly by CP, this method has been applied for large scale production of heterogeneous catalysts.[2] The main drawback of this technique is that there can be large mass loss during the derivation of the final product. Calcination is often required to decompose the material to the active catalyst.

The following method was used to prepare the 31 wt. % Cu/ZrO_2 catalyst in Chapter 4. A 0.5 M mixed solution of $Cu(NO_3)_2.3H_2O$ and $ZrO(NO_3)_2.6H_2O$ was prepared. Na_2CO_3 solution (0.5 M) was added

dropwise to the solution and a pH of 6.5 was maintained. The precipitate was aged in solution for 1 hour at room temperature. The precipitate was filtered under vacuum followed by washing with 6L of warm deionised water. The precipitate was dried in an oven at 110 °C for 16 hours and calcined at the 500 °C (heating rate 2 °C min^{-1}) in static air for 2 hours.

2.2.3 – Oxalate Gel Precipitation (OGP)

Oxalate gel precipitation (OGP) is a variation of the CP procedure discussed in Section 2.2.3, so called because it uses oxalic acid as the precipitating agent, resulting in a sol-gel being formed in solution. The conditions of OGP must be carefully controlled in the same way as CP method.

The supported Cu catalysts and promoted Cu/ZrO_2 catalysts investigated in Chapter 3, Cu/ZrO_2 catalysts in Chapter 4 and CuZn/zeolite and CuZr/Zeolite catalysts in Chapter 5 were prepared by the OGP method. The appropriate metal nitrates were dissolved in 200 mL of ethanol. Solid oxalic acid (0.024 mol) was added into the metal solution, and the resulting precipitate was aged in solution at room temperature for 1 hour. The precipitate was then collected by centrifuge and filtered without a washing step. The material was dried in an oven at 110 °C for 16 hours, and the supported Cu catalysts were calcined at 500 °C (heating rate 2 °C min^{-1}) in static air for 2 hours; for the zeolite catalysts calcination was at 550 °C (heating rate 10 °C min^{-1}) in static air for 2 hours.

2.2.4 – Chemical Vapour Impregnation (CVI)

The chemical vapour impregnation (CVI) method was used in order to synthesise the 20 wt.% CuZnO/ZSM-5, CuZnO/H-Y and CuZnO/mordenite catalysts in Chapter 5, where Cu:Zn = 1. A mixture of $Cu(acac)_2$ (Sigma Aldrich), $Zn(acac)_2$ (Sigma Aldrich) and zeolite (H-ZSM-5 (Alfa Aesar), H-Y (Alfa Aesar) or mordenite (Alfa Aesar)) were mixed thoroughly before transferring to a 50 ml Schlenk flask. The flask was sealed and evacuated at room temperature on a vacuum line ($\sim 10^{-3}$ mbar). The mixture was heated at 120 °C for 1 hour with magnetic stirring under continuous vacuum. The tube was then left to cool and brought to atmospheric pressure in air before collecting. The sample was then calcined at 500 °C (heating rate 2 °C min^{-1}) in static air, for 16 hours) to allow complete decomposition of the acetylacetonate precursors.

2.2.5 – Physical Mixing (PM)

Catalysts prepared by physical mixing are presented in Chapter 5. Physical mixtures of 10% Cu/ZnO, prepared by the oxalate gel method, and commercial H-ZSM-5 (23:1) were made. Two methods of creating physical mixture were employed: the first involved shaking the two catalyst components; and

the second involved grinding the components together, using a pestle and mortar to give the final catalyst.

2.3 – Catalyst Testing

2.3.1 – Reactor Set-up

A custom-built six-bed flow reactor was used for the analysis of all the catalysts towards the CO_2 hydrogenation (250 °C, 20 bar, 30 ml·min^{-1}, 60% H_2, 20% CO_2, 20% N_2). Exhaust gas products were analysed online using a GC Agilent 7890 system fitted with a TCD and a FID detector, and an Agilent CP7557 column with He as the carrier gas. In order to avoid product condensation, post reactor lines and valves prior to the GC were wrapped with heating tape and kept at 130 °C. A thermocouple introduced inside a thermowell placed inside the reactor tube allowed control of the temperature inside the catalyst bed. Simultaneously, a reactor tube was always kept empty to measure the reaction blank activity. A schematic of this is shown below (Figure 2.1).

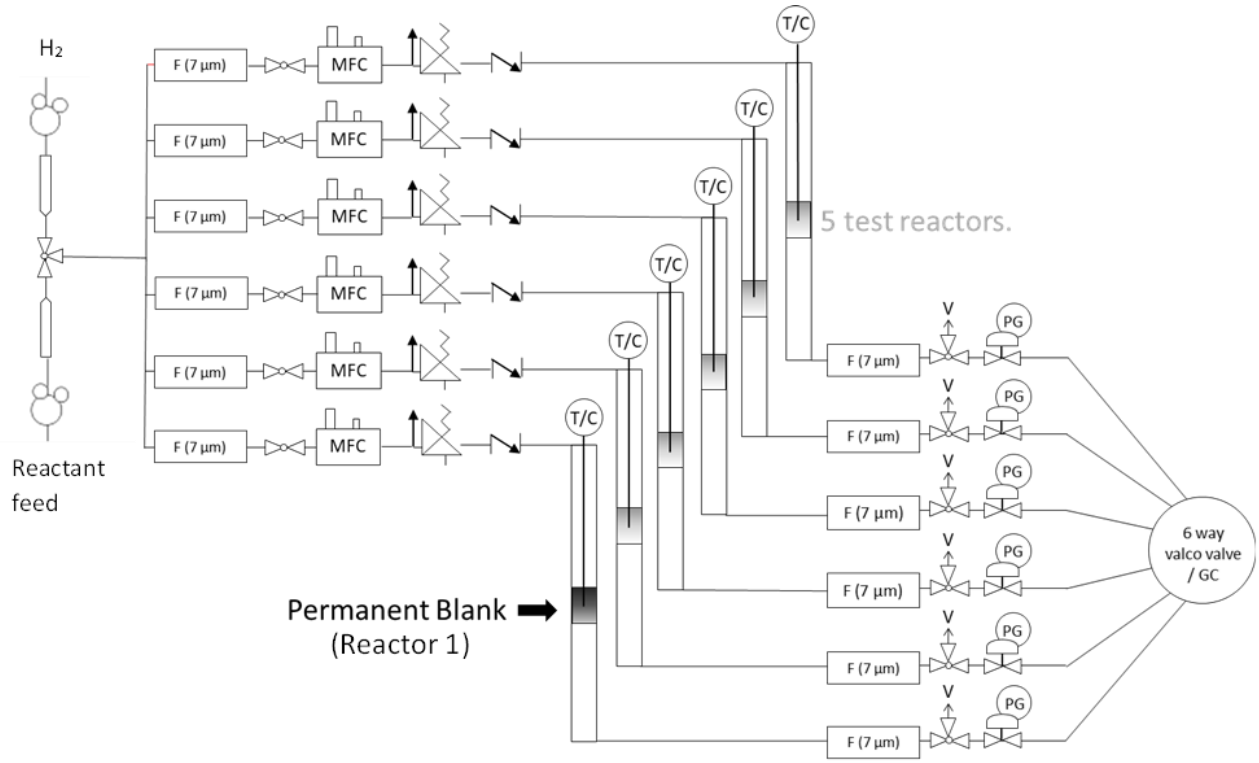

Figure 2.1 – Schematic representation of the six-bed reactor used for CO_2 hydrogenation catalyst testing. Diagram produced by Dr. Robert D. Armstrong, Cardiff Catalysis Institute.

Prior to reactions, catalysts were pelleted (425 - 500 µm) and pre-reduced in situ using 5% H_2/He (30 mL/min) for 1 hour at 220 °C at a ramp rate of 2 °C/min, under atmospheric pressure. Catalysts were placed in the middle of the reactor tube (stainless steel, 0.5 cm x 50 cm), which coincided with the

position of the thermowell, and held in place using quartz wool. Hydrocarbons produced during the reaction including methanol or methane were detected using a flame ionisation detector (FID), while non-hydrocarbon gases like CO, CO_2, and N_2 were analysed using a thermal conductivity detector (TCD).

2.3.2 – Data Calculations

The following calculations (Equations 2.1 to 2.9) were used to determine the CO_2 conversion, product selectivity, and productivities.

Through the ideal gas law (Equation 2.1) where *p* is the pressure of the reaction mixture at the mass flow controller (MFC) (1 bar), *R* is the gas constant (83.15 x 10^{-3} dm^3 bar K^{-1} mol^{-1}), *T* is the temperature (298.15 K) and *V* is the volume (0.03 dm^3 min^{-1} obtained from the flow gas used during the reaction of 30 ml min^{-1}), the total molar gas (*n*) flow was determined.

$$pV = nRT \qquad n = 1.21 \times 10^{-3}\ CO_2\ \text{mol min}^{-1} \qquad \textbf{(Eq. 2.1)}$$

Nitrogen gas was used as internal standard at a concentration of 20 vol. %. A blank reactor was analysed simultaneously to the CO_2 hydrogenation reaction, and CO_2 conversion was calculated according to Equation 2.2.

$$CO_2\ \text{conv. \%} = \frac{\left(\left(\frac{\int \text{Blank CO2 / area count}}{\int \text{Blank N2 / area counts}}\right) - \left(\frac{\int \text{CO2 / area count}}{\int \text{N2 / area counts}}\right)\right)}{\left(\frac{\int \text{Blank CO2 / area count}}{\int \text{Blank N2 / area counts}}\right)} \times 100 \qquad \textbf{(Eq 2.2)}$$

Because the number of moles in the gas phase change during the reaction, a compression factor (CF) was introduced (Equation 2.3).

$$CF = \frac{\int N_2 \text{ / area counts}}{\int \text{Blank } N_2 \text{ / area counts}} \qquad \textbf{(Eq 2.3)}$$

Non-reacted CO_2 was calculated according to Equation 2.4.

$$\text{Non-reacted } CO_2\ \text{mol min}^{-1} = \frac{\frac{\int CO_2 \text{ / area counts}}{rF\ CO_2} \times (\text{Total gas flow / mol min}^{-1})}{CF} \qquad \textbf{(Eq 2.4)}$$

Where *rF* is the response factor obtained from the calibration (area counts per mol^{-1}). CH_3OH productivity was calculated according to Equation 2.5.

$$CH_3OH \text{ mol min}^{-1} = \frac{\left(\left(\frac{\int CH_3OH \,/\, \text{area counts}}{rF\ CH_3OH}\right) x \left(\frac{\text{total gas flow/ml min}^{-1}}{0.25 \text{ ml loop volume}}\right)\right)}{CF} \quad \text{(Eq 2.5)}$$

Productivity of remaining products was obtained following the next calculations (Equation 2.6 representative for CO productivity), were *rF* is the response factor obtained from the corresponding calibration (area counts per ppm^{-1}).

$$CO \text{ mol min}^{-1} = \frac{\frac{\int CO \,/\, \text{area counts}}{rF\ CO} x\ (\text{Total gas flow} \,/\, \text{mol min}^{-1})}{CF} \quad \text{(Eq. 2.6)}$$

The product selectivity based on CO_2 hydrogenation was determined by dividing the productivity of each species times the number of carbons (*nC*) by the productivities of all the products. For instance, CH_3OH and DME selectivity was calculated following Equations 2.7 and 2.8, respectively.

$$CH_3OH \text{ sel. \%} = \left(\frac{CH_3OH \text{ productivity x 1C/ mol min}^{-1}}{\Sigma \text{ productivities}}\right) x\ 100 \quad \text{(Eq. 2.7)}$$

$$DME \text{ sel. \%} = \left(\frac{DME \text{ productivity x 2C/ mol min}^{-1}}{\Sigma \text{ productivities}}\right) x\ 100 \quad \text{(Eq. 2.8)}$$

Molar productivities, obtained in mol min^{-1}, could be normalised to the mass of catalysts used during the reaction (0.5 g) and expressed as mol kg_{cat}^{-1} h^{-1} according to Equation 2.9 as shown for methanol.

$$CH_3OH \text{ prod mol kg}_{cat}^{-1} \text{ h}^{-1} = \left(\frac{CH_3OH \text{ productivity / mol min}^{-1}}{(\text{catalyst mass g / 1000})}\right) x\ 60 \quad \text{(Eq. 2.9)}$$

2.4 – Characterisation

2.4.1 – X-Ray Diffraction

X-ray diffraction is a versatile non-destructive analytical technique for the identification and quantitative determination of the various crystalline forms, known as phases, of compounds present in powdered and solid samples. Identification is achieved by comparing the x-ray diffraction pattern (diffractogram) obtained from an unknown sample with an internationally recognised database containing reference patterns for more than 70, 000 phases. Modern computer-controlled diffractometer systems use automatic routines to measure, record, and interpret the unique diffractograms produced by individual constituents in even highly complex mixtures.

The widths of the peaks in a particular phase pattern provide an indication of the average crystallite size. Large crystallites give rise to sharp peaks, while the peak width increases as crystallite size reduces. Peak broadening also occurs as a result of variations in *d*-spacing caused by micro-strain. However, the relationship between broadening and diffraction angle 2θ is different from that of crystallite size effects, making it possible to differentiate between the two phenomena.

A crystal lattice is a regular three-dimensional distribution (cubic, rhombic, etc.) of atoms in space. These are arranged so that they form a series of parallel planes separated from one another by a distance *d*, which varies according to the nature of the material. For any crystal, planes exist in a number of different orientations – each with its own specific *d* spacing. When a monochromatic x-ray beam with wavelength λ is incident on lattice planes in a crystal at angle ϑ, diffraction occurs only when the distance travelled by the rays reflected from successive planes differs by a complete number *n* of wavelengths.[3] This is described by Bragg's Law (Eq 2.10), and illustrated in Figure 2.2.

$$n\lambda = 2d \sin \vartheta \qquad \text{(Eq. 2.10)}$$

By varying the angle ϑ, the Bragg's Law conditions are satisfied by different *d*-spacings in polycrystalline materials. Plotting the angular positions and intensities of the resultant diffraction peaks produces a pattern that is characteristic of the sample. When a mixture of different phases is present, the diffractogram is formed by addition of the individual patterns.[4]

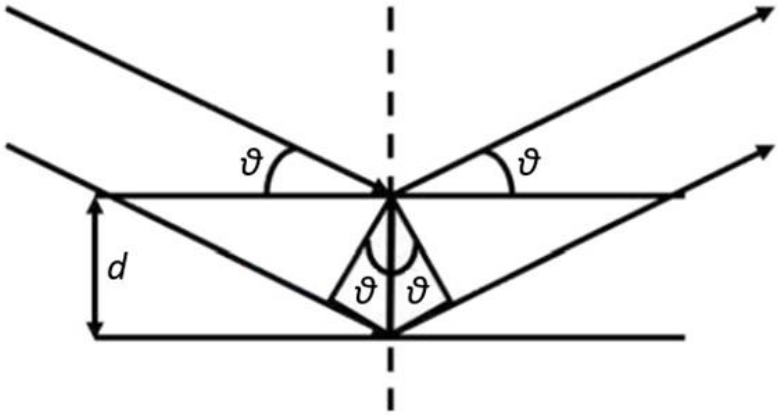

Figure 2.2 – Illustration of x-ray beams interacting with a crystal, from which Bragg's Law is derived.

The average crystallite size of the material can be determined using Scherrer's equation (Equation 2.11). Scherrer's equation is only applicable to particles smaller than 100 nm. XRD reflections must be well defined as the full-width half-maximum (FWHM) is a parameter in the equation, meaning that poorly defined reflections (indicating small particles sizes) cannot always be used to determine the particle size using Scherrer's equation.[5]

$$\text{(Eq. 2.11)} \quad L = \frac{K\lambda}{\beta \cos \theta}$$

L = measure of the crystallite size in the direction perpendicular to the reflecting plane; K = a constant based on crystallite shape (generally 0.9 – 1); λ = x-ray wavelength; β = the peak width (FWHM); ϑ = Bragg angle (the angle between the beam and the normal on the reflecting plane).

Powder x-ray diffraction patterns (PXRD) were obtained using a PANalytical X'Pert Pro fitted with an X'Celerator detector and a CuKα x-ray source operated at 40 kV and 40 mA, 2ϑ = 10–80°. Each sample was scanned from 2ϑ = 10° to 80° for 30 minutes at room temperature. All patterns were matched using the International Centre for Diffraction (ICDD) database. The Cu and Zn particle sizes were calculated using the Scherrer Equation; *Cu (111)* at 2ϑ = 43.3° and *Zn (101)* at 2ϑ = 36.2° respectfully.

2.4.2 – Brunauer–Emmett–Teller (BET) Surface Area Analysis

The Brunauer-Emmett-Teller (BET) method is the most widely used technique for surface area determination. The theory aims to explain the physical adsorption of gas molecules on a solid surface and serves as the basis for an important analysis technique for the measurement of the specific surface area of materials. BET theory applies to systems of multilayer adsorption, and usually utilizes probing gases that do not chemically react with material surfaces as adsorbates to quantify specific surface area. Nitrogen is the most commonly employed gaseous adsorbate used for surface probing by BET methods. For this reason, standard BET analysis is most often conducted at the boiling temperature of N_2.[6,7] This method is an extension of the Langmuir model of monolayer adsorption to cover multilayer adsorption and relies on three key assumptions:

1. Gas molecules can adsorb on a solid in infinite layers
2. There is no interaction between each layer
3. The Langmuir model can be applied to each model

The determination of BET surface area is given by the BET equations show in Equations 2.12-2.14.[8]

(Eq. 2.12) $$\frac{p}{V(p_0-p)} = \frac{1}{V_m C} + \frac{C-1}{V_m C} \cdot \frac{p}{p_0}$$

Where p = equilibrium pressure of the adsorbate at the adsorption temperature; $p0$ = saturation pressure of the adsorbate at the adsorption temperature; V = volume of gas adsorbed at pressure p; V_m = volume of gas required to form a monolayer; C = BET constant, which is related to the heat of adsorption.

(Eq. 2.13) $$S_{\text{total}} = \frac{V_m N_A \sigma}{22414}$$

S_{total} = total surface area; N_A = Avogadro's constant; σ = the adsorption cross section of the adsorbing species; 22414 L mol^{-1} is the molar volume of a gas

(Eq. 2.14) $$S_{\text{BET}} = \frac{S_{total}}{m}$$

S_{BET} = BET surface area; m = mass of the solid sample.

BET surface area measurements were performed on a Quantachrome Nova 2200 using a multipoint N_2 adsorption method. Prior to the analysis, samples were degassed for 3 hours at 120 °C under vacuum. The CuZn/Zeolite and CuZr/Zeolite catalyst surface areas were determined by multi-point N_2 adsorption at 77 K (BET range: P/P_0 = 0.0013-0.0079) on a micromeritics 3-flex instrument according to the Brunauer-Emmett-Teller (BET) method; Prior to the analysis, samples were degassed at 350 °C, at a heating rate of 10°C/min for 9 hours.

2.4.3 – N_2O Pulse Titration to Determine Specific Metal Surface

N_2O titration is used for the determination of the metal surface area. N_2O can oxidise surface metal particles while itself being reduced to N_2, as shown in Equation 2.15 below.[9]

(Eq. 2.15) $N_2O\ (g) + 2Cu^0\ (surface) \rightarrow N_2\ (g) + Cu_2O\ (surface)$

Any unreacted N_2O used during the analysis is trapped before reaching the detector, in this instance a molecular sieve 5 Å (pelleted 1.6 mm, Sigma Aldrich) trap was used. The process relies on the oxidation of the Cu surface; thus the Cu surface area is determined using the amount of N_2 emitted and the catalyst mass (Equation 2.16).

(Eq 2.16) Cu surface area ($m^2\ g^{-1}$) = $$\frac{N_2\ volume\ (ml) \times N_A \times 2}{Catalyst\ mass\ (g) \times 24000\ (ml) \times (1.0 \times 10^{19} \left(\frac{atoms}{m^2}\right))}$$

Whereby N_A = Avagadro's constant = 6.022 x10^{23} (atoms)

The key assumptions are that the amount of N_2 emitted amounts to half a monolayer coverage of oxygen and that the surface density of Cu is 1.47 x 10^{-19} atoms/m^2. The volume of N_2 produced was quantified using a thermal conductivity detector.

Cu surface area analysis was carried out by N_2O pulse titration using a Quantachrome ChemBET. Catalysts were reduced under a flow of 10% H_2/Ar at 220 °C (2 °C min^{-1}, held for 60 min). This was followed by cooling under He. N_2O titration was carried out at 65 °C with a programme of 13 pulses of 113 µl N_2O followed by 3 pulses of N_2 for calibration.

Recent work has shown that if the catalyst is exposed to partial pressures of hydrogen exceeding 0.05 bar then partial reduction of ZnO at Cu interface can occur. This will effect copper surface area results, due to N_2O oxidising both Cu and ZnO_x. In these cases, alternative techniques, such as H_2 TPD, will give more accurate data with respect to copper surface area.[10, 11]

2.4.4 – Temperature Programmed Desorption

Temperature programmed desorption involves monitoring the rate of desorption of chemisorbed molecules as a function of temperature. Adsorption, which can be defined as the enrichment of a fluid adsorbate at the surface of a solid (adsorbent) or the increase in fluid density in the vicinity of an interface,[12] can be categorised as physisorption or chemisorption. Physisorption arises as the result of weak intermolecular forces and is nonspecific, non-dissociative; it occurs only at reasonably low temperatures and is characterised by a low heat of adsorption (< 50 kJ mol^{-1}). Alternatively, chemisorption is characterised by a high heat of adsorption (> 50 kJ mol^{-1}) and can occur over a wide temperature range. Chemisorption is highly specific, monolayer forming and can take place associatively or dissociatively.[13]

TPD typically involves the saturation of a sample with a chemical species (adsorbate) and subsequently heating the sample at a controlled ramp rate to monitor the temperature(s) at which desorption occurs. Following pre-treatment of the adsorbent, the sample is exposed to the adsorbate, generally at ambient temperatures. Any physisorbed species are subsequently removed by flowing an inert gas over the sample before desorption of remaining chemisorbed species is performed. The adsorbent is heated under an inert gas with a constant heating rate ($\beta = dT/dt$ = constant) with any desorbed species monitored by an appropriate detector (generally TCD, FID or quadrupole mass spectrometer (QMS)).[14] The data generated from TPD experiments shows detector signal intensity as a function of time/temperature; since signal intensity is proportional to concentration of detected species as desorbed from the sample surface, it is proportional to the rate of desorption. Calibration of the detector by the direct admission of specific quantities of adsorbates, allows for quantitative measurements of desorbed species.

Acidic probe molecules, such as CO_2 or SO_2, are used to investigate materials with basic sites; basic probe molecules, such as NH_3, pyridine or acetonitrile, are used to investigate materials containing acidic sites. CO_2 and NH_3 are the most widely probe molecules used for investigating the basic and acidic sites of materials, respectively.

Ammonia temperature-programmed desorption (NH_3-TPD) was carried out using a Quantachrome ChemBET TPR/TPD instrument equipped with a thermal conductivity detector (TCD). Each catalyst (0.15

g) underwent a pre-treatment at 400 °C (heating rate: 10 °C/min) for 1 hour under He, to remove any water. The catalysts were then saturated with 10% NH_3/Ar for 15 mins. Physiosorbed NH_3 was removed by heating to 100 °C (heating rate: 10 °C/min) for 1 hour. Finally, NH_3 TPD profiles were recorded under a He flow, from 50 °C to 900 °C using a heating rate of 10 °C/min.

2.4.5 – X-Ray Photoelectron Spectroscopy (XPS)

X-ray photoelectron spectroscopy (XPS) is a commonly used surface technique in catalysis research for the analysis of elemental composition, elemental oxidation state, and metal dispersion. The photoelectron effect is the basis of XPS. An atom absorbs a photon of energy ($h\upsilon$) and ejects a electron with kinetic energy defined by Equation 2.17. The kinetic energy measured by XPS is used to determine the binding energy of the electron, which is characteristic for each element. Because the binding energy is not only characteristic of the element, but affected by the chemical state of the atom, chemical information can be obtained by XPS. XPS is considered surface sensitive, but x-rays can penetrate a sample to a depth of approximately 10 nm.[15]

(Eq 2.17) $E_k = h\upsilon - E_b - \varphi$

E_k = kinetic energy of the ejected photoelectron; $h\upsilon$ = energy of the X-ray photon; E_b = binding energy of the photoelectron with respect to the fermi level; φ = work function of the spectrometer.

If the incident photon is sufficiently energetic, many different levels in the sample may be ionized and thus a spectrum is produced displaying all accessible energy levels as a distribution of photoelectrons with kinetic energies governed by Equation 2.17.[16]

Photoelectron peaks are labelled according to the quantum numbers of the level from which the electron originates. The electron is characterized by a total momentum number $j=l+s$, where l is the orbital momentum number, and s the spin momentum number, which is equal to 1/2 or −1/2. Therefore, whenever $l>0$, the peak is split into a doublet (according to quantum selection rules), with an energy difference called spin-orbit splitting which increases with Z roughly as Z^5.[17]

XPS was performed using a Kratos Axis Ultra-DLD photoelectron spectrometer, using monochromatic Al kα radiation, operating at 144 W power. High resolution and survey scans were performed at pass energies of 40 and 160 eV, respectively. Spectra were calibrated to the C (1s) signal at 284.8 eV and quantified using Casa XPS, using modified Wagner sensitivity factors supplied by the manufacturer.

2.4.6 – Transmission Electron Microscopy (TEM)

In Transmission electron microscopy (TEM) high energy electrons are accelerated onto a thin sample leading to a variety of interactions, these include elastic and inelastically scattered electrons. Elastic scattering occurs when there is no loss of energy of the incident primary electron. Inelastic scattering occurs when there is an interaction that causes loss of energy of the incident primary electron. Inelastically scattered electrons have a longer wavelength and can occur by many mechanisms; the energy is transferred to the specimen generating a range of useful signals that are exploited to characterize the material.[18] The electron beam is then transferred through the instrument's optics. The TEM has an electron gun and electromagnetic lenses that include condenser and objective lenses. The condenser lenses converge and control the electron beam and illuminate the sample, and the objective lens forms the image of the sample and diffraction. The images and diffractions are then magnified by other lenses in the system.

The accelerator voltages are high, to provide electrons with sufficiently high energy (100 – 400 keV) to penetrate the sample. In TEM, the beam is usually spread to encompass the whole sample and as a result does not need to be scanned across the material surface. In addition, the transmission of the electrons through the sample provides more information on the structure of the material, in contrast to scanning electron microscopy (SEM), where the poor depth penetration of the beam insists that only morphology and surface composition can be recorded. The electron beam is refocused after passing through the sample and projected onto a screen. TEM has been previously used to assess the structure and morphology of heterogeneous catalysts as atomic weight contrast, where the scattering increases with atomic number and thickness of the sample, allows for the determination of particle size for supported metal nanoparticles.[19, 20]

Samples are generally dispersed in alcohol and deposited on 3 mm carbon-filmed beryllium, copper or aluminium grids. If carbon or other support films are not desirable, freshly meshed metal grids can be used.

Transmission Electron Microscopy (TEM) images of the catalysts were taken using a JEOL JEM-2100 electron microscope operating at 200 kV.

2.5 – References

1. M. V. Twigg, P. Imperial Chemical Industries, A. Division., *Catalyst Handbook*. 2, Ed., (Manson Pub, London, 1996).
2. P. N. Dyer, R. Pierantozzi, Methods for making a supported iron-copper catalyst, patent file, OSTI identifier 5294907, United States (1985).
3. V. Ramaswamy, *Characterization of Polycrystalline Catalytic Materials Using Powder X-Ray Diffraction*. (Alpha Science International Limited, 2016).
4. C. Hammond, *The Basics of Crystallography and Diffraction*. International Union of Crystallography texts on crystallography (OUP Oxford, 2009).
5. I. V. Krasnikova, I. V. Mishakov, A. A. Vedyagin, in *Carbon-Based Nanofillers and Their Rubber Nanocomposites,* S. Yaragalla, R. K. Mishra, S. Thomas, N. Kalarikkal, H. J. Maria, Eds. (Elsevier, 2019), pp. 75-137.
6. M. Nasrollahzadeh, M. Atarod, M. Sajjadi, S. M. Sajadi, Z. Issaabadi, in *Interface Science and Technology,* Eds. (Elsevier, 2019), vol. 28, pp. 199-322.
7. P. Pourhakkak, A. Taghizadeh, M. Taghizadeh, M. Ghaedi, S. Haghdoust, in *Interface Science and Technology,* (Elsevier, 2021), vol. 33, pp. 1-70.
8. S. Palchoudhury, M. Baalousha, J. R. Lead, in *Frontiers of Nanoscience,* M. Baalousha, J. R. Lead, Eds. (Elsevier, 2015), vol. 8, pp. 153-181.
9. K. Larmier, S. Tada, A. Comas-Vives, C. Copéret, Surface Sites in Cu-Nanoparticles: Chemical Reactivity or Microscopy? *The Journal of Physical Chemistry Letters* **7**, 3259-3263 (2016).
10. M. B. Fichtl, J. Schumann, I. Kasatkin, N. Jacobsen, M. Behrens, R. Schlogl, M. Muhler, O. Hinrichsen, Counting of Oxygen Defects versus Metal Surface Sites in Methanol Synthesis Catalysts by Different Probe Molecules. *Angewandte Chemie International Edition* **53**, 7043-7047 (2014).
11. S. Kuld, C. Conradsen, P. G. Moses, I. Chorkendorff, J. Sehested, Quantification of Zinc Atoms in a Surface Alloy on Copper in an Industrial-Type Methanol Synthesis Catalyst. *Angewandte Chemie International Edition* **53**, 5941-5945 (2014).
12. F. Rouquerol, J. Rouquerol, K. Sing, in *Adsorption by Powders and Porous Solids,* F. Rouquerol, J. Rouquerol, K. Sing, Eds. (Academic Press, London, 1999), pp. 1-26.
13. P. A. Webb, Introduction to chemical adsorption analytical techniques and their applications to catalysis. *Micromeritics Instrument Corp. Technical Publications*, 1-12 (2003).
14. V. Rakić, L. Damjanović, *Temperature-Programmed Desorption (TPD) Methods. In: Auroux A. (eds) Calorimetry and Thermal Methods in Catalysis.* (Springer, Berlin, Heidelberg, 2013), vol. 154.
15. P. van der Heide, *X-ray Photoelectron Spectroscopy: An introduction to Principles and Practices*. (Wiley, 2011).
16. S. Hofmann, *Auger- and X-Ray Photoelectron Spectroscopy in Materials Science: A User-Oriented Guide*. Springer Series in Surface Sciences (Springer Berlin Heidelberg, 2012).
17. A. M. Venezia, X-ray photoelectron spectroscopy (XPS) for catalysts characterization. *Catalysis Today* **77**, 359-370 (2003).

18. B. J. Inkson, in *Materials Characterization Using Nondestructive Evaluation (NDE) Methods,* G. Hübschen, I. Altpeter, R. Tschuncky, H.-G. Herrmann, Eds. (Woodhead Publishing, 2016), pp. 17-43.
19. S. A. Kondrat, P. J. Miedziak, M. Douthwaite, G. L. Brett, T. E. Davies, D. J. Morgan, J. K. Edwards, D. W. Knight, C. J. Kiely, S. H. Taylor, Base-Free Oxidation of Glycerol Using Titania-Supported Trimetallic Au–Pd–Pt Nanoparticles. *ChemSusChem* **7**, 1326-1334 (2014).
20. P. L. Gai, E. D. Boyes, *Electron Microscopy in Heterogeneous Catalysis*. Series in Microscopy in Materials Science (CRC Press, 2003).

Chapter 3

Promoted Cu Catalysts Supported on ZrO_2 for the Hydrogenation of CO_2 to Methanol.

3.1 – Introduction

A wide range of Cu-based heterogeneous catalysts have been explored for the synthesis of MeOH from CO_2, these include: Cu/ZnO/ZrO_2,[1] Cu/CeO_2,[2] CuZnGa,[3] Cu-ZnO[4] and Pd-Cu/SiO_2.[5] ZrO_2 is a promising support for Cu catalysts because of its unique properties: high thermal and mechanical stability, high specific surface area, and amphoteric nature with acid sites to adsorb CO_2 and basic sites that facilitate the hydrogenation of intermediates.[6] Furthermore, ZrO_2 is less hydrophilic than Al_2O_3, which promotes water desorption, enhancing both the MeOH production rate and selectivity.[7]

Co-precipitation is the most common procedure for the synthesis of Cu-based catalysts for CO_2 hydrogenation to MeOH,[8-10] and is favoured over other synthetic procedures including; sol-gel,[11] impregnation[12] and citrate method[13] due to it being a well-established[14], rapid, and economic method that has shown homogeneity in component distribution, uses mild reaction temperatures, and results in uniform particle sizes with weakly agglomerated particles.[15] However, co-precipitation is susceptible to reproducibility issues, since it relies on the precise control of various experimental parameters such as temperature, pH, precursors concentration, and stirring speed, which all highly influence structural and catalytic properties of the final material.[9] On the contrary, the oxalate gel synthesis allows for the reproducible synthesis of small and well dispersed Cu particles. Jingfa *et al*.[16] prepared Cu/ZnO/Al_2O_3 catalysts following several methods for the CO_2 hydrogenation to MeOH, and they reported that catalysts prepared through the oxalate gel method showed higher MeOH productivities compared to catalysts prepared by conventional precipitation routes. Following on from this study, Deng *et al.*[17] demonstrated that highly active and selective Cu/ZnO/ZrO_2 catalysts can be synthesised using this method to achieve finer (12 nm) and more well dispersed particles. It was established that the choice of solvent has a significant impact on the structure of the precipitates, precursors, and catalysts, and subsequently led to different activities; the solvent with the smallest surface tension and largest viscosity (ethanol) was the most beneficial, giving finer particle sizes, as well as more uniformly distributed metal oxides crystallites; this is attributed to the fast nucleation and slow nucleus growth from the more viscous ethanol and reduced shrinkage in volume of the precipitates' structures upon drying. Similar findings were also observed by Koeppel *et al.*[18] where Cu/ZrO_2 catalysts

were prepared via several methods including ion exchange, impregnation, deposition precipitation, and co-precipitation. Precipitation routes were the most effective for active catalyst preparation, compared to the other methods, as they resulted in a high interfacial area between the microcrystalline copper particles stabilised interacting with the amorphous zirconia matrix. From the information above, it can be seen that catalyst synthesis through precipitation, particularly oxalate gel, is highly beneficial and worth further investigation; one such possibility is through the use of different catalyst supports, as outlined in this chapter.

Copper has been one of the most common elements used for the hydrogenation of CO_2 to methanol reaction as it is both active and, more importantly, abundant in comparison to other noble metals such as Pd and Pt that are also active for CO_2 hydrogenation.[19, 20] Although many new active catalyst formulations have been developed, such as Pd/In_2O_3,[21] GaPd/SiO_2[22] and Ni/β-Ga_2O_3,[23] they still carry the problem of incorporating harmful/expensive elements, making them less suitable for commercial use. Instead, the inclusion of such elements (as promoters) is a much better solution. The addition of various promoters/additives to the catalyst are very beneficial towards increasing Cu dispersion, modifying the acid-base and redox properties, and enhancing the catalytic performance and stability. Such promoters may be in the form of oxides, an example being the industrial catalyst with the use of ZnO behaving as both a structural (geometric spacer between Cu nanoparticles) and electronic promoter (via metal-support interactions) for Cu based catalysts;[24] other forms include noble metals such as Au and Pd, where their promotion effects have been linked to a hydrogen spillover mechanism, whereby the reducibility of Cu sites and re-oxidation of the Cu surface is suppressed .[25, 26]

The literature surrounding the synthesis of methanol from CO_2 hydrogenation has predominately been based on Cu catalysts, and this is due to its remarkable hydrogenation activity and abundance. Although the catalyst support is typically viewed as being inert and involved in the dispersion of the active phase, this is far from the truth; indeed, the support has been shown to play an active role during the reaction for various systems. In certain circumstances it can provide thermal stability to the active phase, prevent sintering of metal particles under high reaction temperatures, and can be useful in tuning the surface interaction between the active components of a catalyst, an example of this being the strong metal-support interaction (SMSI), where in some instances the formation of hetero-interfaces between the metal particle and a semiconducting (oxidic) thin layer modifies the electronic structure, resulting in a change in the adsorptive properties of the system.[27, 28]

The synergy between certain metals and oxides can induce large electronic changes in the metal,[29] provide novel active sites[30] or induce variations in the structure or phase of the supported metal particles, which consequently affects the bonding properties and correspondingly the catalytic

performance.[31] The nature of the Cu/ZnO synergy has been studied in much detail with a number of phenomena discussed, such as: the reversible change in morphology of the Cu particles, which is dependent on the reaction conditions i.e. wetting/non-wetting behaviour;[32] and the formation of novel active sites associated with a Cu-Zn surface alloy via the migration of ZnO_x species to the surface of Cu particles,[40] but this is still under debate. The importance of the Cu-ZnO interface in regards to the catalytic activity has been shown many times. For methanol synthesis catalysts, one of the key features is the specific Cu surface area (S_{Cu}), and typically a linear relationship is seen between the Cu surface area and activity; however, deviations from this trend have been observed and can be associated with the synergy effect described above.[33] The potential of intrinsic or synergistic effects, which are responsible for different specific activities of Cu, is not easily determined because surface and interface area are interrelated by morphology and microstructure.

For CO_2 hydrogenation the support is necessary for the binding of CO_2 and intermediates, and the nature of the oxide support, i.e. acidic and basic properties, are crucial towards changing the reaction environment on the catalyst surface. In addition, the reducibility of an oxide is important as having the presence of an oxygen vacancy allows stronger binding of CO_2, and therefore an increase in activity, which has been shown for a number of different supports including CeO_2, where the increased methanol selectivity is associated with the formation of monodentate/bidentate carbonates that form from the reaction of CO_2 with coordinatively unsaturated O^{2-} on CeO_2 in the presence of oxygen vacancies (V_0).[34] Graciani *et al*. presented detailed theoretical and experimental evidence of a new site for the activation of CO_2 in the form of carboxylate ($CO_2^{\delta-}$) at the copper–ceria interface. The rate of methanol production on CeO_x/Cu(111) was around 200 times greater than that on Cu(111), and about 14 times greater than that over traditional Cu/ZnO catalysts.[35]

A study by Kattel *et al.* looked at the use of bimetallic PtCo on various reducible supports including CeO_2, ZrO_2 and TiO_2, and revealed a remarkable difference in selectivity across the supports. The result has been attributed to both the different dominant reaction pathways and the role of the metal-oxide interface towards promoting the heterogeneity of the active sites. Unlike the binding of C-bound species, the binding of C,O-bound and O-bound species can be tuned selectively at the interface. Changing the support from TiO_2 to ZrO_2 did not affect the dominant RWGS and CO hydrogenation pathway; however, CO formation was hindered, and CH_4 was preferentially formed over ZrO_2.[36]

Other studies have also shown the benefits of using reducible supports like CeO_2 and ZrO_2 and reveal similar results as above with Cu. Wang *et al.* found that the selectivity of the catalyst can be tuned via the metal-support interaction, and by combining the structural characterisations with in-situ DRIFTS it was concluded that the changes in reaction adsorption intermediates ultimately affected the

distribution of the final products, mainly CO and CH_3OH. In order to improve on these results, the interaction of the Cu species with the support is essential as this will result in the formation of more Cu-support interfaces, which favour the binding and activation of CO_2, and greater concentration of oxygen vacancies that can strengthen CO_2 adsorption and stabilisation of key carbon intermediates by promoting the charge accumulation and redistribution.[34]

To gain a deeper understanding of the support effect for the hydrogenation of CO_2 to methanol, a variety of different supports were investigated. The supports differed by their acid-base properties and include MgO, MnO, La_2O_3, ZnO, ZrO_2, CeO_2 and Al_2O_3. As shown by Tagawa *et al.*, the choice of support can have a major influence on the catalytic performance through CO_2 adsorption on the Cu surface and hydrogenation of intermediates, they showed that: the use of a basic support led to an increase in the concentration of the formate intermediate on Cu and therefore an increase in activity; using an acidic support allowed an increase in methanol selectivity due to increased reactivity of the reaction intermediate but low activity; and furthermore by choosing an amphoteric support such as Al_2O_3 the combined effects mentioned above are observed resulting in even higher activity.[37]

Apart from varying the type of support, the addition of suitable promoters to the catalyst have been shown to be effective towards improving catalytic activity or stability. Palladium is a common dopant used for promoting higher MeOH rates during CO_2 hydrogenation. For example, Fujimoto *et al.* found that by doping a CuZnAl/SiO_2 catalyst with Pd, MeOH yield increased from 8.9 % to 11.2 % when assessed towards the CO_2 hydrogenation at (240 °C , CO_2/H_2 = 9, 15 bar, W/F = 5g-cat.h/mol). Moreover, higher stability was observed for the Pd-doped counterpart. The activity for the Cu-Zn-Al catalyst dropped remarkably in the presence of steam and high temperatures (260 °C) due to catalyst oxidation; however, no change in activity was observed in the Pd-doped catalyst. The higher MeOH productivity was attributed to Pd hydrogen spill-over to adjacent Cu centres, which promotes the reduction of Cu^{2+} to Cu^{+} active sites for methanol formation.[38] Sahibzada *et al.* compared the effect of Pd doping on commercial Cu/ZnO/Al_2O_3 catalysts, prepared via a two-stage precipitation, under industrially relevant conditions (5 MPa, 250 °C), Pd was added into the Cu-Zn-Al catalyst by impregnation or by physically mixing Pd/Al with CZA, and promotion effect was observed for both Pd-doping methods compared to CZA (14 mol h^{-1} g_{Cu}^{-1} at 4 % CO_2 conversion); CO_2 conversion increases by almost double from increasing Pd concentration (4 wt.% and 12 wt.%) for physically mixed catalysts, whilst a higher promotion effect (35%) was observed when (4 wt. %) Pd was impregnated (14 mol h^{-1} g_{Cu}^{-1}) but no further rise in activity was observed with increasing Pd concentration (12 wt.%). Again, the promotion effect of Pd was assigned to hydrogen spillover and the formation of Cu^{+} active sites. They also noted that the promotion effect was greater at higher flow rates (lower conversions).[39]

The addition of Pd not only promotes the formation of Cu^+ active sites, but it also alloys with Cu leading to active phases for MeOH production. For instance, Jiang and co-workers prepared a series of bimetallic Pd-Cu catalysts supported on amorphous and mesoporous silica. They concluded that the combination of Cu and Pd led to a strong synergistic promotion of CH_3OH formation rate compared to the monometallic equivalents when the Pd/(Pd + Cu) atomic ratios were within 0.25–0.34 for amorphous silica supported Pd–Cu catalysts. Furthermore, XRD analysis suggested that alloy formation, specifically PdCu and $PdCu_3$, are more favourable for methanol formation rather than CO formation.[5] From computational studies, it was concluded that the PdCu alloy was more active than the $PdCu_3$ alloy (based on (111) surface analysis); the higher activity of PdCu was attributed to under co-ordinated Pd atoms at the surface, which promoted both CO_2 and H_2 adsorption and activation. Overall, the Pd-Cu alloy structure has a major effect on the catalytic reaction pathway, and the presence of water can significantly influence the formation of CH_3OH from CO_2 hydrogenation through acceleration of the CO_2 conversion by reducing the kinetic barriers, altering the rate-limiting step and enhancing the TOF.[99, 40]

Hu *et al.* prepared a series of Pd-doped Cu/ZnO catalysts *via* a polyol method with a Cu:Pd molar ratio of 0.005, 0.01, 0.02, 0.03, and 0.04. When tested for the CO_2 hydrogenation (CO_2/H_2 – 1:3, 36 mL min^{-1}, 45 bar and 230 – 290 °C) a volcano plot between methanol yield and Pd loading was obtained, with 1 wt. % Pd at the top. 1 wt. % Pd-doped Cu/ZnO catalyst showed an increase in the methanol space time yield (STY) by a factor of 2.5, and an increase of MeOH turnover frequency (TOF) by a factor of 3.5, compared to Cu/ZnO. The increase in MeOH productivity that was observed with increasing Pd concentration up to 1 wt. % was attributed to hydrogen spill over; however, excess of Pd translated in a decrease in surface Cu area and concomitant loss of activity. [41]

As well as Pd, other noble metals such as Pt and Ag are often a prime choice as promoters or additions to a catalyst. Tada *et al*. examined the effect of Ag as a promoter for Cu/ZrO_2 catalysts, by varying the loading from 0 – 5 wt %, and they found a monotonical increase in methanol selectivity from 39 % (Cu/ZrO_2) to 65 % (5 wt% $Ag/Cu/ZrO_2$). It was also noted that a strong synergy between the Cu and Ag, most likely through the formation of an alloy, contributes towards the differences in intrinsic activity between the promoted and unpromoted catalyst.[42] Zeng *et al.* prepared atomically dispersed Pt/MoS_2 catalysts with a Pt loading up to 7.5%, although not at promoter levels, they reported that the synergetic interaction between neighbouring Pt monomers reduces the activation energy and enhances the catalytic activity relative to isolated Pt monomers in CO_2 hydrogenation.[43] Other non-noble metal additions have also been investigated for CO_2 hydrogenation to MeOH, these include Ni and Ce; Frei and co-workers studied the in-depth promotion of Indium catalysts with Ni; interestingly, up to 10 wt% Ni resulted in the formation of $InNi_3$ patches along the oxide surface and this led to higher catalyst stability, increased methanol productivity and suppressed methane formation compared to

pure In_2O_3.[44] Gao *et al.* investigated the use of various rare earth metals, including ceria, as a promoter for Cu/Zn/Al catalysts and discovered that incorporating these promoters led to higher BET surface areas, Cu surface area, and Cu dispersion, and subsequently greater methanol productivity than the pure Cu/Zn/Al catalysts.[45] Seeing the benefits of introducing Pt, Ag, Ni and Ce to a catalyst it was decided that their addition as promoters would be investigated for Cu/ZrO_2.

The work detailed in this chapter aims to explore various supported Cu catalysts prepared via the oxalate gel synthesis method, with a particular focus on Cu/ZrO_2, towards the conversion of CO_2 to MeOH. The role of various promoters (Pd, Pt, Ce, Ni and Ag) and the stability of these catalysts is also investigated.

3.2 – Results and Discussion

3.2.1 – Effect of Support on Cu Catalysts Synthesised by Oxalate Gel Precipitation

As described previously, the support employed not only serves as a material where Cu nanoparticles are deposited but it also plays an important role in modifying the catalysts properties.[46] Hence, the first aim of this chapter was to prepare and study Cu catalysts on several supports (ZrO_2, Al_2O_3, ZnO, MgO, La_2O_3, CeO_2 and MnO) and study their catalytic activity for CO_2 hydrogenation to MeOH. Catalysts were prepared following the oxalate gel methodology described in the experimental section (Chapter 2, Section 2.3). The Cu loading for all the catalysts were fixed at 31 wt. % to allow comparison between the different supports; after preparation, catalysts were dried in static air at 500 °C for 2 h, 10 °C min^{-1}. Prior to reaction, catalysts were pelleted (425–600 µm), and 0.5 g of pelleted catalyst was secured with quartz wool in the reactor tube and pre-reduced *in-situ* with 5 % H_2/He (220 °C, 1 h, 2 °C min^{-1}). After reduction, the reactor was allowed to cool to 50 °C, the gas flow was switched from 5 % H_2/He to the reaction mixture (20 % CO_2, 60 % H_2, 20 % N_2) and was pressurised to 20 bar at a flow rate of 30 ml min^{-1}. Catalyst activity was assessed between 150 and 250 °C, for a total of 50 h.

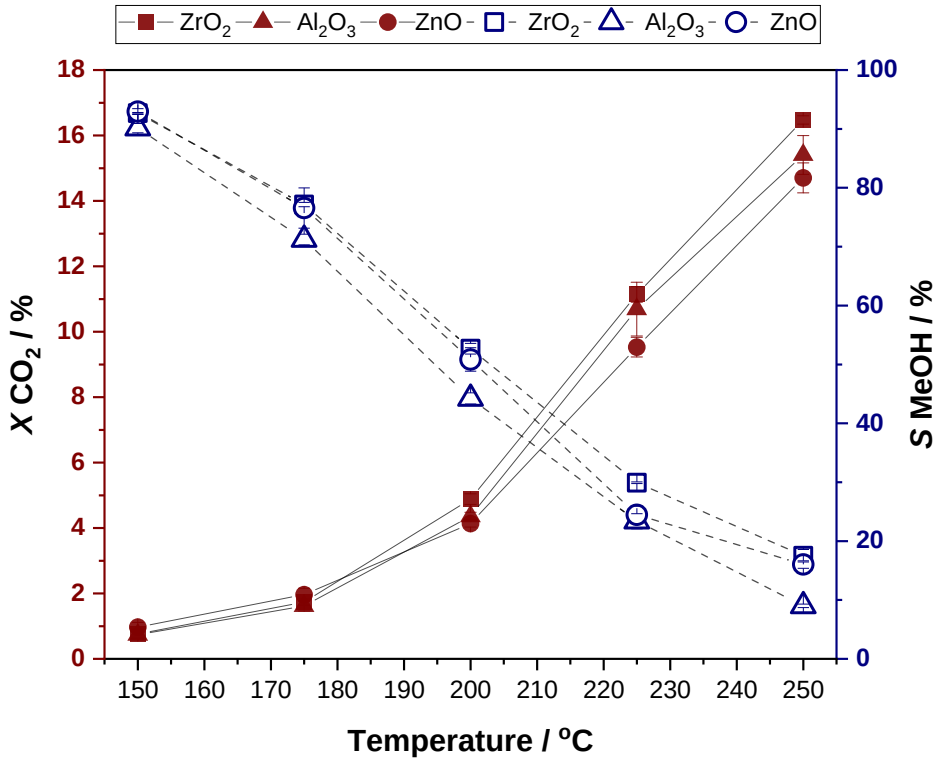

Figure. 3.1a - CO_2 conversion (left-red filled symbols) and methanol selectivity (right-blue open symbols) for Cu/ZrO_2, Cu/Al_2O_3 and Cu/ZnO catalysts. ***In-situ* reduction conditions**; 1 h at 220 °C in 5% H_2/He (2 °C min^{-1}, 1 bar, 30 ml min^{-1} STP). **Reaction conditions:** 150 - 250 °C, 10 h dwells (total = 50 h), 30 ml min^{-1} (STP) of CO_2 : N_2 : H_2 (1:1:3), P(total) = 20 bar.

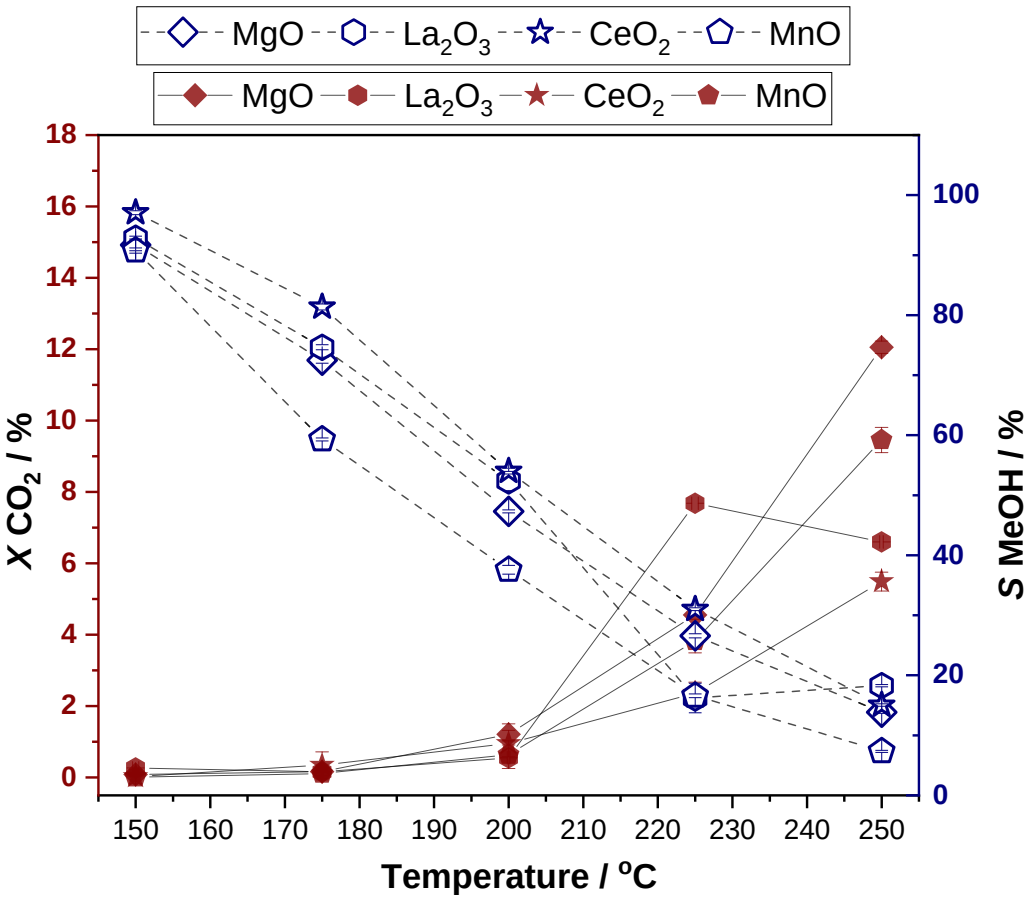

Figure. 3.1b - CO_2 conversion (left-red filled symbols) and methanol selectivity (right-blue open symbols) for Cu/MgO, Cu/La_2O_3, Cu/CeO_2, and Cu/MnO catalysts. ***In-situ* reduction conditions**; 1 h at 220 °C in 5%H_2/He (2 °C min^{-1}, 1 bar, 30 ml min^{-1} STP). **Reaction conditions:** 150 - 250 °C, 10 h dwells (total = 50 h), 30 ml min^{-1} (STP) of CO_2 : N_2 : H_2 (1:1:3), P(total) = 20 bar.

Energy input is necessary for the activation of CO_2,[47] which is observed by the low CO_2 conversion (< 1 %) at low temperature for all catalysts (Figure 3.1). Increasing reaction temperature leads to an increase in the CO_2 conversion; however, this is at the expense of MeOH selectivity. The decrease in MeOH selectivity is explained by the reaction thermodynamics (Equation 3.1); MeOH synthesis is favoured at low temperature and high pressure,[48] whilst CO formation via reverse water gas shift (RWGS) is favoured at high temperatures (Equation 3.2). No other products (e.g., CH_4 or DME, which can originate from CO_2 methanation or MeOH dehydration, respectively) were detected.

(Eq. 3.1) $CO_2 + 3H_2 \rightleftharpoons CH_3OH + H_2O$ $\Delta H_{25°C} = -49.5$ KJ mol^{-1}

(Eq. 3.2) $CO_2 + H_2 \rightleftharpoons CO + H_2O$ $\Delta H_{25°C} = 41.2$ kJ mol^{-1}

The catalysts can be divided into two catalytic trends: the first group are Cu/ZnO, Cu/ZrO_2 and Cu/Al_2O_3 (Figure 3.1a) and the second group are Cu/MgO, Cu/La_2O_3, Cu/CeO_2 and Cu/MnO (Figure 3.1b). Despite the variation in the supports used, there is little difference between the catalysts; the error bars show a good reproducibility between all the catalysts measured. The first group of catalysts (Cu-ZrO_2, Cu-Al_2O_3 and Cu-ZnO) show slightly higher activity compared to the other supports, and the MeOH selectivity falls within the same range across the temperatures, with the largest errors seen at the lowest temperatures and conversions. Al_2O_3, ZnO and ZrO_2 follow a similar trend for CO_2 conversion and MeOH selectivity up to 200 °C; at higher temperatures, the supports can be differentiated by their individual activity. At 250 °C CO_2 conversion for Cu/Al_2O_3 and Cu/ZnO was 15.4 and 14.7 %, respectively, whilst MeOH selectivity was 9.0 and 16.0 %. In comparison, the Cu/ZrO_2 catalyst achieved the highest conversion (16.4 %) and MeOH selectivity (17.5 %) at 250°C.

Figure 3.1b shows CO_2 conversion and MeOH selectivity for the second group of catalysts (Cu/MgO, Cu/La_2O_3, Cu/CeO_2 and Cu/MnO). This group shows less activity and selectivity than the previous group of catalysts, with very low conversion observed below 200 °C. Cu-La_2O_3 shows a rapid increase in CO_2 conversion from 0.5 % to 7.7 % when the reaction temperature is increased from 200 °C to 225 °C; however, the CO_2 conversion suddenly drops at a higher temperature, which might be associated with catalyst deactivation. The remaining supports show a steady increase in CO_2 conversion above 200 °C. Similar MeOH selectivity was observed for this group of catalysts; however, clear differences in CO_2 conversion where detected. The results most likely reflect a change in the basicity of the supports, where an increase in basicity results in an in higher CO_2 uptake and stronger adsorption of CO_2.[49]

A comparison of the CO_2 conversion and MeOH selectivity between all the supports is shown in Figure 3.2. As discussed above, there is a noticeable difference between the two sets of supports, although all supports show near identical selectivity at the start with small changes over the course of the reaction. Differences between the conversion become apparent, with the maximum conversion of 12% for the second set of supports (MgO) and 16% for the first set of catalysts (ZrO_2).

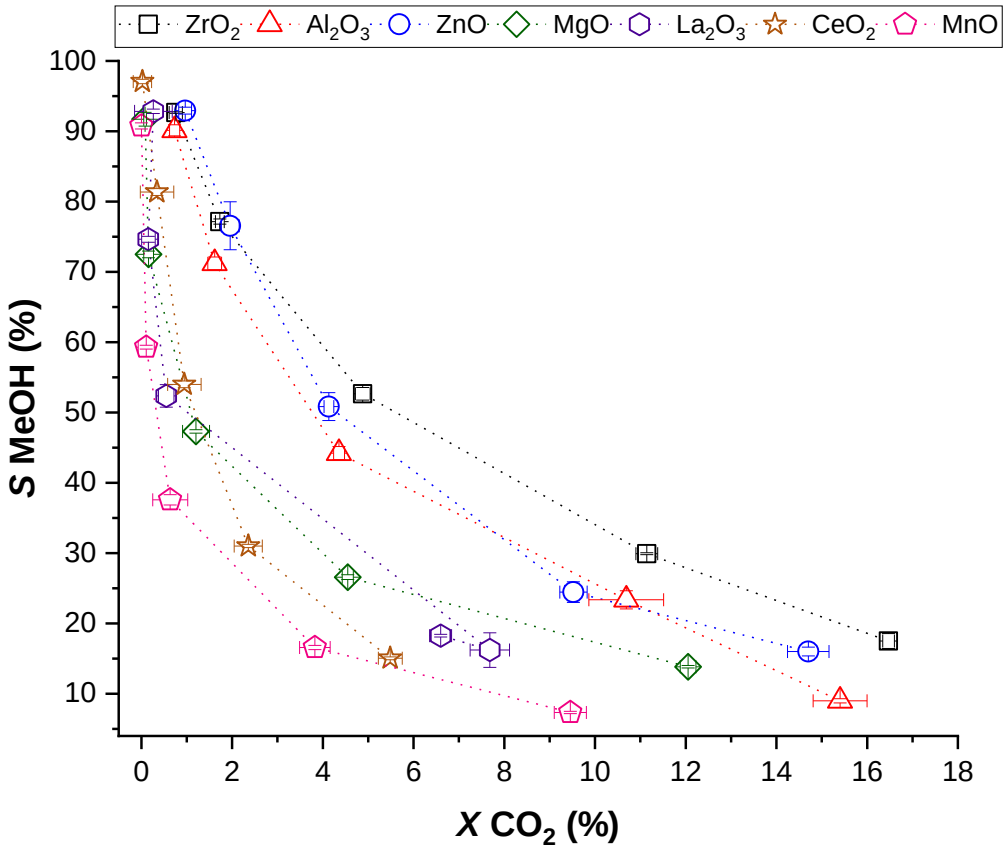

Figure. 3.2 - Methanol selectivity and CO_2 conversion for Cu/ZrO_2, Cu/Al_2O_3, Cu/ZnO, Cu/MgO, Cu/La_2O_3, Cu/CeO_2, and Cu/MnO catalysts. ***In-situ* reduction conditions**; 1 h at 220 °C in 5% H_2/He (2 °C min^{-1}, 1 bar, 30 ml min^{-1} STP). **Reaction conditions:** 150 - 250 °C, 10 h dwells (total = 50 h), 30 ml min^{-1} (STP) of CO_2 : N_2 : H_2 (1:1:3), P(total) = 20 bar.

The MeOH and CO productivities for the supported Cu catalysts at 250 °C are shown in Table 3.1. Of the supports tested, ZrO_2 achieved the highest MeOH productivity of 811 $mmol_{MeOH}Kg_{cat}^{-1}h^{-1}$, and MnO attained the lowest MeOH productivity of 215 $mmol_{MeOH}Kg_{cat}^{-1}h^{-1}$. ZnO is also a suitable support and the most comparable with ZrO_2 with regards to the methanol and CO productivity. These results support existing literature where the promoting effects of ZnO and ZrO_2 have been verified; the active sites in conventional Cu-ZnO catalysts are said to be a mixture of partial or completely reduced Cu,[50] with a strong synergistic contact with ZnO or partially reduced ZnO_x.[51, 52] The presence of ZnO has been argued to contribute in a number of ways including; increased number of active sites by favouring the dispersion of reduced Cu, stabilising Cu^+ sites on the surface and reducibility of Cu^{2+} species and catalysing the hydrogenation of carbon oxides via close contact between the basic sites available on ZnO and various Cu species.[53-55] In addition, the role of ZrO_2 in Cu based catalysts has also been emphasised, where its addition can tune the dissociation of H_2 and subsequent spillover of atomic hydrogen,[56-58] alter reaction pathways,[59] increase the metal dispersion and surface area, and enhance

the binding of key intermediates for further conversion,[60-62] as well as modifying key surface properties (e.g., basicity and defect concentration).[63, 64] The benefits listed above explain why the majority of mixed catalysts used for methanol production are based on ZnO and ZrO_2 in conjunction with Al_2O_3.

Table 3.1: *Activity of supported Cu catalysts at 250 °C.*

Catalyst	*X* CO_2 %	*S* MeOH %	*S* CO %	MeOH Productivity ($mmol_{MeOH}kg_{cat}^{-1}h^{-1}$)	CO Productivity ($mmol_{CO}kg_{cat}^{-1}h^{-1}$)
Cu/ZnO	14.7	16.0	83.8	717	3753
Cu/ZrO_2	16.5	17.5	82.2	811	3802
Cu/Al_2O_3	15.4	9.0	91.0	408	4133
Cu/MgO	12.1	13.8	86.2	501	3119
Cu/MnO	9.5	7.3	92.7	215	2716
Cu/La_2O_3	6.6	18.3	81.7	421	1884
Cu/CeO_2	5.5	15.0	84.9	252	1422

As mentioned previously, the study by Tagawa *et al.* shows that the choice of support can have a major influence on the catalytic performance through CO_2 adsorption on the Cu surface and hydrogenation of intermediates. A range of supports were tested in their work; these include MgO (basic), SiO_2-Al_2O_3 and Al_2O_3 (acidic), SiO_2 (neutral) and TiO_2 and ZrO_2 (amphoteric). They showed that the use of a strong basic support (MgO) led to a destabilisation of the formate species preventing hydrogenation to MeOH and instead an increase in CO concentration via the RWGS reaction; similar findings were shown for the neutral support (SiO_2) where the surface concentration of formate was small. Using an acidic support allowed an increase in methanol selectivity due to increased reactivity of the reaction intermediate; however, the acidic nature prevented the adsorption of CO_2 and consequently the conversion was low. Furthermore, by choosing an amphoteric support such as TiO_2 one can take advantage of both the basic sites to adsorb CO_2 to form the formate species and the acid sites to activate the formate species for hydrogenation to form methanol via a methoxy species. Differences between the amphoteric supports can be attributed to the increased concentration of formate and ease of hydrogenation to the methoxy species.[37] The results discussed in the literature above reflect the trends observed in Table 3.1, with the first group of catalysts (amphoteric) being the most active, and the more neutral and basic supports being the less active towards CO_2 hydrogenation to methanol.

The physiochemical properties of the supported Cu catalysts (Table 3.2) were also characterised in order to investigate their influence on the catalytic activity observed above. The XRD data is shown in Figure 3.3.

Table 3.2: *Physiochemical properties of supported Cu catalysts.*

Catalyst	BET Surface area (m^2/g)	Cu Surface area (m^2/g)	CuO particle size (nm)*
Cu/ZnO	18	10	21
Cu/ZrO_2	57	11	10
Cu/Al_2O_3	55	25	8
Cu/MgO	74	23	5
Cu/MnO	37	27	20
Cu/La_2O_3	22	10	15
Cu/CeO_2	35	20	13

**Calculated via Scherrer equation for CuO ($\bar{1}11$) at 35.5°*

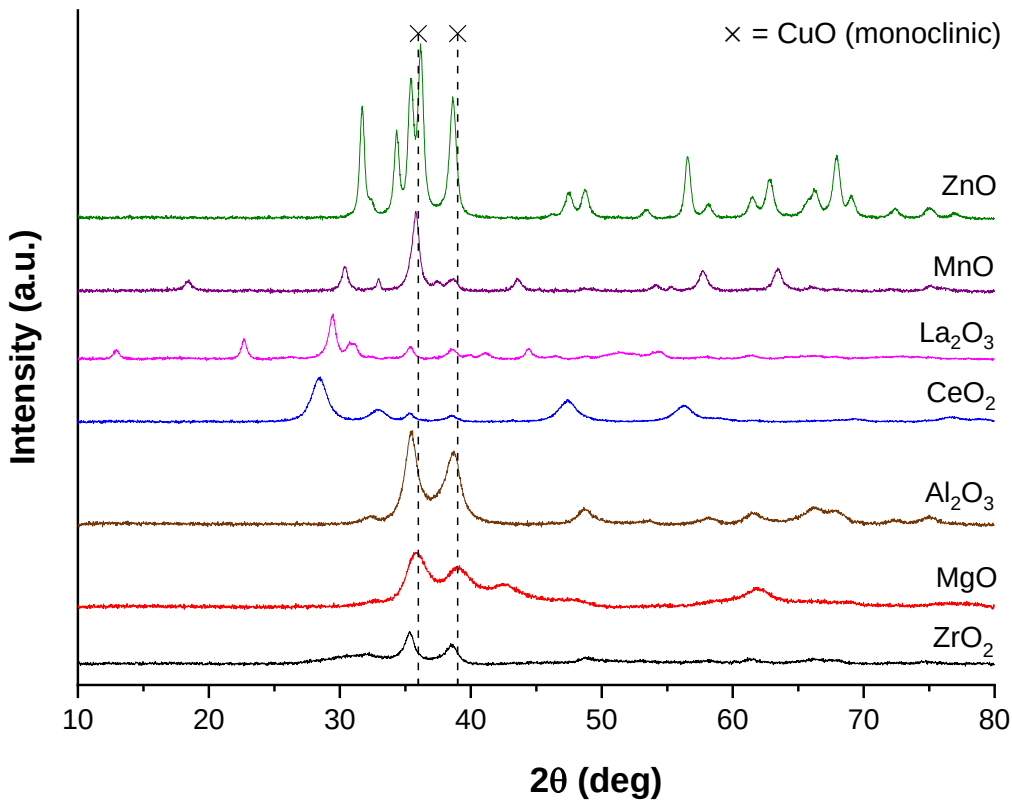

Figure 3.3 - XRD patterns for calcined supported Cu catalysts, the CuO (monoclinic) regions have been highlighted.

The XRD patterns above show the major peaks for CuO (monoclinic) at 2θ = 36°and 39° for all the calcined catalysts, these however, vary in intensity and peak width suggesting a large variation in the CuO particle sizes between the supports. The reflections for the individual supports, particularly ZrO_2, include peaks in close proximity to the CuO peaks (*t*-ZrO_2 = 31.5°). The variety is also reflected by the values calculated using the Scherrer equation CuO ($\bar{1}11$) at 35.5°; the first group of catalysts show some of the largest CuO particle sizes, with ZnO measuring 21 nm compared to the second group of catalysts such as MgO, giving a CuO particle size of 5 nm. The relationship between the overall surface area of the catalysts and the metal particle size and surface area are illustrated in Figure 3.4. Looking at the overall surface area of the supports, there is no specific trend in relation to the CuO particle size and Cu surface area; however, a fairly linear trend, with the exception of MnO, is established between the total surface area and CuO particle size, where an increase in the surface area shows a decrease in the size of the metal particles. Comparing with the specific Cu surface area, no clear trend is shown; despite ZrO_2 and ZnO belonging to the group of the most active supports, the specific metal surface areas are significantly lower compared to the other supports. This suggests that an increase in Cu surface area does not correlate with an increase in methanol activity as discussed previously.

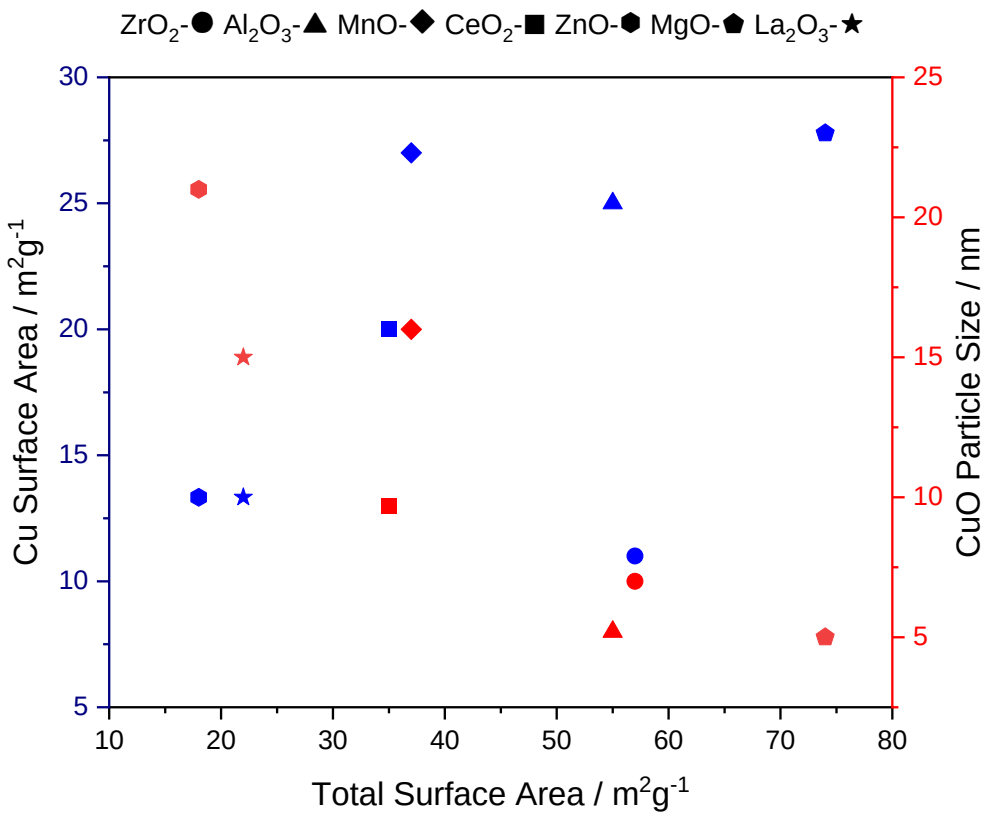

Figure. 3.4 – Total surface area of supported Cu catalysts vs Cu surface area (blue symbols) and CuO particle size (red symbols).

3.2.3 – Pd Promoted Cu/ZrO_2 Catalysts

As the Cu/ZrO_2 catalyst showed promising results, with reasonable methanol productivities and CO_2 conversion compared to the other supports tested, it was decided that the catalyst would be optimised further through the addition of various promotors including Pd. The addition of Pd to the catalyst is beneficial as it can modify the structure and surface electronic properties, which will subsequently affect the stability of intermediates and transition states and thus alter the reaction path and modulate the selectivity. It is also crucial towards hydrogen activation and maintaining the Cu particles in a reduced state, by acting as the dissociation sites for H_2 and serving as an exit route for H_2 via inverse spillover during the desorption process, and therefore suppressing the re-oxidation of the Cu surface via a hydrogen spillover mechanism.

Based on the promoting effect of Pd-doping observed on several Cu-based catalysts for the CO_2 hydrogenation to MeOH,[25, 39, 65] a series of Pd-doped Cu/ZrO_2 catalysts (Pd:Cu molar ratio – 1 : 0.005, 1 : 0.01, 1 : 0.02 and 1 : 0.03) were prepared through the oxalate gel method. For the preparation of Pd-doped Cu/ZrO_2 catalysts via oxalate gel, the desired amount of $Pd(NO_3)_2$ was added simultaneously with $Cu(NO_3)_2$ and $Zr(NO_3)_2$ precursors and precipitated with oxalic acid to induce its precipitation; further details of the synthetic process can be found in the experimental section (Chapter 2, Section 2.3). Catalysts are named as Pd(0.005)Cu/ZrO_2, Pd(0.01)Cu/ZrO_2, Pd(0.02)Cu/ZrO_2 and Pd(0.03)Cu/ZrO_2 following the order of Pd:Cu molar ratios listed above. Prior to reaction (150 – 250 °C, $CO_2/H_2/N_2$ – 1:3:1, 30 ml/min, 20 bar and total 50 h) catalysts were calcined, pelleted, and pre-reduced as described previously.

As observed in Figure 3.5, no significant promoting effect in terms of greater CO_2 conversion or improved MeOH selectivity was observed for Pd-promoted Cu/ZrO_2 catalysts compared to Cu/ZrO_2. Slight differences observed between the catalysts fall within the experimental error with signs of deactivation observed for both Pd(0.02)Cu/ZrO_2 and Pd(0.03)Cu/ZrO_2 over the temperature range studied. Pd(0.005)Cu/ZrO_2 and Pd(0.01)Cu/ZrO_2 show a slight increase in CO_2 conversion in comparison to Cu/ZrO_2, which is more apparent at 225°C where Cu/ZrO_2 achieves a conversion of 11% and Pd(0.005)Cu/ZrO_2 and Pd(0.01)Cu/ZrO_2 achieve a conversion of 13%; despite this difference, a decrease in methanol selectivity is also observed for these catalysts meaning any changes observed are within error and are not correlated to the addition of a promoter.

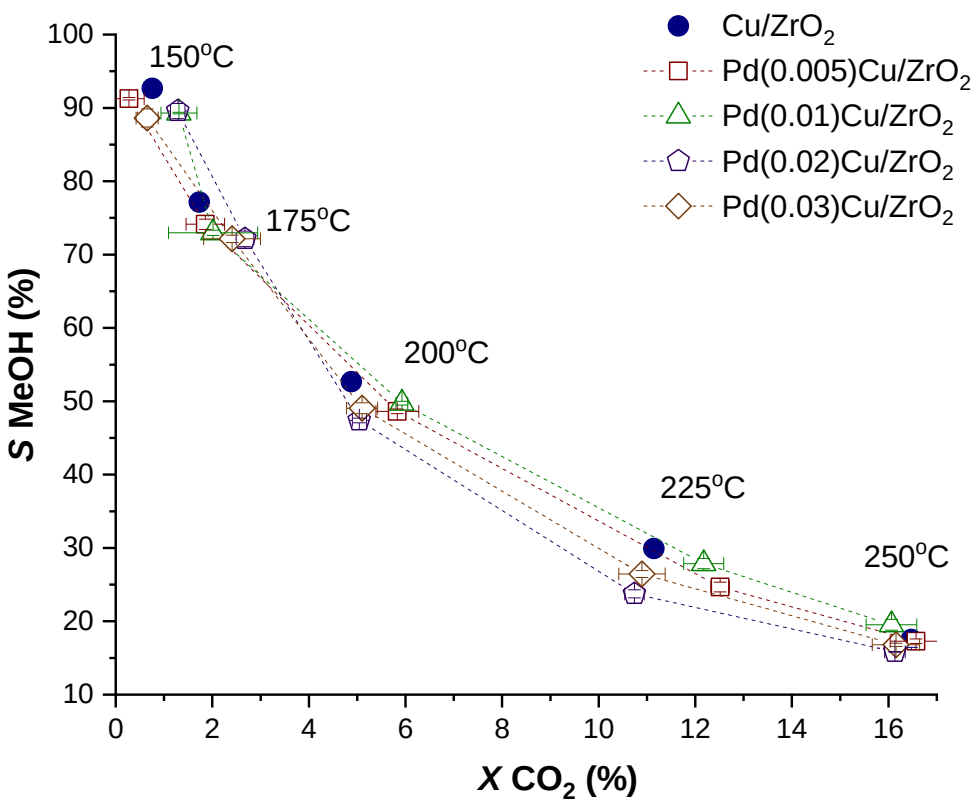

Figure 3.5 - Activity of $CuZrO_2$ - Pd promoted catalysts (Cu:Pd = 1 : 0.005 – 1 : 0.03) vs unpromoted Cu/ZrO_2 . *In-situ* reduction conditions; 1 h at 220°C in 5% H_2/He (2°C min^{-1}, 1 bar, 30 ml min^{-1} STP). Reaction conditions: 150 - 250°C, 10 h dwells (total = 50 h), 30 ml min^{-1} (STP) of CO_2 : N_2 : H_2 (1:1:3)(GHSV = 3,333 h^{-1}), P(total) = 20 bar.

One hypothesis to explain the lack of promoting effect is the low concentration of Pd on the surface of the catalyst, and therefore limited interaction between the Pd and Cu species. Instead, Pd may be more concentrated in the bulk of the material and hence unable to perform H_2 spillover. One method to determine the concentration of species on the surface is XPS, as shown in Figure 3.7. Catalyst specific surface area was determined by N_2 adsorption (BET), while Cu surface area was determined by N_2O adsorption. BET surface area and Cu surface area are shown in Table 3.3. BET surface area seems to greatly increase with the addition of Pd from 57 m^2 g^{-1} for Cu/ZrO_2 to 82 m^2 g^{-1} for $Pd(0.03)Cu/ZrO_2$, suggesting the addition of the promoter during the oxalate gel method and subsequent calcination alters the porosity and catalyst structure. The same trend was observed for Cu surface area, which increased from 11.0 for Cu/ZrO_2 to 11.6 for $Pd(0.03)Cu/ZrO_2$ with increasing Pd loading. According to previous reports, higher Cu surface area would most likely have translated into higher activity; However, this was not reflected in our catalytic data. Based on results observed by Kapteijn[(66)] and Pachatouridou[(67)], we can conclude that Pd is active for N_2O decomposition even in small quantities, with the rate of decomposition reflected by an increase in metal loading, and hence, in this case N_2O pulse titration is not a reliable technique to quantify the Cu surface area. In addition to Pd contributing

to the associated errors for the Cu surface area, Hinrichsen *et al.* found that N_2O titration was indicative of both Cu surface area and oxygen defects present at the copper-zinc interface.[10] Moreover, Muhler and co-workers reported that N_2O titration catalysts are prone to significant structural changes, which might lead to errors in the Cu surface area determination.[68] In our case, N_2O titration was not conclusive to elucidate whether higher Cu surface area observed with increasing Pd concentration is related to surface Pd or to higher BET catalyst surface area. Nevertheless, it seems that neither the BET surface area nor the Cu surface area significantly affects the catalytic activity for MeOH formation.

Table 3.3: *Physiochemical properties of Pd promoted catalysts and Cu/ZrO_2.*

Catalyst	Cu:Pd molar ratio	BET Surface area (m^2/g)	*Cu Surface area (m^2/g)
Cu/ZrO_2	-	57	11.0
Pd (0.005)Cu/ZrO_2	1 : 0.005	63	5.7
Pd (0.01)Cu/ZrO_2	1 : 0.01	65	8.6
Pd (0.02)Cu/ZrO_2	1 : 0.02	79	7.4
Pd (0.03)Cu/ZrO_2	1 : 0.03	82	11.6

**Pd (0) also catalytically active for N_2O decomposition.*

Phase differences between Pd-promoted catalysts were studied by XRD (Figure 3.6). The XRD pattern recorded for Cu/ZrO_2 shows characteristic peaks of monoclinic CuO at 36°, 39° and 49° corresponding to ($\bar{1}11$), (111) and ($\bar{2}02$) planes (PDF ref. 01-089-5896) and tetragonal zirconia (t-ZrO_2) at 31.5° and 61° for (101) and (211) planes (PDF ref. 01-078-3194). Peaks corresponding to both crystallite phases, CuO and t-ZrO_2, were broad and with low intensity, this indicates that the crystallites sizes were fairly small and that some amorphous material might be present. The addition of Pd seems to not affect the crystallite size of CuO and the peaks for the t-ZrO_2 phases are almost identical. No additional crystalline phases were observed for Pd-doped Cu/ZrO_2 catalysts, moreover, no Pd, PdO, CuPd or Cu_3Pd were detected, with the exception of Pd(0.03)Cu/ZrO_2 catalyst, were the formation of PdO is observed as a very low intensity peak at 34° and 43°. The XRD results indicate that Pd is either well dispersed throughout the material or smaller than the XRD detection limit (clusters smaller than 2 nm).

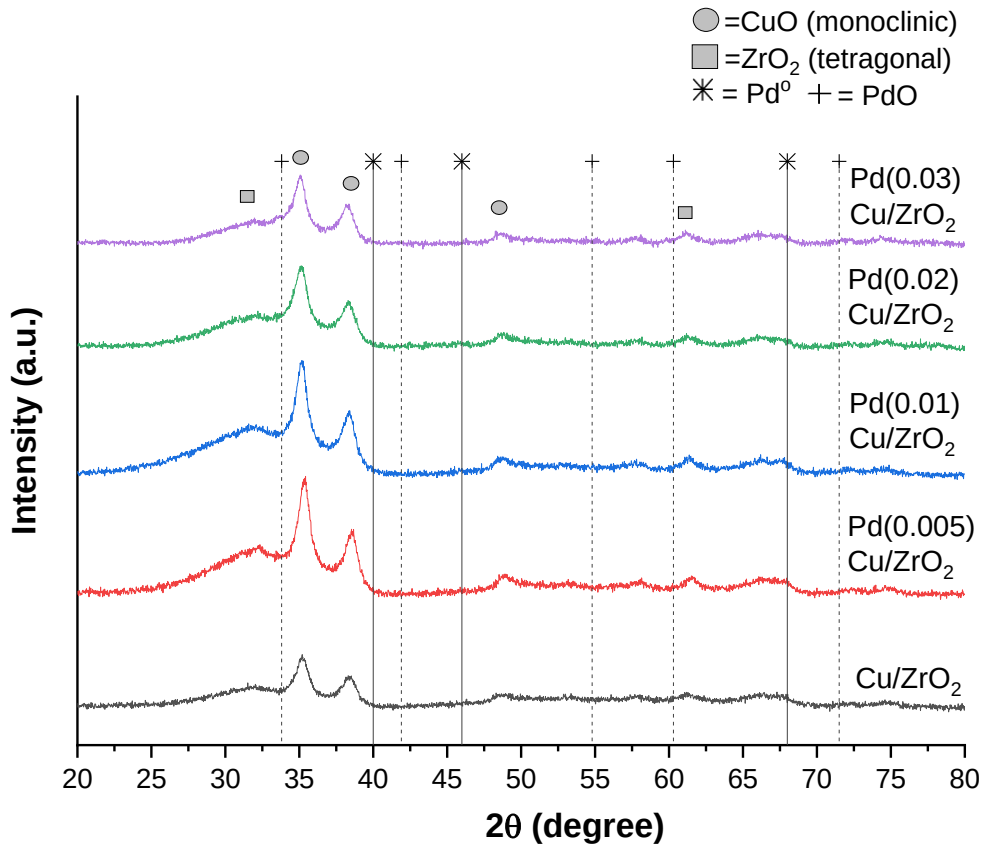

Figure 3.6 - XRD patterns for Cu/ZrO_2 catalyst and series of Pd promoted catalysts in the range Cu : Pd molar ratio (1 : 0.005 – 1 : 0.03.)

XPS analysis was carried out on the samples in order to determine the quantity of surface Pd and any changes in oxidation state. The XPS data (Figure. 3.7) reveals changes in the Pd peaks between the different catalysts. Metallic Pd is reported to have a binding energy (BE) *ca*. 335 eV,[69] and the upward shift observed in the Pd peaks indicates the presence of PdO rather than Pd^0. Due to the overlap of Pd and Zr $3p_{3/2}$, atomic percentages of the Pd were calculated from fits taken from bulk materials. The calculated concentrations of surface Pd, shown in Table 3.4, were significantly lower than expected, which can arise from Pd being present as large particles (poor dispersion) or the Pd being present within the bulk of the support or metal present (Cu). From the XRD data, it is most likely that the majority of the promoter remains trapped within the bulk of the support or present as a dilute alloy with Cu where it is unavailable for reaction. Hence, little change in activity is observed between the promoted catalysts compared to the unpromoted Cu/ZrO_2 catalyst.

Table 3.4: *Summary of XPS data for Pd regions on Pd promoted catalysts.*

Catalyst	BINDING ENERGY (eV) Pd $3d_{3/2}$	BINDING ENERGY (eV) Pd $3d_{5/2}$	Total Atomic Percentage
Pd 1 (0.22 nominal wt% Pd)	341.5	336.2	1.9
Pd 2 (0.43 nominal wt% Pd)	341.4	336.1	2.3
Pd 3 (0.86 nominal wt% Pd)	341.4	336.1	0
Pd 4 (1.30 nominal wt% Pd)	342.0	336.7	2.8

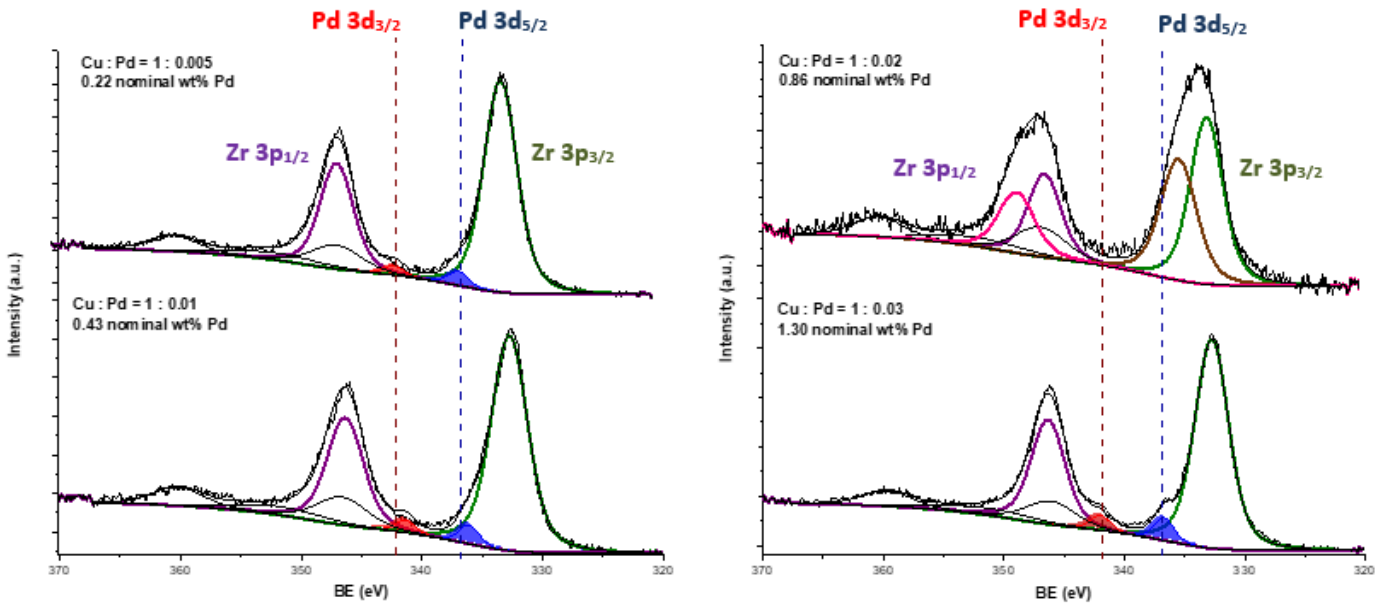

Figure. 3.7 - XPS Spectra for Initial Cu/ZrO_2 catalysts prepared via oxalate gel with the addition of Pd promoters in the range Cu : Pd molar ratio (1 : 0.005 – 1 : 0.04). The Pd $3d_{5/2}$ and Pd $3d_{3/2}$ have been highlighted.

Based on our XRD results, it can be suggested that co-precipitation of $Pd(NO_3)_2$, $Cu(NO_3)_2$ and $Zr(NO_3)_2$ via oxalate gel led to well dispersed materials, broad and low intense CuO and t-ZrO_2 peaks were observed while no Pd related peaks were detected. Moreover, XPS characterisation suggests that Pd in homogeneously distributed throughout the material, and hence most of it is placed in the bulk of the material unable to significantly enhance MeOH rates via hydrogen spillover. This conclusion agrees with results observed by Melián-Cabrera *et al.*, where it was shown that the precipitation order for catalyst synthesis has a remarkable influence on the properties of the active phases and, consequently, on the catalytic performance for the hydrogenation of CO_2 to methanol (P = 60 bar, CO_2/H_2 = 3, and T = 180–240 °C.) An enhanced methanol yield at 240 °C was observed for the Pd based Cu-ZnO catalyst prepared via sequential precipitation (11 mol MeOH/(h kg_{Cat})) compared to the reference CuO-ZnO (9 mol MeOH/(h kg_{Cat})) and this was attributed to a synergistic effect of Pd on the active Cu sites, which facilitated the H_2-spillover mechanism. The catalyst prepared via co-precipitation resulted in very low methanol yields, almost inactive, compared to the reference Cu-ZnO catalyst which was due to significant changes in the bulk and surface properties of the catalyst: large CuO particle sizes, very low copper surface area, difficulty in CuO reduction, and greater instability towards sintering.[65, 70]

3.2.4 – Additional Promoters for Cu/ZrO₂

As shown in the previous section, the simultaneous co-precipitation of $Pd(NO_3)_2$, $Cu(NO_3)_2$ and $Zr(NO_3)_4$ during the oxalate gel synthesis resulted in a homogenous distribution of the three elements throughout the material and hence most of the Pd was not at the surface of the catalyst where required, resulting in no promoting effect. To concentrate promoters at the surface of the catalyst, Cu/ZrO_2 was prepared though the standard oxalate method, followed by promoter (Pd, Pt, Ag, Ni or Ce) post-impregnation, this is described in Section 2.21.

All promoted catalysts were prepared with a Cu to promoter molar ratio of 1:0.01. Prior to reaction, catalysts were dried (110 °C, 4 h), pelleted (425–600 µm) and pre-reduced *in situ* in 5% H_2/He (2 °C min^{-1}, 1 bar, 30 ml min^{-1}). CO_2 hydrogenation was assessed at 225 C, 20 bar, 18 h, 30 ml min^{-1}, 20 % CO_2, 60 % H_2, 20 % N_2.

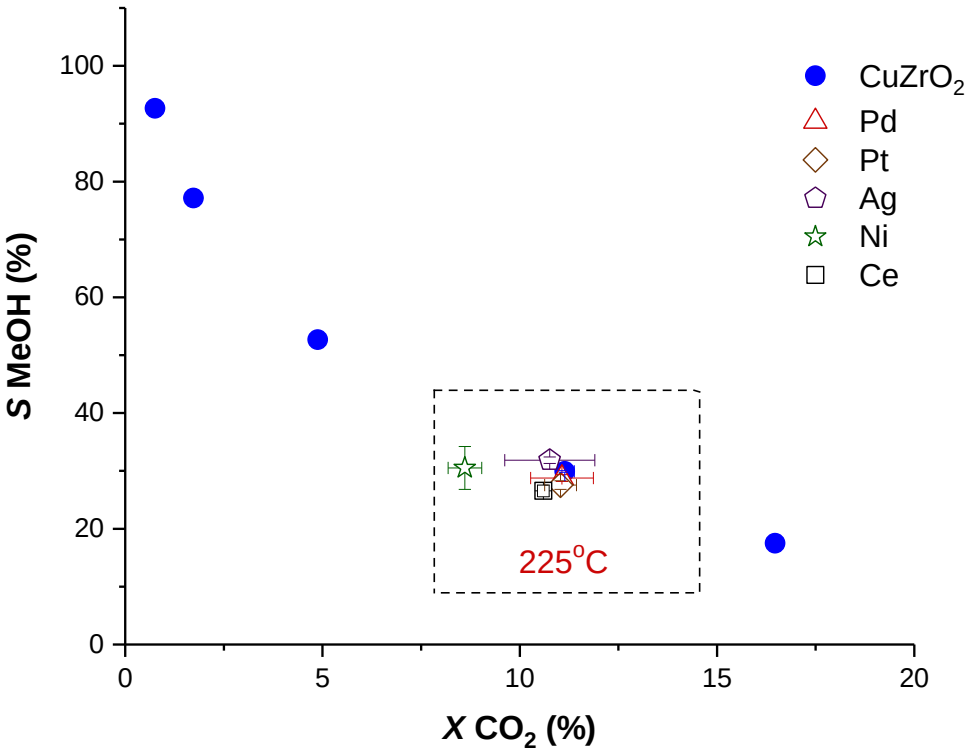

Figure 3.8- Activity of Cu/ZrO_2 catalyst vs various promoters at a Cu:X molar ratio of 1:0.01. ***In-situ* reduction conditions**; 1 h at 220 °C in 5% H_2/He (2 °C min^{-1}, 1 bar, 30 ml min^{-1} STP). **Reaction conditions:** Isothermal test at 225 °C, 18 h dwell, 30 ml min^{-1} (STP) of CO_2 : N_2 : H_2 (1:1:3), P(total) = 20 bar.

As observed in Figure 3.8, no significant differences in CO_2 conversion or MeOH selectivity were observed between promoted and unpromoted Cu/ZrO_2 catalysts, with the exception of the $NiCu/ZrO_2$ which performs slightly worse, with lower CO_2 conversion (8.6 %) compared to Cu/ZrO_2 (11.1 %). When comparing MeOH productivity (Figure 3.9), it seems that the additions of Pd, Pt, Ag, Ni or Ce have a poisoning effect rather than a promoting one. The highest MeOH productivity of 890 mmol $kg_{MeOH}^{-1}h^{-1}$ was recorded for Cu/ZrO_2 catalyst, and addition of a metal at low loadings seems to result in a lack of interaction between the active Cu sites, leading to lower MeOH productivity. The lowest MeOH productivity, observed for Ni-promoted Cu/ZrO_2 catalyst, can be attributed to a lower CO_2 conversion (8.7%) and slightly higher formation of CH_4 when compared with the other promoted catalysts, as shown in Table 3.5. Of the promoted catalysts tested, Pd and Pt resulted in the highest CO productivities, and the addition of Ag to Cu/ZrO_2 allows for an increase in DME and MeOH productivity at similar CO_2 conversions with a decrease in CO productivity.

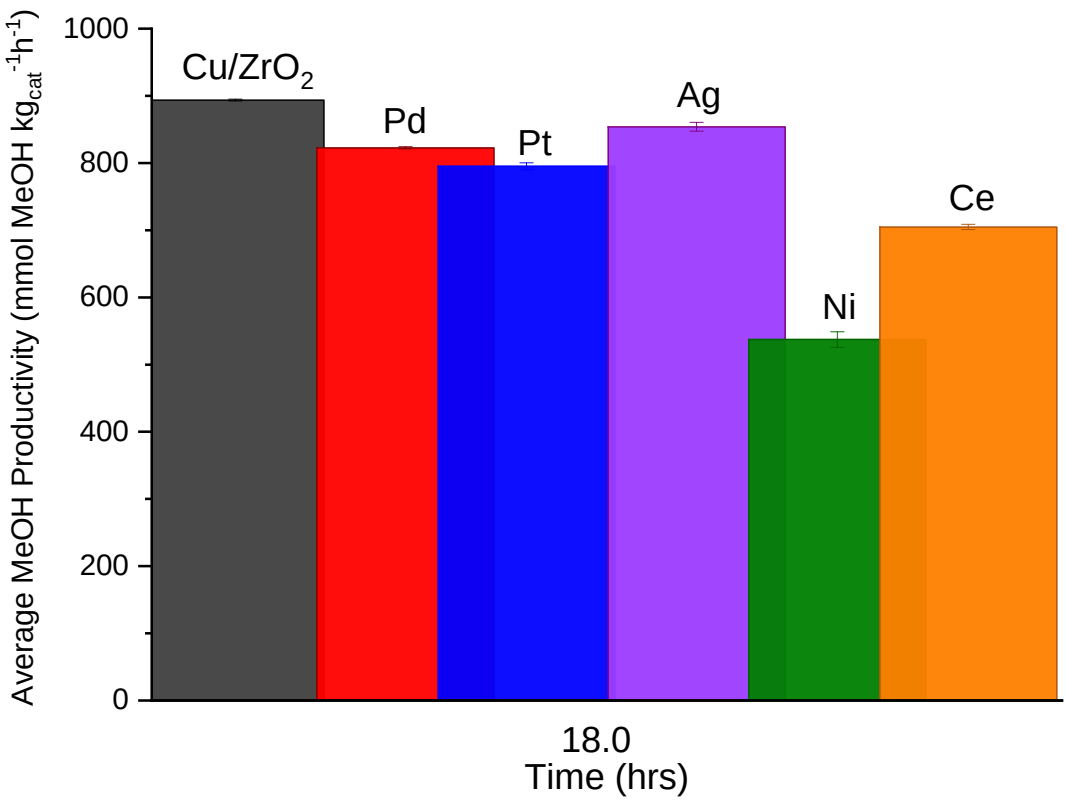

Figure 3.9 – Methanol productivity data of Cu/ZrO_2 catalyst vs various promoters at a Cu:X molar ratio of 1:0.01. ***In-situ* reduction conditions**; 1 h at 220 °C in 5% H_2/He (2 °C min^{-1}, 1 bar, 30 ml min^{-1} STP). **Reaction conditions:** Isothermal test at 225 °C, 18 h dwell, 30 ml min^{-1} (STP) of CO_2 : N_2 : H_2 (1:1:3), P(total) = 20 bar.

Table 3.5: *productivity data for post-impregnation Cu/ZrO_2 promoted catalysts at 225 °C. Promoters at a Cu:X molar ratio of 1:0.01.*

Catalyst	*X* CO_2 %	MeOH Productivity ($mmol_{MeOH}kg_{cat}^{-1}h^{-1}$)	DME Productivity ($mmol_{DME}kg_{cat}^{-1}h^{-1}$)	CH_4 Productivity ($mmol_{CO}kg_{cat}^{-1}h^{-1}$)	CO Productivity ($mmol_{CO}kg_{cat}^{-1}h^{-1}$)
Cu/ZrO_2	11.13	881	2.59	0.08	2059
Cu/ZrO_2 - Pd	10.60	822	1.91	0.09	2052
Cu/ZrO_2 - Pt	11.10	795	2.23	0.09	2054
Cu/ZrO_2 - Ag	10.67	854	2.39	0.09	1844
Cu/ZrO_2 - Ni	8.70	537	1.78	0.13	1474
Cu/ZrO_2 - Ce	10.59	705	1.90	0.08	1979

3.2.5 – Catalyst Stability & Comparison between Cu/ZrO_2 and CZA catalysts

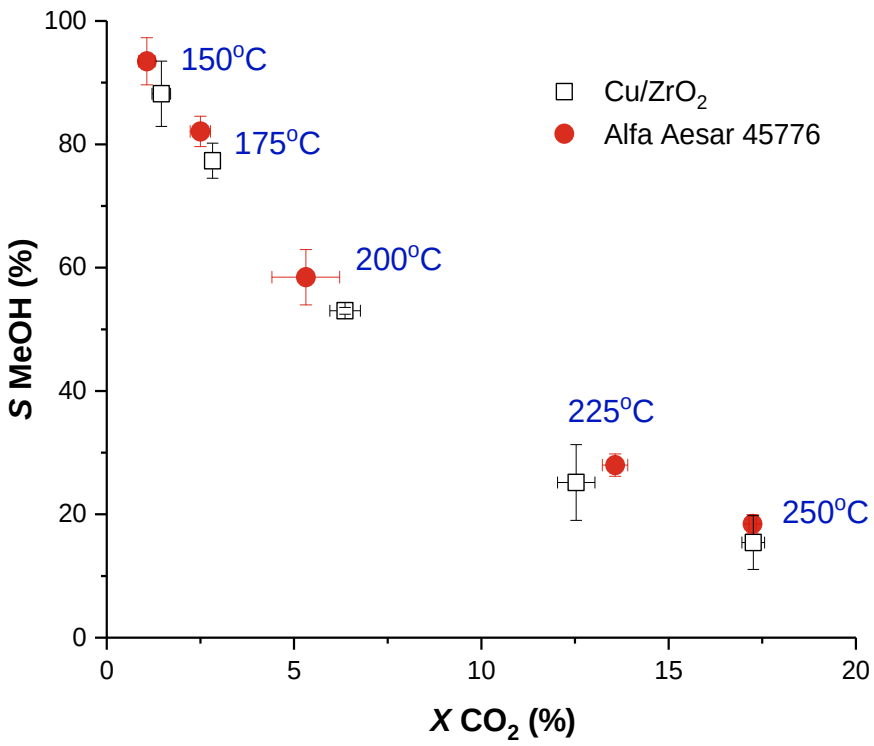

Figure. 3.10 – *MeOH selectivity and CO_2 conversion of Cu/ZrO_2 catalyst vs Commercial Alfa Aesar catalyst.* ***In-situ*** **reduction conditions**; 1 h at 220 °C in 5% H_2/He (2 °C min^{-1}, 1 bar, 30 ml min^{-1} STP). **Reaction conditions:** 150 - 250 °C, 9 h dwells (total = 45 h), 30 ml min^{-1} (STP) of CO_2 : N_2 : H_2 (1:1:3)(GHSV = 3,333 h^{-1}), P(total) = 20 bar.

Once it was determined that the use of ZrO_2 as a support gave the best catalytic results, among a series of other supports (Section 3.2.1) employed for the synthesis of Cu-containing catalysts prepared via oxalate gel, we wanted to compare the Cu/ZrO_2 to a benchmark methanol synthesis CZA catalyst (Alfa Aesar, 45776). Catalysts were tested as previously described.

As observed in Figure 3.10, Cu/ZrO_2 prepared by the oxalate gel method presents comparable CO_2 conversion and MeOH selectivity to the commercial $Cu/ZnO/Al_2O_3$ (CZA) catalyst over the temperature range studied, with an initial selectivity of 88% at 150 °C which then drops to 15.4% at 250 °C for Cu/ZrO_2 and a selectivity change of 93% to 18.4% for the commercial catalyst. A similar trend is seen for the conversion with Cu/ZrO_2, increasing from 1.5 to 17.3% and the commercial catalyst increasing from 1.1 to 17.2%. Moreover, the trend line reflects an equilibrium limit where a decrease in methanol selectivity and an increase in CO_2 conversion are seen as the temperature is increased.

As important as CO_2 conversion and MeOH selectivity are when selecting an active catalyst, so is the catalyst stability. There are several pathways in which a solid catalyst can decay and they can be grouped into six intrinsic mechanisms. These include vapour formation; vapour-solid and/or solid-solid interactions; attrition/crushing; poisoning, which is the strong chemisorption (may be reversible) of reactants, products or impurities in the feed onto sites otherwise available for catalysis, and can potentially induce changes in the electronic or geometric structure;[71] fouling – the physical (mechanical) deposition of species from the fluid phase onto the catalyst surface, which results in activity loss due to blockage of sites and/or pores (e.g. coke and carbon deposition in porous catalysts); and thermal degradation and sintering – thermally induced deactivation of catalysts that results from sintering, which is the loss of catalytic surface area due to crystallite growth of the catalytic phase and loss of support area due to support collapse, which normally occurs at higher temperatures (> 500 °C) and are generally accelerated by the presence of water vapour. Understanding of these pathways allows for further optimisation of catalyst design and improved reaction conditions and thus increases the longevity of the catalyst during the process.[72]

In an industrial process catalysts are expected to remain stable under reaction conditions for as long as two years.[73 74] For example, in a methanol synthesis plant from a syngas feedstock ($CO+CO_2+H_2$), typical conditions adopted are 200–320 °C and 5–10 MPa, and variations in the synthesis gas phase composition have shown a close correlation between activity loss and loss of Cu surface area, suggesting that an important cause of deactivation is sintering, which may be promoted by over-reduction of Cu.[75] Studies have also indicated that when CO_2 is used as the feed, severe deactivation on Cu-based catalysts occur.[76] One of the major contributors to deactivation is the formation of water;

notably, one third of the H_2 is consumed to produce water, which is significantly wasteful compared to the commercial methanol production via synthesis gas.[77] Water is known to behave as a strong oxidant at elevated temperatures; under these conditions, the water oxidises the active Cu^0 to the less active $Cu^{2+}$and thus reduces the number of active sites available for reaction. Wu *et al.* found that water produced during methanol synthesis from a CO_2-rich feed (CO_2 (22%), CO (3%), H_2 (75%)) accelerated the crystallization of Cu and ZnO in a $Cu/ZnO/ZrO_2/Al_2O_3$ catalyst, and led to the deactivation of the catalyst; they also showed that the addition of colloidal silica to the catalyst greatly improved the catalyst stability by suppressing the crystallization of Cu and ZnO.[78] Li *et al.* demonstrated that a Zr doped Cu-Zn-Zr-Al catalyst enhanced the stability for CO_2 hydrogenation by promoting the reduction of CuO, formed from the oxidation of Cu by water, in the presence of H_2.[79]

The addition of CO into the gas feed, or gas recirculation, can improve the lifetime of Cu- based catalysts for the CO_2 hydrogenation to MeOH; however, we investigated catalysts stability using a 20 % CO_2, 60 % H_2 and 20 % N_2 gas feed. The stability of Cu/ZrO_2 and the benchmark CZA catalysts was assessed at a reaction flow of 30 ml min^{-1} and 20 bar pressure, 150 – 350 °C and total reaction time of 100 hrs. (Figure 3.11.)

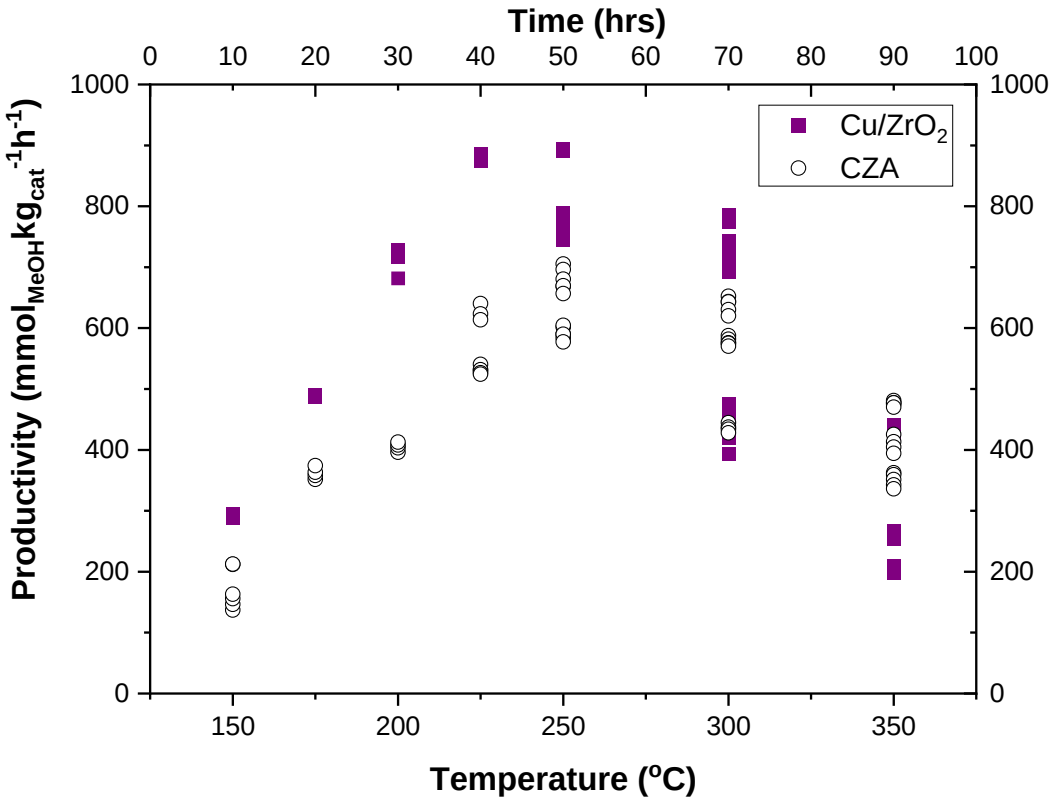

Figure 3.11 – Methanol productivity data over 100 hrs. for Cu/ZrO_2 and commercial $Cu/ZnO/Al_2O_3$ (CZA) catalysts. ***In-situ* reduction conditions**; 1 h at 220 °C in 5% H_2/He (2 °C min^{-1}, 1 bar, 30 ml min^{-1} STP). **Reaction conditions:** temperature ramp study 150-225 °C, 10 hr dwell, 2° C/min (total 40 hrs) then 250, 300 and 350 °C, 20 hr dwell, 2 °C/min (total 60 hrs); 30 ml min^{-1} (STP) of CO_2 : N_2 : H_2 (1:1:3), P(total) = 20 bar.

Figure 3.11 above shows an increase in methanol productivity for both catalysts from 150 °C – 250 °C, with Cu/ZrO_2 achieving a maximum productivity of 894 $mmol_{MeOH}kg_{cat}^{-1}h^{-1}$, compared with 705 $mmol_{MeOH}kg_{cat}^{-1}h^{-1}$ for the commercial catalyst. After 50 hrs, the productivity decreases for both catalysts, particularly for the Cu/ZrO_2 catalyst, which shows a drop in productivity of 78%, as the temperature increases up to 350 °C. However, when comparing the methanol selectivity and CO_2 conversion in Figure 3.12 (below), the catalysts remain fairly stable.

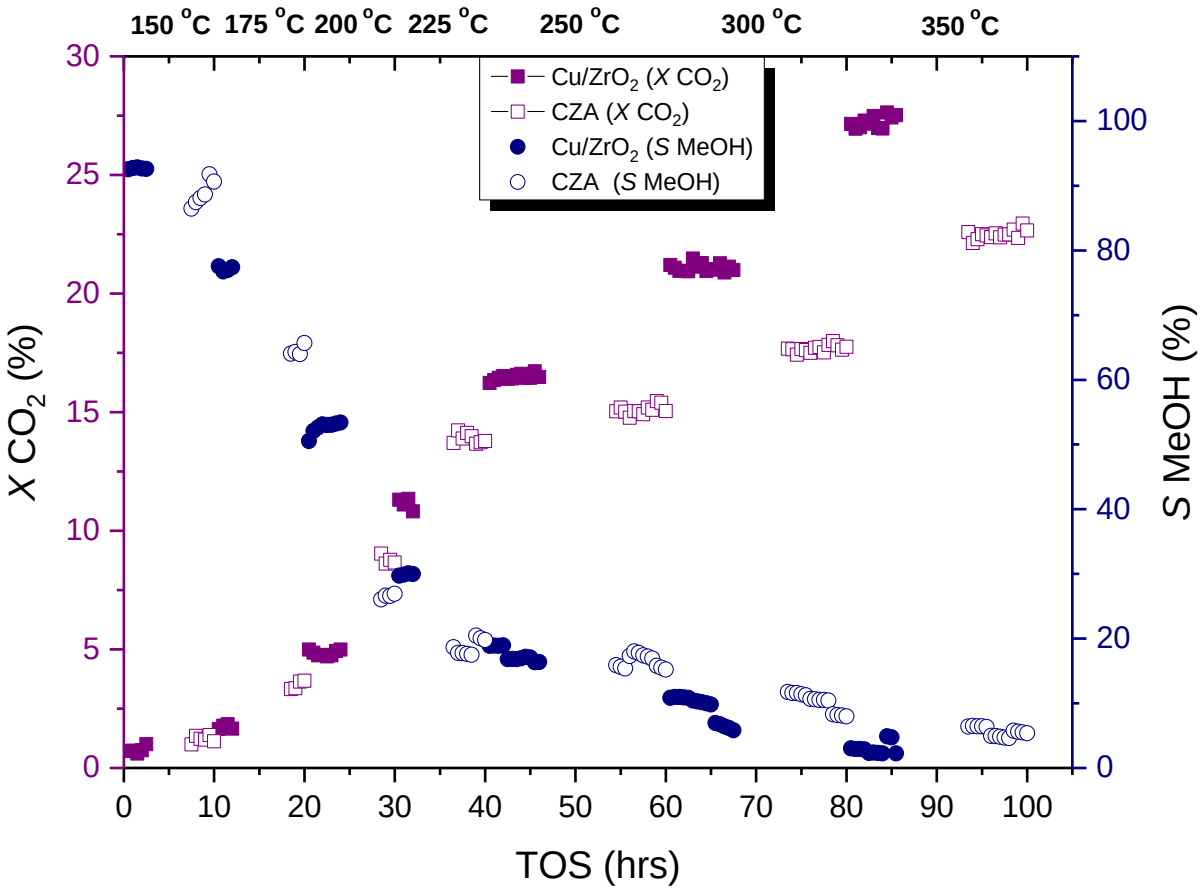

Figure 3.12 – Methanol selectivity and CO_2 conversion data over 100 hrs for Cu/ZrO_2 and commercial $Cu/ZnO/Al_2O_3$ (CZA) catalysts. ***In-situ* reduction conditions**; 1 h at 220 °C in 5% H_2/He (2 °C min^{-1}, 1 bar, 30 ml min^{-1} STP). **Reaction conditions:** temperature ramp study 150-225 °C, 10 hr dwell, 2 °C/min (total 40 hrs) then 250, 300 and 350 °C, 20 hr dwell, 2 °C/min (total 60 hrs); 30 ml min^{-1} (STP) of CO_2 : N_2 : H_2 (1:1:3), P(total) = 20 bar.

As expected, an increase in CO_2 conversion and decrease in methanol selectivity is observed with increasing temperature, however there is a dramatic decrease in methanol selectivity for both catalysts as the temperature increases above 175 °C, the initial selectivity for both catalysts are around 90% and this falls to less than 5% by the end of the study. The methanol selectivity drops at a faster rate for the CZA catalyst compared to the Cu/ZrO_2 catalyst up until the reaction reaches 250°C after 40 hrs, where both catalysts achieve 18% methanol selectivity. The conversion and selectivity data across the

temperature range studied remains stable within the dwelling periods. The CZA catalyst shows a higher CO_2 conversion (9 %) than the Cu/ZrO_2 catalyst (5 %) after 30 hrs of reaction where the temperature reaches 200 °C; after increasing the temperature to 250 °C (50 hrs) the opposite is observed, and this difference is further increased as the reaction proceeds until the end (100 hrs) where there is a difference of 5% between the catalysts.

The significant change in CO_2 conversion and MeOH selectivity of the catalysts with increasing temperature can be associated with the increase in Cu particle size i.e., sintering as you approach higher temperatures, accompanied by the formation of water both from the reaction and the RWGS reaction leading to increased oxidation and deactivation of active sites.

Kurtz and co-workers conducted a rapid aging test where a selection of catalysts (Cu/ZnO, Cu/Al_2O_3 and Cu/ZnO/Al_2O_3) were tested under a 50 Nml min^{-1} flow of synthesis gas (14% He, 72% H_2, 4% CO_2, and 10% CO) and the temperature was gradually increased from 200 °C to 500 °C, with 50 °C increments and held for 8 h at each temperature, over a total of 125 hours. They concluded that the ZnO containing catalyst, that exhibited a pronounced deactivation behaviour compared to the other catalysts, was due to thermal sintering of the Cu crystallites. The addition of Al_2O_3 was beneficial as a structural promoter and inhibited the thermal sintering of the Cu crystallites.[80] Spencer and Twigg also found that copper containing catalysts are susceptible to thermal sintering via a surface migration process, particularly at temperatures above 300 °C, and this is markedly accelerated by the presence of even traces of chloride.[81] Additional stabilisers and promoters such as alumina, alkaline earth oxides and other oxides were shown to play a number of important roles, including the inhibition of sintering and absorption of catalyst poisons.[82] These findings suggest that attention to catalyst design, particularly with the addition of promoters or oxides, can prove highly beneficial towards the stability of the catalyst; furthermore, control of other parameters such as the gas composition, temperature, and especially water removal are necessary to enhance the catalyst lifetime. One suggestion to alleviate H_2O-induced catalyst sintering as well as increasing methanol selectivity and reducing the overall energy consumption is to optimise reactor design.

3.3 – Conclusions

Synthesis of catalysts for CO_2 hydrogenation to methanol via an oxalate gel precipitation method has been shown to be successful and reproducible. Comparing the activity of a number of supported Cu catalysts (Cu/ZnO, Cu/ZrO_2, Cu/Al_2O_3, Cu/MgO, Cu/La_2O_3, Cu/CeO_2 and Cu/MnO) shows the influence the supports have on the catalyst. Ultimately, a change in the basicity or acidity of the supports results in changes to the catalyst performance most likely associated with changes to the intermediate species during the reaction, as reported in previous studies. Amphoteric supports were the most successful due to availability of basic sites to adsorb CO_2 and acid sites to activate formate species; ZrO_2 achieved the highest MeOH productivity of 811 $mmol_{MeOH}kg_{cat}^{-1}h^{-1}$ of all the supports tested.

Addition of Pd to Cu/ZrO_2 catalysts at promoter levels (0.2 – 1.3 wt%) via the oxalate gel method proved unsuccessful, with no increase in methanol productivity, which is attributed to the homogeneous distribution of the Pd species within the bulk of the catalyst as opposed to the surface where it would be required for hydrogen spillover.

Addition of various promoters (Pd, Pt, Ag, Ni and Ce) to the Cu/ZrO_2 catalyst via post impregnation increased the concentration of surface metal species; however, no significant differences in CO_2 conversion or MeOH selectivity were observed between promoted and unpromoted Cu/ZrO_2 catalysts, with the exception of the NiCu/ZrO_2 with lower CO_2 conversion and higher methane selectivity. The lack of promotion effect observed for the promoted catalysts is likely due to the low metal loadings and proximity to the active Cu sites.

Cu/ZrO_2 prepared by the oxalate gel method presents comparable CO_2 conversion and MeOH selectivity to the commercial Cu/ZnO/Al_2O_3 (CZA) catalyst over 150 – 250 °C. Comparing the stability of the catalysts over 100 hrs and increasing the temperature range from 150 – 350 °C, both Cu/ZrO_2 and the CZA catalyst remain fairly stable over time, but both catalysts show significant changes in CO_2 conversion and MeOH selectivity after 250 °C (total 60 hrs). The changes observed in the catalysts can be associated with an increase in Cu particle size i.e., sintering as you approach higher temperatures, accompanied by the formation of water from the RWGS reaction leading to increased oxidation and deactivation of active sites.

Recommendations for future work include; post-reaction characterization, particularly XRD, to determine the level of sintering and XPS to investigate any changes in surface oxidation. Also, the measurement of catalyst support basicity and acidity via CO_2 and NH_3-TPD.

3.4 – References

1. X. Dong, F. Li, N. Zhao, F. Xiao, J. Wang, Y. Tan, CO_2 hydrogenation to methanol over Cu/ZnO/ZrO_2 catalysts prepared by precipitation-reduction method. *Applied Catalysis B: Environmental* **191**, 8-17 (2016).
2. P. Sripada, J. Kimpton, A. Barlow, T. Williams, S. Kandasamy, S. Bhattacharya, Investigating the dynamic structural changes on Cu/CeO_2 catalysts observed during CO_2 hydrogenation. *Journal of Catalysis* **381**, 415-426 (2020).
3. W. Cai, P. R. de la Piscina, J. Toyir, N. Homs, CO_2 hydrogenation to methanol over CuZnGa catalysts prepared using microwave-assisted methods. *Catalysis Today* **242**, 193-199 (2015).
4. C. Tisseraud, C. Comminges, A. Habrioux, S. Pronier, Y. Pouilloux, A. Le Valant, Cu-ZnO catalysts for CO_2 hydrogenation to methanol: Morphology change induced by ZnO lixiviation and its impact on the active phase formation. *Molecular Catalysis* **446**, 98-105 (2018).
5. X. Jiang, N. Koizumi, X. Guo, C. Song, Bimetallic Pd–Cu catalysts for selective CO_2 hydrogenation to methanol. *Applied Catalysis B: Environmental* **170-171**, 173-185 (2015).
6. N. Nomura, T. Tagawa, S. Goto, Effect of acid-base properties on copper catalysts for hydrogenation of carbon dioxide. *Reaction Kinetics and Catalysis Letters* **63**, 21-25 (1998).
7. J. Wambach, A. Baiker, A. Wokaun, CO_2 Hydrogenation over Metal/zirconia Catalysts. *Phys. Chem. Chem. Phys.* **1**, 5071 (1999).
8. S.-i. Fujita, S. Moribe, Y. Kanamori, M. Kakudate, N. Takezawa, Preparation of a coprecipitated Cu/ZnO catalyst for the methanol synthesis from CO_2 — effects of the calcination and reduction conditions on the catalytic performance. *Applied Catalysis A: General* **207**, 121-128 (2001).
9. E. Frei, A. Schaadt, T. Ludwig, H. Hillebrecht, I. Krossing, The Influence of the Precipitation/Ageing Temperature on a Cu/ZnO/ZrO_2 Catalyst for Methanol Synthesis from H_2 and CO_2. *ChemCatChem* **6**, 1721 (2014).
10. C. Baltes, S. Vukojević, F. Schüth, Correlations between synthesis, precursor, and catalyst structure and activity of a large set of CuO/ZnO/Al_2O_3 catalysts for methanol synthesis. *Journal of Catalysis* **258**, 334-344 (2008).
11. L. Angelo, Study of $CuZnMO_x$ Oxides (M = Al, Zr, Ce, CeZr) for the Catalytic Hydrogenation of CO_2 into Methanol. *C. R. Chim.* **18**, 250 (2015).
12. K. K. Bando, K. Sayama, H. Kusama, K. Okabe, H. Arakawa, In-situ FT-IR study on CO_2 hydrogenation over Cu catalysts supported on SiO_2, Al_2O_3, and TiO_2. *Applied Catalysis A: General* **165**, 391-409 (1997).
13. A. Karelovic, A. Bargibant, C. Fernández, P. Ruiz, Effect of the structural and morphological properties of Cu/ZnO catalysts prepared by citrate method on their activity toward methanol synthesis from CO_2 and H_2 under mild reaction conditions. *Catalysis Today* **197**, 109-118 (2012).
14. K. y. Shimomura, K. Ogawa, M. Oba, Y. Kotera, Copper oxide-zinc oxide-alumina catalyst: The structure of a copper oxide-zinc oxide-alumina catalyst for methanol synthesis. *Journal of Catalysis* **52**, 191-205 (1978).
15. G. J. Hutchings, J. C. Védrine, in *Basic Principles in Applied Catalysis,* M. Baerns, Ed. (Springer Berlin Heidelberg, Berlin, Heidelberg, 2004), pp. 215-258.
16. D. Jingfa, S. Qi, Z. Yulong, C. Songying, W. Dong, A novel process for preparation of a Cu/ZnO/Al_2O_3 ultrafine catalyst for methanol synthesis from CO_2 + H_2: comparison of various preparation methods. *Applied Catalysis A: General* **139**, 75-85 (1996).

17. Y. Ma, A practical approach for the preparation of high activity Cu/ZnO/ZrO_2 catalyst for methanol synthesis from CO_2 hydrogenation. *Applied Catalysis A: General* **171**, 45-55 (1998).
18. R. A. Koeppel, A. Baiker, A. Wokaun, Copper/zirconia catalysts for the synthesis of methanol from carbon dioxide: Influence of preparation variables on structural and catalytic properties of catalysts. *Applied Catalysis A: General* **84**, 77-102 (1992).
19. O. A. Ojelade, S. F. Zaman, A Review on Pd Based Catalysts for CO_2 Hydrogenation to Methanol: In-Depth Activity and DRIFTS Mechanistic Study. *Catalysis Surveys from Asia* **24**, 11-37 (2020).
20. K. Sun, A highly active Pt/In_2O_3 catalyst for CO_2 hydrogenation to methanol with enhanced stability. *Green Chemistry* **22**, 5059-5066 (2020).
21. N. Rui, CO_2 hydrogenation to methanol over Pd/In_2O_3: effects of Pd and oxygen vacancy. *Applied Catalysis B: Environmental* **218**, 488-497 (2017).
22. E. M. Fiordaliso, Intermetallic $GaPd_2$ Nanoparticles on SiO_2 for Low-Pressure CO_2 Hydrogenation to Methanol: Catalytic Performance and In Situ Characterization. *ACS Catalysis* **5**, 5827-5836 (2015).
23. H. Choi, S. Oh, S. B. Trung Tran, J. Y. Park, Size-controlled model Ni catalysts on Ga_2O_3 for CO_2 hydrogenation to methanol. *Journal of Catalysis* **376**, 68-76 (2019).
24. F. Liao, Morphology-Dependent Interactions of ZnO with Cu Nanoparticles at the Materials' Interface in Selective Hydrogenation of CO_2 to CH_3OH. *Angewandte Chemie International Edition* **50**, 2162-2165 (2011).
25. E. J. Choi, Y. H. Lee, D.-W. Lee, D.-J. Moon, K.-Y. Lee, Hydrogenation of CO_2 to methanol over Pd–Cu/CeO_2 catalysts. *Molecular Catalysis* **434**, 146-153 (2017).
26. O. Martin, Zinc-Rich Copper Catalysts Promoted by Gold for Methanol Synthesis. *ACS Catalysis* **5**, 5607-5616 (2015).
27. F. Solymosi, Importance of the Electric Properties of Supports in the Carrier Effect. *Catalysis Reviews* **1**, 233-255 (1968).
28. S. J. Tauster, Strong metal-support interactions. *Accounts of Chemical Research* **20**, 389-394 (1987).
29. K. Mudiyanselage, Importance of the Metal–Oxide Interface in Catalysis: In Situ Studies of the Water–Gas Shift Reaction by Ambient-Pressure X-ray Photoelectron Spectroscopy. *Angewandte Chemie International Edition* **52**, 5101-5105 (2013).
30. J. Graciani, Highly active copper-ceria and copper-ceria-titania catalysts for methanol synthesis from CO_2. *Science* **345**, 546 (2014).
31. J. A. Rodriguez, Hydrogenation of CO_2 to Methanol: Importance of Metal–Oxide and Metal–Carbide Interfaces in the Activation of CO_2. *ACS Catalysis* **5**, 6696-6706 (2015).
32. J. D. Grunwaldt, A. M. Molenbroek, N. Y. Topsøe, H. Topsøe, B. S. Clausen, In Situ Investigations of Structural Changes in Cu/ZnO Catalysts. *Journal of Catalysis* **194**, 452-460 (2000).
33. T. Fujitani, J. Nakamura, The effect of ZnO in methanol synthesis catalysts on Cu dispersion and the specific activity. *Catalysis Letters* **56**, 119-124 (1998).
34. W. Wang, Z. Qu, L. Song, Q. Fu, CO_2 hydrogenation to methanol over Cu/CeO_2 and Cu/ZrO_2 catalysts: Tuning methanol selectivity via metal-support interaction. *Journal of Energy Chemistry* **40**, 22-30 (2020).
35. J. Graciani, Highly Active Copper-ceria and Copper-ceria-titania Catalysts for Methanol Synthesis from CO_2. *Science* **345**, 546 (2014).
36. S. Kattel, CO_2 Hydrogenation over Oxide-Supported PtCo Catalysts: The Role of the Oxide Support in Determining the Product Selectivity. *Angewandte Chemie International Edition* **55**, 7968-7973 (2016).
37. T. Tagawa, N. Nomura, M. Shimakage, S. Goto, Effect of supports on copper Catalysts for Methanol Synthesis from $CO_2 + H_2$. *Research on Chemical Intermediates* **21**, 193-202 (1995).

38. K. Fujimoto, Y. Yu, in *Studies in Surface Science and Catalysis,* T. Inui, K. Fujimoto, T. Uchijima, M. Masai, Eds. (Elsevier, 1993), vol. 77, pp. 393-396.
39. M. Sahibzada, D. Chadwick, I. S. Metcalfe, Hydrogenation of carbon dioxide to methanol over palladium-promoted Cu/ZnO/Al_2O_3 catalysts. *Catalysis Today* **29**, 367-372 (1996).
40. X. Jiang, Origin of Pd-Cu bimetallic effect for synergetic promotion of methanol formation from CO_2 hydrogenation. *Journal of Catalysis* **369**, 21-32 (2019).
41. B. Hu, Hydrogen spillover enabled active Cu sites for methanol synthesis from CO_2 hydrogenation over Pd doped CuZn catalysts. *Journal of Catalysis* **359**, 17-26 (2018).
42. S. Tada, S. Satokawa, Effect of Ag loading on CO_2-to-methanol hydrogenation over Ag/CuO/ZrO_2. *Catalysis Communications* **113**, 41-45 (2018).
43. H. Li, Synergetic interaction between neighbouring platinum monomers in CO_2 hydrogenation. *Nature Nanotechnology* **13**, 411-417 (2018).
44. M. S. Frei, Nanostructure of nickel-promoted indium oxide catalysts drives selectivity in CO_2 hydrogenation. *Nature Communications* **12**, 1960 (2021).
45. P. Gao, Influence of modifier (Mn, La, Ce, Zr and Y) on the performance of Cu/Zn/Al catalysts via hydrotalcite-like precursors for CO_2 hydrogenation to methanol. *Applied Catalysis A: General* **468**, 442-452 (2013).
46. H.-W. Chen, J. M. White, J. G. Ekerdt, Electronic effect of supports on copper catalysts. *Journal of Catalysis* **99**, 293-303 (1986).
47. G. Zhao, X. Huang, X. Wang, X. Wang, Progress in catalyst exploration for heterogeneous CO_2 reduction and utilization: a critical review. *Journal of Materials Chemistry A* **5**, 21625-21649 (2017).
48. A. Karelovic, P. Ruiz, The role of copper particle size in low pressure methanol synthesis via CO_2 hydrogenation over Cu/ZnO catalysts. *Catalysis Science & Technology* **5**, 869-881 (2015).
49. K. Chen, X. Duan, H. Fang, X. Liang, Y. Yuan, Selective hydrogenation of CO_2 to methanol catalyzed by Cu supported on rod-like $La_2O_2CO_3$. *Catalysis Science & Technology* **8**, 1062-1069 (2018).
50. I. U. Din, M. S. Shaharun, M. A. Alotaibi, A. I. Alharthi, A. Naeem, Recent developments on heterogeneous catalytic CO_2 reduction to methanol. *Journal of CO_2 Utilization* **34**, 20-33 (2019).
51. Y. Choi, K. Futagami, T. Fujitani, J. Nakamura, The role of ZnO in Cu/ZnO methanol synthesis catalysts — morphology effect or active site model? *Applied Catalysis A: General* **208**, 163-167 (2001).
52. S. Natesakhawat, Active Sites and Structure–Activity Relationships of Copper-Based Catalysts for Carbon Dioxide Hydrogenation to Methanol. *ACS Catalysis* **2**, 1667-1676 (2012).
53. S. Dang, A review of research progress on heterogeneous catalysts for methanol synthesis from carbon dioxide hydrogenation. *Catalysis Today* **330**, 61-75 (2019).
54. S. Zander, The Role of the Oxide Component in the Development of Copper Composite Catalysts for Methanol Synthesis. *Angew. Chem., Int. Ed.* **52**, 6536 (2013).
55. H. Ren, Methanol synthesis from CO_2 hydrogenation over Cu/γ-Al_2O_3 catalysts modified by ZnO, ZrO_2 and MgO. *Journal of Industrial and Engineering Chemistry* **28**, 261-267 (2015).
56. K.-D. Jung, A. T. Bell, Role of Hydrogen Spillover in Methanol Synthesis over Cu/ZrO_2. *Journal of Catalysis* **193**, 207-223 (2000).
57. T. Witoon, J. Chalorngtham, P. Dumrongbunditkul, M. Chareonpanich, J. Limtrakul, CO_2 hydrogenation to methanol over Cu/ZrO_2 catalysts: Effects of zirconia phases. *Chemical Engineering Journal* **293**, 327-336 (2016).
58. Y. H. Wang, Structure-activity relationships of Cu-ZrO_2 catalysts for CO_2 hydrogenation to methanol: interaction effects and reaction mechanism. *RSC Advances* **7**, 8709-8717 (2017).
59. M. Z. Ramli, S. S. A. Syed-Hassan, A. Hadi, Performance of Cu-Zn-Al-Zr catalyst prepared by ultrasonic spray precipitation technique in the synthesis of methanol via CO_2 hydrogenation. *Fuel Processing Technology* **169**, 191-198 (2018).

60. S. Kattel, B. Yan, Y. Yang, J. G. Chen, P. Liu, Optimizing Binding Energies of Key Intermediates for CO_2 Hydrogenation to Methanol over Oxide-Supported Copper. *Journal of the American Chemical Society* **138**, 12440-12450 (2016).
61. M. Saito, T. Fujitani, M. Takeuchi, T. Watanabe, Development of copper/zinc oxide-based multicomponent catalysts for methanol synthesis from carbon dioxide and hydrogen. *Applied Catalysis A: General* **138**, 311-318 (1996).
62. Y. Zhang, J. Fei, Y. Yu, X. Zheng, Methanol synthesis from CO_2 hydrogenation over Cu based catalyst supported on zirconia modified γ-Al_2O_3. *Energy Conversion and Management* **47**, 3360-3367 (2006).
63. K. Samson, Influence of ZrO_2 Structure and Copper Electronic State on Activity of Cu/ZrO_2 Catalysts in Methanol Synthesis from CO_2. *ACS Catal.* **4**, 3730 (2014).
64. P. Gao, Fluorine-modified Cu/Zn/Al/Zr catalysts via hydrotalcite-like precursors for CO_2 hydrogenation to methanol. *Catalysis Communications* **50**, 78-82 (2014).
65. I. Melián-Cabrera, M. López Granados, J. L. G. Fierro, Effect of Pd on Cu-Zn Catalysts for the Hydrogenation of CO_2 to Methanol: Stabilization of Cu Metal Against CO_2 Oxidation. *Catalysis Letters* **79**, 165-170 (2002).
66. F. Kapteijn, J. Rodriguez-Mirasol, J. A. Moulijn, Heterogeneous catalytic decomposition of nitrous oxide. *Applied Catalysis B: Environmental* **9**, 25-64 (1996).
67. E. Pachatouridou, Nitrous oxide decomposition over Al_2O_3 supported noble metals (Pt, Pd, Ir): Effect of metal loading and feed composition. *Journal of Environmental Chemical Engineering* **3**, 815-821 (2015).
68. M. Muhler, L. P. Nielsen, E. Törnqvist, B. S. Clausen, H. Topsøe, Temperature-programmed desorption of H_2 as a tool to determine metal surface areas of Cu catalysts. *Catalysis Letters* **14**, 241-249 (1992).
69. M. Brun, A. Berthet, J. C. Bertolini, XPS, AES and Auger parameter of Pd and PdO. *Journal of Electron Spectroscopy and Related Phenomena* **104**, 55-60 (1999).
70. I. Melián-Cabrera, M. L. Granados, J. L. G. Fierro, Pd-Modified Cu–Zn Catalysts for Methanol Synthesis from CO_2/H_2 Mixtures: Catalytic Structures and Performance. *Journal of Catalysis* **210**, 285-294 (2002).
71. L. L. Hegedus, R. W. McCabe, in *Studies in Surface Science and Catalysis,* B. Delmon, G. F. Froment, Eds. (Elsevier, 1980), vol. 6, pp. 471-505.
72. C. H. Bartholomew, M. D. Argyle, *Advances in Catalyst Deactivation*. (MDPI AG, 2016).
73. C. H. Bartholomew, M. D. Argyle, *Advances in Catalyst Deactivation*. (MDPI AG, 2018).
74. H. H. Kung, Deactivation of methanol synthesis catalysts - a review. *Catalysis Today* **11**, 443-453 (1992).
75. J. T. Sun, I. S. Metcalfe, M. Sahibzada, Deactivation of Cu/ZnO/Al_2O_3 Methanol Synthesis Catalyst by Sintering. *Industrial & Engineering Chemistry Research* **38**, 3868-3872 (1999).
76. M. B. Fichtl, Kinetics of deactivation on Cu/ZnO/Al_2O_3 methanol synthesis catalysts. *Applied Catalysis A: General* **502**, 262-270 (2015).
77. M. Mikkelsen, M. Jørgensen, F. C. Krebs, The teraton challenge. A review of fixation and transformation of carbon dioxide. *Energy & Environmental Science* **3**, 43-81 (2010).
78. J. Wu, M. Saito, M. Takeuchi, T. Watanabe, The stability of Cu/ZnO-based catalysts in methanol synthesis from a CO_2-rich feed and from a CO-rich feed. *Applied Catalysis A: General* **218**, 235-240 (2001).
79. C. Li, X. Yuan, K. Fujimoto, Development of highly stable catalyst for methanol synthesis from carbon dioxide. *Applied Catalysis A: General* **469**, 306-311 (2014).
80. M. Kurtz, H. Wilmer, T. Genger, O. Hinrichsen, M. Muhler, Deactivation of Supported Copper Catalysts for Methanol Synthesis. *Catalysis Letters* **86**, 77-80 (2003).
81. M. V. Twigg, M. S. Spencer, Deactivation of Copper Metal Catalysts for Methanol Decomposition, Methanol Steam Reforming and Methanol Synthesis. *Topics in Catalysis* **22**, 191-203 (2003).

Chapter 4

Phase Composition of Cu/ZrO_2 Catalysts and Their Impact on the Hydrogenation of CO_2 to MeOH.

4.1 – Introduction

As discussed previously the catalytic support has been shown to play an active and essential role in many systems including the hydrogenation of CO_2 to methanol. More recently, the interest towards the support composition of Cu/ZrO_2 catalysts has risen in order to gain a deeper understanding of the catalyst structure and possible reaction mechanisms.

ZrO_2 exists as three crystal forms: cubic, tetragonal and monoclinic; the isolation or mixture of these phases depends on the preparation method, particle size, defects and calcination temperature. The monoclinic phase is said to be the most stable at room temperature compared to the other two polymorphs, with the metastable tetragonal phase readily converted to the monoclinic phase at < 1170 °C and the cubic phase being stable >2370 °C.[1] The transition temperature, however, varies according to the defect degree of the crystallographic lattice and the existence of any additives.

The polymorphic nature of ZrO_2 has divided many researchers over its influence on the catalytic activity. A study by Bell and Jung looked at the effects of copper supported on monoclinic (*m*-ZrO_2) and tetragonal zirconia (*t*-ZrO_2) towards methanol synthesis using either CO or CO_2 as the feed. Their results showed that the catalyst supported by *m*-ZrO_2 was 4.5 times more active for methanol synthesis from CO_2/H_2 than that supported by *t*-ZrO_2 (H_2/CO_x = 3, 60 mL/min, 275 °C, 7 bar), which is associated with a higher affinity of adsorbed intermediates to methanol. When using CO/H_2 as the feed, the *m*-ZrO_2 catalyst was found to be 7.5 times more active. The overall findings are a contribution of the ZrO_2 phase, where an increase in activity for *m*-ZrO_2 is expected with an increase in surface area, as well as the ratio of the surface area of Cu to that of ZrO_2.[2] On the other hand, a number of studies have claimed that crystallisation of the zirconia (transformation from amorphous zirconia) is less catalytically active.[3] Early studies by Baiker *et al.*[4] showed that the lower Cu surface area combined with the crystallization of amorphous ZrO_2 (*am*-ZrO_2) had a negative effect on the selectivity and activity of the Cu/ZrO_2 catalyst; the importance of a strong metal-support interaction was stressed. Sun and co-workers conducted studies on Cu supported onto different zirconia polymorphs, using CO feeds, and discovered

that the Cu/t-ZrO_2 catalyst, with a high Cu dispersion, showed greatest activity and selectivity to methanol compared to the two other catalysts. The CO conversion and space-time yield were only 11.30 %, 0.11 g/ml h^{-1} and 9.28 %, 0.07 g/ml h^{-1} for Cu/*am*-ZrO_2 and Cu/*m*-ZrO_2 catalysts, respectively, whereas the Cu/*t*-ZrO_2 catalyst was up to three times more active (13.96 %, 0.22 g/ml h^{-1}) for methanol synthesis.[5] Recent studies by Tada *et al.* found that the interfacial sites on Cu/*am*-ZrO_2 that are obtained by reducing the prepared amorphous Cu–Zr–O oxides without forming crystalline CuO particles, are more active than those on Cu/*t*-ZrO_2 and Cu/*m*-ZrO_2. Methanol adsorbs more weakly on *am*-ZrO_2 than on *m*-ZrO_2, allowing the suppression of unwanted methanol decomposition and consequently a higher methanol selectivity.[6] Also, if the Cu loading of Cu/*am*-ZrO_2 decreases from 12 to 19 to 6–8 wt. % (the solubility limit of Cu species in *am*-ZrO_2), the turnover frequencies (TOFs), methanol production per exposed Cu sites at weight/volume flow rate (W/F) of 430 g_{cat} s L(STP)$^{-1}$, increase from 16 to 18 to 29–39 h^{-1} respectively.[7]

Although the differences in activity have been associated with support crystallographic structure, it is important to take into account the influence of catalyst preparation conditions, especially the acid-base environment as this can impact the surface hydroxylation and consequent activity. Indeed, a number of catalytic active sites can be found on the surface of zirconia, which include Brönsted acidic and basic hydroxyl groups, and coordinatively unsaturated Lewis acidic-base $Zr^{4+}O^{2-}$ pairs.[8-12] It has been shown that all of these sites are crucial towards reactions involving CO and CO_2.[47, 13] Differences in the methanol formation between the polymorphs are a reflection of the discrepancies in the concentration of these structural defects. Previous studies by Bell and co-workers found that the adsorption capacity of CO_2 is an order of magnitude higher for *m*-ZrO_2 (2–3 µmol/m^2) compared to *t*-ZrO_2 (0.1 µmol/m^2), which has been attributed to the increased concentration and basicity of hydroxyl groups as well as higher Lewis acidity/basicity of Zr^{4+}/ O^{2-} pairs present on the *m*-ZrO_2 surface. The adsorption capacity of CO_2 on both *m*-ZrO_2 and *t*-ZrO_2 was shown to increase with surface area, suggesting that the surface density of adsorption sites increases with surface area. Furthermore, adsorption of CO_2 on monoclinic ZrO_2 produces bicarbonate and monodentate and bidentate carbonates, whereas bidentate and polydentate carbonates are formed on tetragonal ZrO_2.[14]

An interesting study by Samson and co-workers looked at the effect of the various factors mentioned above for the activity of Cu/ZrO_2 catalysts in the synthesis of methanol from CO_2. Their findings show that the methanol formation rate increases with increasing *t*-ZrO_2 phase in the catalyst, and the active centers are Cu^+ ions incorporated into the ZrO_2 lattice near oxygen vacancies. In addition, when investigating the acid sites formed, the addition of CuO onto the polymorphs resulted in an increase in Brønsted acid sites and an even larger increase (4-5 x) in the concentration of Lewis acid sites when

compared to those in the pure support; however, comparing the strength of the Lewis acid sites for the two polymorphs, the tetragonal zirconia was far greater than the monoclinic. A linear correlation was established between catalytic activity and acidity of the catalysts for both Brønsted and Lewis centres. In contrast to the previous studies, no correlation was found between the methanol formation rate and Cu surface area.[63]

Similar findings were also reported by Bueno and co-workers when studying copper catalysts supported on different ZrO_2 polymorphs for ethanol dehydrogenation to acetaldehyde and ethyl acetate. The catalytic properties of the Cu catalysts supported on *am*-, *m*-, or *t*-ZrO_2 phase were associated with the specific electron density of supported copper species (Cu^0 and Cu^+) defined by the particle size and the interface at the copper metal oxide support. The active surface sites for the Cu/ *m*-ZrO_2 catalyst showed that greater ethyl acetate formation is determined by the high oxygen mobility from the bulk *m*-ZrO_2 phase to copper species, causing a high density of basic sites and a more heterogeneous distribution of the surface copper species (Cu^0 /Cu^+).[15]

Lin *et al*. conducted a study on a unique catalyst with a ZrO_2/Cu inverse configuration in which the domains of amorphous zirconia only covered a small fraction of the metallic copper surface. The catalysts were synthesised using a modified co-precipitation technique where oxalic acid was used for precipitation. The best ZrO_2/Cu catalyst (ZrO_2/Cu-0.1) displayed 3 times higher activity for the hydrogenation of CO_2 to methanol when compared with conventional Cu/ZrO_2 catalysts. (220 °C , CO_2/H_2 = 1:3, 30 bar). AP-XPS and DRIFTs characterizations showed that the ZrO_2 species were in a highly reduced state and intermediates of formate and methoxy were formed and consumed on the inverse ZrO_2/Cu much faster than on the Cu/ZrO_2 configuration. The high activity is mainly ascribed to the formation of a highly reactive HCOO-Cu intermediate adsorbed on the metallic Cu component of the inverse ZrO_2/Cu catalyst.[16]

The work detailed in this chapter aims to explore the impact of varying the calcination temperature and reduction temperature of the Cu/ZrO_2 catalysts prepared via oxalate gel, towards their hydrogenation of carbon dioxide to methanol. The deposition of Cu onto the ZrO_2 polymorphs by oxalate gel and wet impregnation is also investigated to understand the effects of preparation method and support phase on catalytic activity.

4.2 – Results and Discussion

4.2.1 – Variation of Calcination Temperature

The effects of ZrO_2 phase transformation through varying the calcination temperature were explored using Cu/ZrO_2 catalysts prepared via the oxalate gel method. The catalysts were also compared against a Cu/ZrO_2 catalyst with the same metal loading (31 wt.%) prepared by a standard co-precipitation method. The catalysts were calcined at various temperatures (400, 500 and 700 °C) under static air with a ramp rate of 2 °C/min for 2 hrs. The catalysts were then tested for their activity towards CO_2 hydrogenation through a temperature ramp study (150 – 250 °C, with 10 h dwells at each temperature). at P(total) of 20 bar. The results are shown in Figure 4.1.

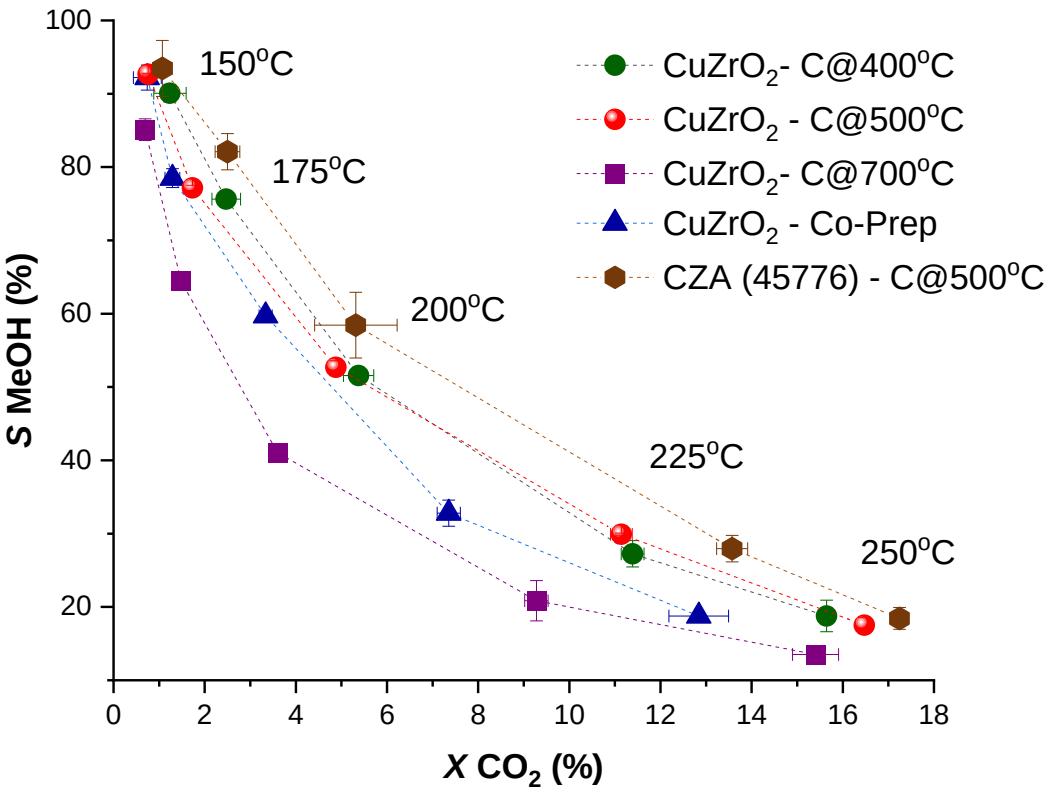

Figure. 4.1 – CO_2 conversion vs MeOH selectivity of Cu/ZrO_2 catalysts prepared via oxalate gel and co-prep calcined at various temperatures (400, 500 & 700 °C) compared with Commercial Alfa Aesar $Cu/ZnO/Al_2O_3$ (CZA) catalyst. ***In-situ* reduction conditions**; 1 h at 220 °C in 5% H_2/He (2 °C min^{-1}, 1 bar, 30 ml min^{-1} STP). **Reaction conditions:** 150 - 250 °C, 10 h dwells (total = 50 h), 30 ml min^{-1} (STP) of $CO_2 : N_2 : H_2$ (1:1:3), P(total) = 20 bar.

The methanol selectivity data for each catalyst in Figure 4.1 is shown to decrease, and CO_2 conversion increase, as the temperature is raised from 150 – 250 °C. Comparing the catalysts prepared via the oxalate gel method it can be seen that increasing the calcination temperature above 500 °C results in a loss in both the conversion and selectivity, which becomes more significant after 175 °C where the methanol selectivity drops to 41%. The catalysts calcined at 400 and 500 °C display very similar results, and are closest to the performance of the commercial CZA catalyst, which indicates that there are very small changes between the structure of the two calcined catalysts. The Cu/ZrO_2 catalyst prepared by a standard co-precipitation method is less active than the oxalate gel catalysts calcined at 400 and 500 °C. There is a clear change in the conversion data for all the catalysts, particularly after 200 °C, with a 5% difference between the co-prep catalyst and catalyst calcined at 500 °C, although there is little difference between the methanol selectivity of the catalysts calcined at the lower temperatures.

The differences between the calcined catalysts become more apparent when comparing the MeOH productivity over the different temperatures, as shown in Figure 4.2.

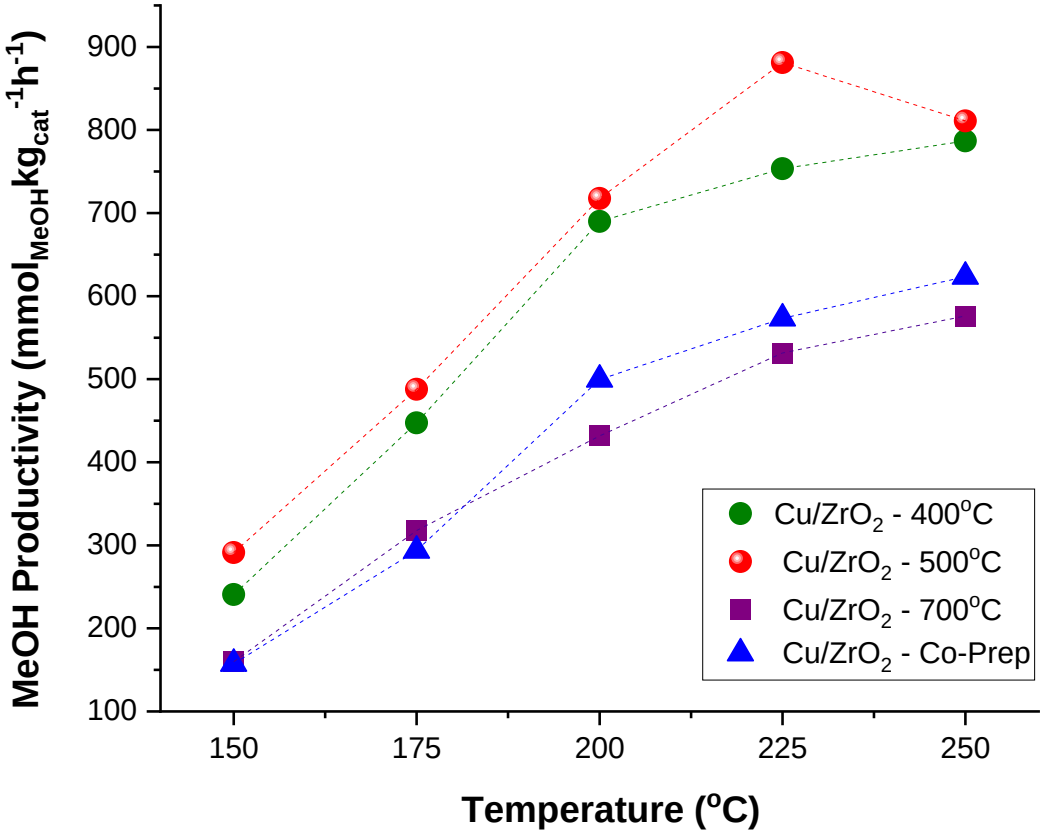

Figure. 4.2 – Methanol productivity of Cu/ZrO_2 catalysts prepared via oxalate gel and co-precipitation calcined at various temperatures (400, 500 & 700 °C).

The catalyst calcined at 500 °C achieves the highest MeOH productivity of 881 $mmol_{MeOH}kg_{cat}^{-1}h^{-1}$ at 225 °C, followed closely by the catalyst calcined at 400 °C. The productivity for the catalyst calcined at 700°C and catalyst prepared via co-precipitation remains level up to 175°C at 300 $mmol_{MeOH}kg_{cat}^{-1}h^{-1}$ before the co-prep catalyst overtakes the former at 200 °C. The Cu/ZrO_2 catalyst calcined at 700 °C displays the lowest productivity of 576 $mmol_{MeOH}kg_{cat}^{-1}h^{-1}$ for all the catalysts tested. The general trend of an initial increase in productivity and decrease over higher catalytic temperatures is apparent in the majority of the catalysts tested, as expected with an increased rate of CO production from competing reactions.

The trends shown above suggest that the use of higher calcination temperatures cause a change in the structure of the catalyst and subsequently reduces the catalyst activity; the activity is also influenced by the catalyst preparation method. To investigate further, the catalysts were characterised using N_2O pulse titration and standard BET method to compare the surface area in relation to the activity of the catalysts. The results for this are shown in Table 4.1.

Table 4.1: *Physiochemical properties of calcined Cu/ZrO_2 catalysts*.

Catalyst	BET Surface area (m^2/g)	Cu Surface area (m^2/g)	Cu Particle Size (nm)*
Cu/ZrO_2 – C@400°c	53	11.4	11
Cu/ZrO_2 – C@500°c	57	10.8	11
Cu/ZrO_2 – C@700°c	22	11.5	17
Cu/ZrO_2 – Co-Prep	98	7.80	24
Alfa Aesar (45776)-CZA	72	20.2	11

**Calculated via Scherrer equation for Cu (111) at 43.6°*

Comparing the surface area data above, in Table 4.1 there are a range of surface areas between the catalysts. The catalysts calcined at 400 and 500 °C show identical Cu particle sizes (11 nm) and very similar surface area values; as mentioned previously, the work by Bell and co-workers established that the surface density of adsorption sites for CO_2 increases with an increase in surface area, particularly for *t*-ZrO_2, and this reflects well with the activity data for the catalyst calcined at 500 °C. However, the least active catalysts (co-prep and Cu/ZrO_2 calcined at 700 °C) have BET surface area that vary significantly. The co-prep catalyst has the highest overall surface area (98 m^2/g) but the specific Cu

surface area is marginally lower than the other catalysts, as well as containing larger Cu particles; but this catalyst performs slightly better than the catalyst calcined at 700°C, which has a very low BET surface area and most likely poor Cu dispersion and lack of CO_2 adsorption sites across the surface. These findings support the studies by Sun and co-workers, where greater Cu dispersion was linked to higher methanol activity and selectivity, and oppose the work of Bell and Jung where the most crystalline polymorph (*m*-ZrO_2) was the most active. The commercial catalyst shows both high surface area (72 m^2/g) and low Cu particle size (11 nm); the information suggests that the surface area and particle size may be a factor influencing the methanol activity but it is not the determining factor, and likely a combination of factors, such as the catalyst surface properties and metal-support interactions, as there is no clear trend in methanol productivity between the surface areas and Cu particle sizes displayed between the catalysts.

XRD analysis was performed on all of the catalysts and the resulting patterns are shown in Figure 4.3.

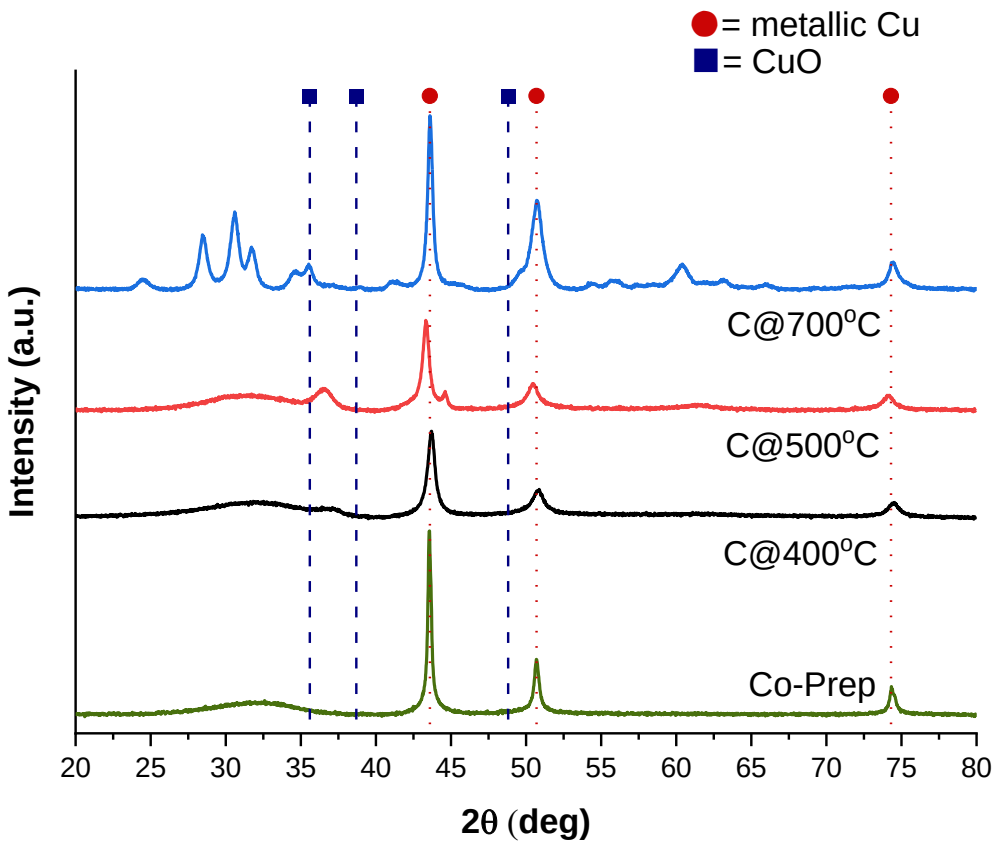

Figure 4.3. – XRD patterns for the reduced Cu/ZrO_2 catalysts calcined at 400, 500 and 700 °C and Cu/ZrO_2 prepared via co-precipitation. Peaks for metallic Cu have been highlighted with red circles and CuO with blue squares.

The XRD patterns show an increase in crystallinity as the calcination temperature is increased from 400 to 700°C. Comparing the two preparation methods, the co-precipitation catalyst is more crystalline than to the Cu/ZrO_2 catalysts prepared via the oxalate gel method. The most intense reflections observed at 2θ = 43.6° are assigned to metallic Cu (111), which was used to estimate the Cu particle size using the Scherrer equation (Table 4.1); the remaining Cu^0 peaks are located at 50.7° and 74.3° and correspond to the (200) and (220) planes respectively (PDF ref. 01-071-4609). Peaks for CuO are also included, the major reflections are observed at 2θ = 35.6, 38.7 and 48.8° and correspond to the ($\bar{1}11$), (111) and ($\bar{2}02$) planes respectively. Comparing the XRD patterns, the catalyst calcined at 700 °C shows low intensity peaks for CuO; no CuO peaks are found in the remaining catalysts. The increase peak width between the catalysts corresponds to an increase in the Cu particle size. Partial phase transformation of the ZrO_2 from tetragonal (*t*-ZrO_2) to monoclinic (*m*-ZrO_2) at 700°C is also observed, indicated by the formation of additional peaks at 2θ = 24.5, 28.5, 30.6 and 31.7°; only very small reflections were observed for tetragonal zirconia, with the majority being monoclinic. These phase transformations at the calcination temperatures used are well known for ZrO_2, and the addition of elements such as Cu have little effect on the temperature, suggesting the incorporation of Cu into the matrix does not have a major impact on the phase transition temperatures of ZrO_2.[17, 18]

The reflections for the most active catalyst (calcined at 500 °C) are very similar to those of the catalyst calcined at 400 °C; however, the peaks for tetragonal zirconia at 2θ = 36.5° and 60.3° are more pronounced and there is the additional peak for monoclinic zirconia at 44.6°. The co-prep and catalyst calcined at 400 °C are more amorphous, with broad peaks around 33° assigned to tetragonal zirconia, and no signs of monoclinic zirconia are seen. The slight differences in the structure of the catalyst may be the cause for changes in the catalytic activity, with mixed phases of tetragonal and monoclinic zirconia being more favourable, as opposed to a complete transition to monoclinic zirconia that leads to larger Cu particles and hence a dramatic decrease in methanol activity.

In order to study this in more detail Selected Area Electron Diffraction (SAED) patterns were taken of the catalysts as shown in Figure 4.4.

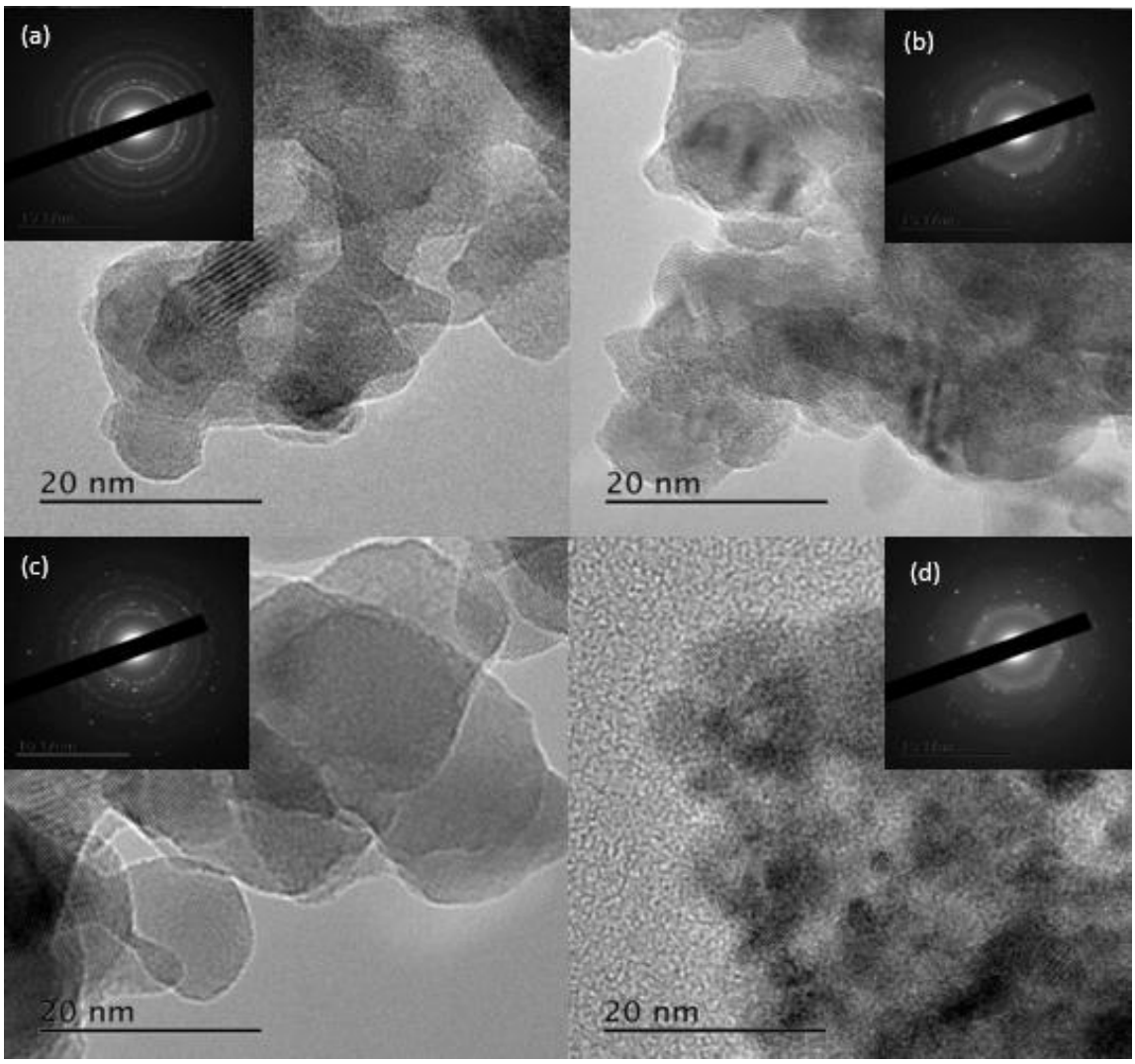

Figure 4.4. – TEM images with corresponding SAED patterns for (a): Cu/ZrO_2-400 °C, (b): Cu/ZrO_2-500 °C, (c): Cu/ZrO_2-700 °C and (d): Cu/ZrO_2 – Co-Prep.

The SAED patterns show an increase in crystallinity with an increase in calcination temperature for the catalysts prepared via the oxalate gel method, as shown in the XRD patterns (Figure 4.3.). The crystallinity is evident by the rise in bright spots and disappearance of the diffuse rings corresponding to the amorphous layers. From Figure 4.4, the catalyst prepared via the co-precipitation method is most crystalline and the presence of multiple fringes shows the presence of larger CuO particles across the surface. The large lattice fringes in the remaining images are due to zirconia, and it is difficult to identify the presence of the CuO due to the inhomogeneity of the sample.

Combining the information above, it can be concluded that the increase in crystallinity and Cu particle size at higher temperatures, coupled with changes in the zirconia phase (transformation of tetragonal to monoclinic), lead to a decrease in methanol activity.

4.2.2 – Variation of Reduction Temperature

Changes in reduction temperature have been shown to impact the metal particle size and therefore increase the productivity of a catalyst. In this section, the changes in reduction temperature of the Cu/ZrO_2 catalysts will be explored and comparisons between the activity investigated.

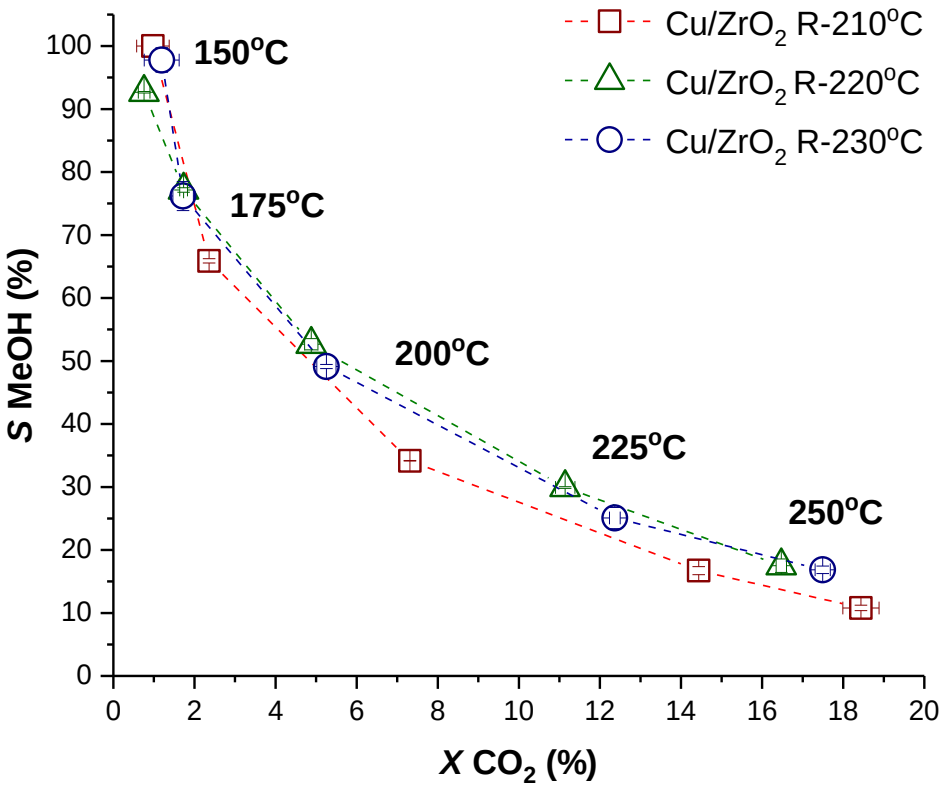

Figure. 4.5 - Activity of Cu/ZrO_2 catalysts prepared via oxalate gel and reduced at various temperatures (210, 220 & 230 °C). ***In-situ* reduction conditions**; 1 h in 5 %H_2/He (2 °C min^{-1}, 1 bar, 30 ml min^{-1} STP). **Reaction conditions:** 150 - 250 °C, 10 h dwells (total = 50 h), 30 ml min^{-1} (STP) of CO_2 : N_2 : H_2 (1:1:3), P(total) = 20 bar.

Figure 4.5 compares the methanol selectivity and CO_2 conversion between Cu/ZrO_2 catalysts pre-reduced *in-situ* with 5 % H_2/He at three different temperatures – 210, 220 and 230 °C. A small temperature range was chosen for the reduction in order to prevent sintering of the Cu particles, and consequent loss of catalytic activity. The catalysts all have a high methanol selectivity (above 93 %), at the start, and this then drops with an increase in temperature and conversion. Although the catalyst reduced at the lower temperature (210 °C) shows the greatest decrease in methanol selectivity (66 %) above 200 °C, the CO_2 conversion remains greater than the other reduced catalysts. Very little difference is observed between the Cu/ZrO_2 catalysts reduced at 210 and 220 °C, at testing temperatures below 250 °C; the catalyst reduced at 220 °C slightly outperforms the other catalyst in

regard to the methanol selectivity between 175 – 225 °C, yet the CO_2 conversion remains somewhat greater for the catalyst calcined at 230 °C. The data suggests that a small change in the reduction temperature of the Cu/ZrO_2 catalysts has very little influence on the overall performance of the catalyst, which is most likely due to the Cu particles becoming fully reduced at temperatures ≥ 220 °C, as reflected in the XRD patterns (Figure 4.5). Any temperatures below this are likely to result in the presence of unreduced Cu species and consequently a reduction in methanol activity.

Work by Ramírez and co-workers looked at the influence of the calcination and reduction temperature over Cu/ZnO catalysts at atmospheric pressure. The best combination of calcination and reduction temperature was 10CuZnO-350-200 (*A*CuZnO-*B*-*C*: *A*, loading percentage; B, calcination temperature; C, reduction temperature), which gave the highest conversion to methanol. When they increased the calcination temperature more than 350 °C, the TPR showed that the α and β peaks corresponding to the reduction of Cu(II) to Cu(I) and Cu(I) to Cu(0) merged together. This proved that the reduction became harsher and also there is an increase in particle size with calcination temperature. Interestingly, the influence of reduction temperature on particle size was the opposite. The size of Cu(0) decreased with reduction temperature. Studies on the methane–methanol selectivity of this catalyst proved the role of Cu oxidation states in governing the product selectivity. 10CuZnO-350-150 resulted in higher methane selectivity than methanol, which the authors attributed to the unreduced Cu(I) and Cu(II) because they observed these species in the XRD. Thus, for methanol, the best reduction temperature was identified as 200 °C, and it gave good conversion below 250 °C for methanol, where CO selectivity was less. A reduction temperature of 400 °C yielded CuZn alloy, which generated good selectivity to methanol only at >200 °C. This study suggests a fine balance between the calcination and reduction temperatures is required to obtain the optimal Cu state and catalytic activity.[19]

4.2.3 – Variation of Cu Deposition

As shown in the previous sections the variation of calcination and reduction parameters has marginal effect on the catalysts. In order to observe a more significant change and to establish the effect of changing the phase of the support without impacting the Cu particles, Cu was deposited onto different calcined ZrO_2 phases; amorphous (*am*-ZrO_2), tetragonal (*t*-ZrO_2) and monoclinic (*m*-ZrO_2), all prepared via the oxalate gel method through two preparation methods. The first method was oxalate gel, and the second method was wet impregnation (WI). The Cu loading for all catalyst were fixed at 31 wt. %; after preparation catalysts were dried in static air at 500 °C for 2 h, 10 °C min^{-1}. Prior to reaction catalysts were pelleted (425–600 µm), and 0.5 g of pelleted catalyst was secured with quartz wool in the reactor tube and pre-reduced *in-situ* with 5 % H_2/He (220 °C, 1 h, 2 °C min^{-1}). After reduction, the reactor was allowed to cool to 50 °C, the gas flow was switched from 5 % H_2/He to the reaction mixture (20 % CO_2, 60 % H_2, 20 % N_2) and was pressurised to 20 bar at a flow rate of 30 ml min^{-1}. Catalyst activity was assessed between 150 and 250 °C, for a total of 50 h.

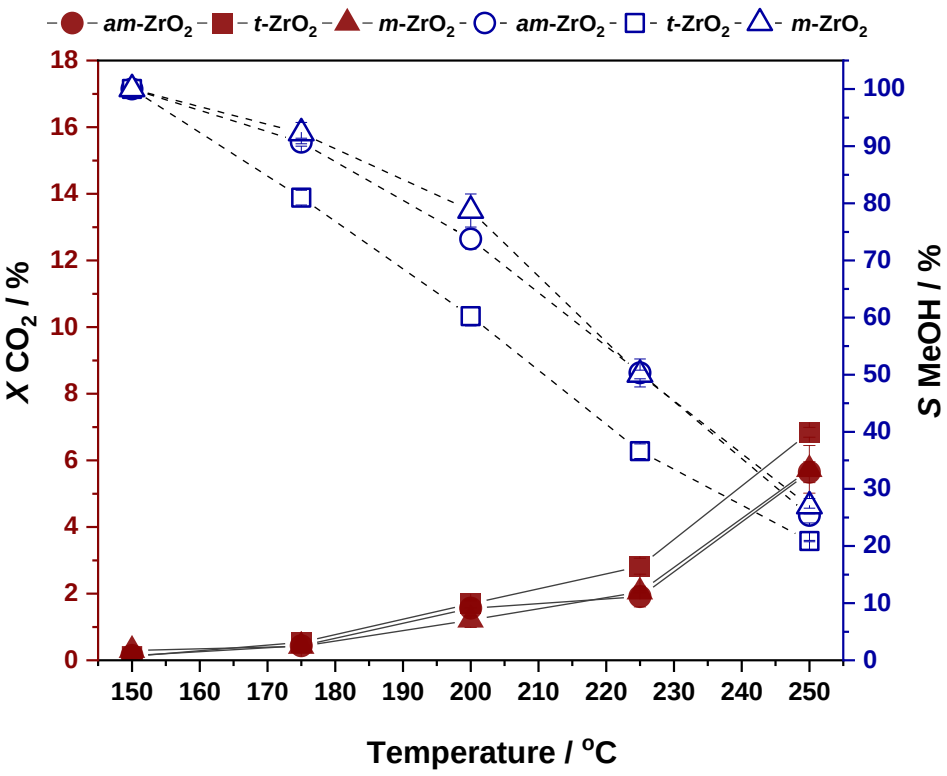

Figure. 4.6a - Activity of Cu/ZrO_2 catalysts with 3 different ZrO_2 phases- *am*-ZrO_2 (400-OG), *t*-ZrO_2 (500-OG) and *m*-ZrO_2 (700-OG) prepared via oxalate gel. ***In-situ* reduction conditions**; 1 h, 220 °C in 5% H_2/He (2 °C min^{-1}, 1 bar, 30 ml min^{-1} STP). **Reaction conditions:** 150 - 250 °C, 10 h dwells (total = 50 h), 30 ml min^{-1} (STP) of CO_2 : N_2 : H_2 (1:1:3), P(total) = 20 bar.

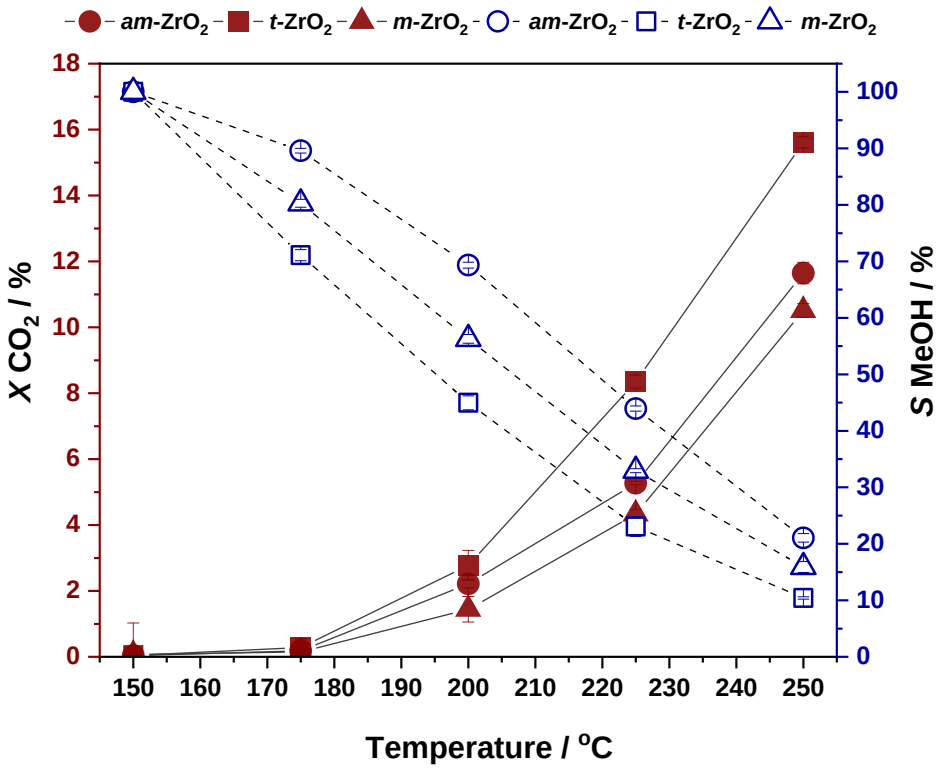

Figure. 4.6b - Activity of Cu/ZrO_2 catalysts with 3 different ZrO_2 phases- *am*-ZrO_2 (400-OG), *t*-ZrO_2 (500-OG) and *m*-ZrO_2 (700-OG) prepared via wet impregnation. ***In-situ* reduction conditions**; 1 h, 220 °C in 5 % H_2/He (2 °C min^{-1}, 1 bar, 30 ml min^{-1} STP). **Reaction conditions:** 150 - 250 °C, 10 h dwells (total = 50 h), 30 ml min^{-1} (STP) of CO_2 : N_2 : H_2 (1:1:3), P(total) = 20 bar.

The catalysts can be split according to their Cu deposition methods: Figure 4.6a shows the catalysts prepared via oxalate gel; and Figure 4.6b shows the catalysts prepared via wet impregnation. As seen previously for Cu/ZrO_2, the CO_2 conversion increases with temperature and the selectivity towards methanol decreases. The catalysts prepared via the oxalate gel show very similar conversions (1.6 %) up to 200 °C, and beyond this only a small increase (1 %) is observed for the tetragonal ZrO_2 catalyst (500-OG). On the other hand, Cu/*t*-ZrO_2 displays the lowest methanol selectivity across the temperature range studied, compared to the other catalysts, with a difference of up to 12%. Both the amorphous ZrO_2 (400-OG) and monoclinic ZrO_2 (700-OG) exhibit comparable methanol selectivities. In contrast, the catalysts prepared via wet impregnation can be distinguished more easily according to the crystallographic phases of ZrO_2; noticeably, the conversions are higher and the methanol selectivities lower when compared to the oxalate gel catalysts. For the wet impregnation catalysts, clear differences are observed at 225 °C and above; the tetragonal ZrO_2 catalyst reaches a maximum CO_2 conversion of 16%, followed by 12% for amorphous ZrO_2 and 11% for monoclinic ZrO_2. Differences in methanol selectivity can be observed from 175 °C onwards; amorphous ZrO_2 maintains the highest methanol selectivity across the temperature range falling to 21% at 250 °C, in contrast to monoclinic ZrO_2 at 16% and tetragonal ZrO_2 at 10%.

Table 4.2: *Activity of Cu/ZrO_2 catalysts with varying ZrO_2 phases at 225 °C.*

Catalyst	*X* CO_2 %	*S* MeOH %	*S* CO %	MeOH Productivity ($mmol_{MeOH}kg_{cat}^{-1}h^{-1}$)	CO Productivity ($mmol_{CO}kg_{cat}^{-1}h^{-1}$)
Cu/ZrO_2-400-OG	1.9	50.3	49.5	323	319
Cu/ZrO_2-500-OG	2.8	36.6	63.4	226	392
Cu/ZrO_2-700-OG	2.1	50.0	50.0	281	281
Cu/ZrO_2-400-WI	5.3	43.9	55.9	521	662
Cu/ZrO_2-500-WI	8.3	23.1	76.9	460	1531
Cu/ZrO_2-700-WI	4.3	33.0	67.0	333	677

The difference in activity between the catalysts is highlighted in Table 4.2, where the reaction data is provided for 225 °C. As described above, the wet impregnation catalysts are more active compared to the oxalate gel catalysts. Interestingly, both sets the tetragonal ZrO_2 catalysts display a higher CO_2 conversion and significantly lower methanol selectivity. Furthermore, the amorphous Cu/ZrO_2 catalysts achieve the highest methanol productivity, when compared against the tetragonal and monoclinic phases, at 323 and 521 $mmol_{MeOH}kg_{cat}^{-1}h^{-1}$, respectively.

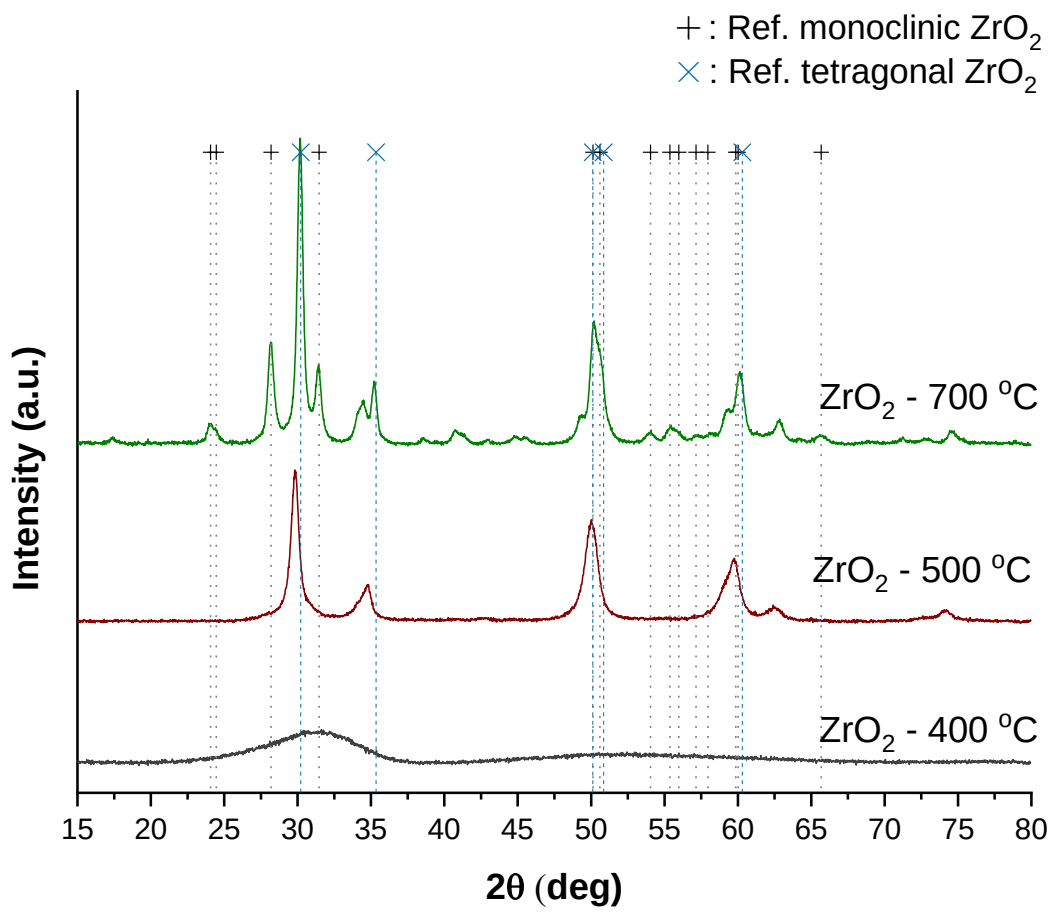

Figure 4.7. – XRD patterns for synthesised ZrO_2 catalysts calcined at 400, 500 and 700 °C; reference peaks for monoclinic ZrO_2 have been highlighted with + and reference peaks for tetragonal ZrO_2 have been highlighted with x in blue.

XRD analysis was performed on the synthesised ZrO_2 supports before Cu deposition, in order to determine if the calcination at the various temperatures formed the phases expected, and to identify any presence of mixed phases (Figure. 4.7). The crystallinity of the supports increases with an increase in the calcination temperature as expected; at 500 °C, a change from amorphous ZrO_2 to tetragonal ZrO_2 is observed, with characteristic peaks at 29.8°, 34.8°, 50.0°, 59.8°, 62.6° and 74.2° corresponding to (101), (002), (112), (211), (202) and (220) planes. As the temperature is increased further from 500 to 700 °C, a partial phase transition from tetragonal to monoclinic zirconia is seen. Reference data for monoclinic ZrO_2 (PDF ref num. 01-078-0047) and tetragonal ZrO_2 (PDF ref num. 01-078-3194) has been added for comparison; the most prominent peaks for the monoclinic ZrO_2 are 24.1°, 24.4°, 28.2°, 31.5° and 50.3° corresponding to (011), (110), ($\bar{1}$11), (111) and (220) planes. To understand the potential changes in the support structure, additional XRD patterns were taken of the calcined catalysts after Cu deposition, via both the oxalate gel and wet impregnation (Figure 4.8).

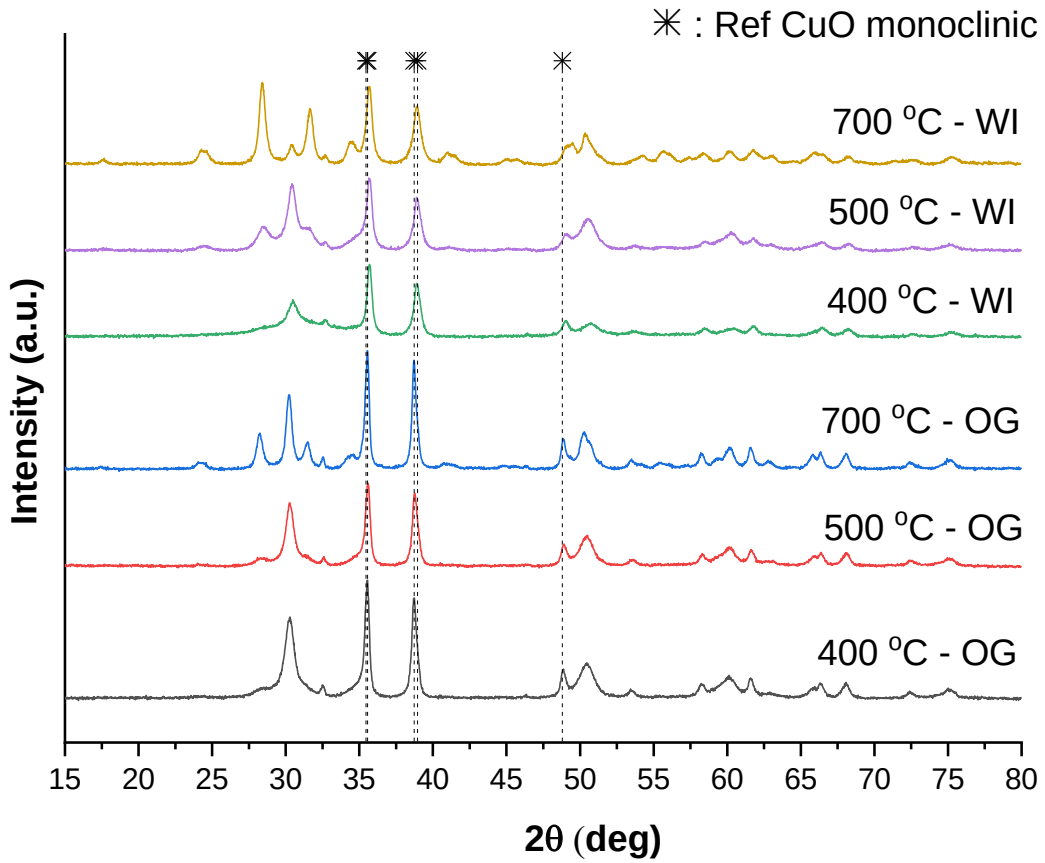

Figure 4.8. – XRD patterns for calcined Cu/ZrO_2 catalysts, post Cu deposition onto ZrO_2 400, 500 and 700 °C via oxalate gel and wet impregnation. Reference peaks for monoclinic CuO have been highlighted.

The XRD patterns in Figure 4.8 show an increase in crystallinity for both series of catalysts from 400 to 700 °C. Comparing the two preparation methods (wet impregnation and oxalate gel), the reflections observed for the ZrO_2 phases and CuO are very similar; differences are observed primarily in the peak intensities and widths, with the series of catalysts prepared via wet impregnation having less intense and more broad peaks, the series of catalysts prepared via oxalate gel displaying sharper and more intense peaks. The results suggests that the CuO particles deposited onto the Cu/ZrO_2 catalysts via wet impregnation are smaller than those deposited via the oxalate gel method.

The most intense reflections observed at 2θ = 35.6° are assigned to monoclinic CuO ($\bar{1}11$), which was used to estimate the CuO particle size using the Scherrer equation (Table 4.2). The remaining CuO peaks are located at 38.9° and 48.8° and correspond to the (100) and ($\bar{2}02$) planes, respectively (PDF ref. 01-089-5896). The peaks for the various ZrO_2 phases are also shown for each catalyst, as was shown in Figure 4.7 for the supports before Cu deposition. The reflections expected for tetragonal and monoclinic zirconia are maintained, with Cu/ZrO_2-500 °C exhibiting peaks for both monoclinic and

tetragonal zirconia and the Cu/ZrO_2-700°C exhibiting peaks for monoclinic zirconia; only this is true for both the wet impregnation and oxalate gel catalysts. The only exception was the Cu/ZrO_2-400°C system, where the amorphous support has now transformed, compared to no Cu, with reflections matching those of tetragonal zirconia; this is more pronounced for the oxalate gel catalyst.

Table 4.2: *Physiochemical properties of Cu/ZrO_2 catalysts calcined at 400, 500 and 700 °C and prepared via oxalate gel and wet impregnation*.

Catalyst	BET Surface area (m^2/g)	Cu Surface area (m^2/g)	CuO Particle Size (nm)*
Cu/ZrO_2 – C@400°c-OG	94	5.11	34
Cu/ZrO_2 – C@500°c- OG	50	4.58	31
Cu/ZrO_2 – C@700°c- OG	20	5.04	37
Cu/ZrO_2 – C@400°c-WI	41	9.00	29
Cu/ZrO_2 – C@500°c-WI	33	7.94	25
Cu/ZrO_2 – C@700°c-WI	17	8.30	23

**Calculated via Scherrer equation for CuO ($\bar{1}11$) at 35.6°*

Comparing the two sets of catalysts, the BET surface areas vary according to the temperature used to calcine the support of the catalysts, with the monoclinic ZrO_2-supported Cu catalyst calcined at the higher temperature of 700 °C giving the lowest BET surface area, in contrast to the less crystalline supported Cu catalyst calcined at 400 °C that gives the highest BET surface area. The CuO particle sizes remain fairly similar, as expected from the XRD patterns in Figure 4.8; the catalysts prepared by wet impregnation achieve smaller CuO particles than those prepared by the oxalate gel method. On the other hand, there are greater differences between the two sets of catalysts when comparing the Cu surface areas. The same trend is observed in both sets of catalysts; the Cu surface area increases as the calcination temperature of the catalyst support decreases. This trend correlates with the reaction data shown in Figures 4.6a and 4.6b, where the activity towards methanol production goes in the order 400 > 700 > 500°C. Despite having higher CO_2 conversions, the methanol selectivity of the mixed ZrO_2 phase-supported Cu catalysts (500 °C) were lower than the other catalysts.

The results described above can be linked to both the type of method used to deposit the Cu in the support, and to the type of support phase present. Choosing a less crystalline support and adding Cu particles with larger surface areas, that are more well dispersed, is more favourable towards an increase in catalyst performance. The results match the work of Baiker *et al.*, as mentioned at the beginning, where the combination of an increase in support crystallinity and low Cu surface area results indicates a weakened metal-support interaction and subsequently lower activity. In addition, Bell and co-workers also emphasised the importance of acid-base sites on the support surface, this environment is influenced by the type of preparation method used, and from the data the deposition of the Cu onto the ZrO_2 supports through wet impregnation helped maintain the integrity of key structural defects compared to the catalysts where the Cu was deposited through the oxalate gel method. Furthermore, the adsorption capacity of CO_2 increases with surface area; therefore, the increased surface area of the Cu/ZrO_2-400 catalysts can be linked to an increase in surface density of the adsorption sites and hence an increase in the adsorption capacity of CO_2.

4.3 – Conclusions

The formation of the three zirconia phases – amorphous (*am*-ZrO_2), tetragonal zirconia (*t*-ZrO_2) and monoclinic zirconia (*m*-ZrO_2) are possible through varying the calcination temperatures of the Cu/ZrO_2 catalysts prepared via the oxalate gel method. Temperatures ≥ 700°C afford more crystalline *m*-ZrO_2, a temperature of 500 °C results in a majority *t*-ZrO_2 phase, and temperatures ≤ 400°C achieves *am*-ZrO_2. When comparing the catalysts with a co-precipitation catalyst of the same Cu loading (31 wt.%), increasing the calcination temperature above 500 °C resulted in a loss in both the catalytic conversion and selectivity; the catalysts calcined at 400 and 500 °C displayed very similar results and were closest to the performance of the commercial CZA catalyst, which indicates that there are very small changes only between the structure of the two calcined catalysts. The Cu/ZrO_2 catalyst prepared by a standard co-precipitation method was more active than the oxalate gel catalyst when calcined at 700 °C. The catalyst calcined at 500 °C achieved the highest MeOH productivity of 881 $mmol_{MeOH}kg_{cat}^{-1}h^{-1}$ and the Cu/ZrO_2 catalyst calcined at 700 °C displayed the lowest productivity of 576 $mmol_{MeOH}kg_{cat}^{-1}h^{-1}$. These results reflect an increase in Cu surface area and Cu dispersion.

In addition, small change in the reduction temperature of the Cu/ZrO_2 catalysts had very little influence on the overall performance of the catalyst, which is most likely due to the Cu particles becoming fully reduced at temperatures ≥ 220 °C, as reflected in the XRD patterns. Any temperatures below 220 °C are likely to result in the presence of unreduced Cu species and consequently a reduction in methanol activity.

Cu was deposited onto the pre-synthesised ZrO_2 supports via wet impregnation and the oxalate gel method. The wet impregnation catalysts were more active than the oxalate gel catalysts, with the more amorphous Cu/ZrO_2 catalysts achieving the highest methanol productivity. Again, an increase in Cu surface area and Cu dispersion leads to an increase in activity, likely due to stronger metal-support interactions; in addition, increased surface area of the Cu/ZrO_2-400 catalysts can be linked to an increase in surface density of the adsorption sites and hence an increase in the adsorption capacity of CO_2. Overall, the type of preparation method used, as well as the ZrO_2 phase, Cu surface area and Cu dispersion, all play an important part towards the catalyst activity.

Future work recommendations include enhanced characterisation of catalysts, such as *in-situ* XRD to follow the changes in the support phases under reaction conditions. Also investigating additional methods to add Cu to the supports.

4.4 – References

1. V. B. Raghavendra, S. Naik, M. Antony, G. Ramalingam, M. Rajanathi, S. Raghavan, Amorphous, Monoclinic, and Tetragonal Porous Zirconia Through a Controlled Self-Sustained Combustion Route. *Journal of the American Ceramic Society* **94**, 1747-1755 (2011).
2. K. T. Jung, A. T. Bell, Effects of Zirconia Phase on the Synthesis of Methanol over Zirconia-Supported Copper. *Catalysis Letters* **80**, 63-68 (2002).
3. R. A. Köppel, C. Stöcker, A. Baiker, Copper- and Silver–Zirconia Aerogels: Preparation, Structural Properties and Catalytic Behavior in Methanol Synthesis from Carbon Dioxide. *Journal of Catalysis* **179**, 515-527 (1998).
4. A. Baiker, M. Kilo, M. Maciejewski, S. Menzi, A. Wokaun, in *Studies in Surface Science and Catalysis,* L. Guczi, F. Solymosi, P. TÉTÉNyi, Eds. (Elsevier, 1993), vol. 75, pp. 1257-1272.
5. Z.-Y. Ma, C. Yang, W. Wei, W.-H. Li, Y.-H. Sun, Catalytic performance of copper supported on zirconia polymorphs for CO hydrogenation. *Journal of Molecular Catalysis A: Chemical* **231**, 75-81 (2005).
6. S. Tada, A. Katagiri, K. Kiyota, T. Honma, H. Kamei, A. Nariyuki, S. Uchida, S. Satokawa, Cu Species Incorporated into Amorphous ZrO_2 with High Activity and Selectivity in CO_2-to-Methanol Hydrogenation. *The Journal of Physical Chemistry C* **122**, 5430-5442 (2018).
7. S. Tada, A. Katagiri, K. Kiyota, T. Honma, H. Kamei, A. Nariyuki, K. Kon, T. Toyao, K. I. Shimizu, S. Satokawa, Design of Interfacial Sites between Cu and Amorphous ZrO_2 Dedicated to CO_2-to-Methanol Hydrogenation. *ACS Catalysis* **8**, 7809-7819 (2018).
8. T. Yamaguchi, Application of ZrO_2 as a catalyst and a catalyst support. *Catalysis Today* **20**, 199-217 (1994).
9. C. Morterra, G. Cerrato, M. Signoretto, On the role of the calcination step in the preparation of active (superacid) sulfated zirconia catalysts. *Catalysis Letters* **41**, 101-109 (1996).
10. C. Morterra, G. Cerrato, V. Bolis, S. Di Ciero, M. Signoretto, On the strength of Lewis- and Brønsted-acid sites at the surface of sulfated zirconia catalysts. *Journal of the Chemical Society, Faraday Transactions* **93**, 1179-1184 (1997).
11. C. Morterra, G. Cerrato, S. Di Ciero, IR study of the low temperature adsorption of CO on tetragonal zirconia and sulfated tetragonal zirconia. *Applied Surface Science* **126**, 107-128 (1998).
12. K. Tanabe, Surface and catalytic properties of ZrO_2. *Materials Chemistry and Physics* **13**, 347-364 (1985).
13. F. Arena, G. Italiano, K. Barbara, S. Bordiga, G. Bonura, L. Spadaro, F. Frusteri, Solid-state Interactions, Adsorption Sites and Functionality of Cu-ZnO/ZrO_2 Catalysts in the CO_2 Hydrogenation to CH_3OH. *Appl. Catal., A* **350**, 16 (2008).
14. X.-M. Liu, G. Q. Lu, Z.-F. Yan, Nanocrystalline zirconia as catalyst support in methanol synthesis. *Applied Catalysis A: General* **279**, 241-245 (2005).
15. A. G. Sato, D. P. Volanti, D. M. Meira, S. Damyanova, E. Longo, J. M. C. Bueno, Effect of the ZrO_2 phase on the structure and behaviour of supported Cu catalysts for ethanol conversion. *Journal of Catalysis* **307**, 1-17 (2013).
16. C. Wu, L. Lin, J. Liu, J, Zhang, F. Zhang, T. Zhou, N. Rui, S. Yao, Y. Deng, F. Yang, W. Xu, J. Luo, Y. Zhao, B. Yan, D. X. Wen, J. A. Rodriguez, D. Ma, Inverse ZrO_2/Cu as a highly efficient methanol synthesis catalyst from CO_2 hydrogenation. *Nature Communications* **11**, 5767 (2020).

17. N. C. Horti, M. D. Kamatagi, S. K. Nataraj, M. N. Wari, S. R. Inamdar, Structural and optical properties of zirconium oxide (ZrO_2) nanoparticles: effect of calcination temperature. *Nano Express* **1**, 010022 (2020).
18. R. Srinivasan, L. Rice, B. H. Davis, Critical Particle Size and Phase Transformation in Zirconia: Transmission Electron Microscopy and X-ray Diffraction Studies. *Journal of the American Ceramic Society* **73**, 3528-3530 (1990)
19. J. Díez-Ramírez, F. Dorado, A. R. de la Osa, J. L. Valverde, P. Sánchez, Hydrogenation of CO2 to Methanol at Atmospheric Pressure over Cu/ZnO Catalysts: Influence of the Calcination, Reduction, and Metal Loading. *Industrial & Engineering Chemistry Research* **56**, 1979-1987 (2017).

Chapter 5

Cu/Zn Zeolite Catalysts for the Indirect Conversion of CO_2 to hydrocarbons.

5.1 – Introduction

We have already discussed in Chapter 3 the significance of methanol among the possible CO_2 hydrogenation products, not only because CH_3OH is an essential product in its own right but it can also be blended with gasoline and used as an intermediate for the production of numerous important chemicals.[16] CH_3OH is currently produced over $Cu/ZnO/Al_2O_3$ catalysts from syngas ($CO + H_2 + CO_2$) at 200-300 °C and 80-120 bar.[1] Under laboratory testing conditions (20-50 bar), the CO_2 hydrogenation to CH_3OH is limited to the 200-270 °C range, as at lower temperatures little CO_2 conversion is observed, whereas at higher temperatures CH_3OH productivity is limited by the equilibrium due to the promotion of the reverse water gas shift (RWGS) reaction.[2]

CH_3OH productivity from CO_2 can be enhanced by simultaneously dehydrating CH_3OH to dimethyl ether (DME). The simultaneous dehydration is achieved by combining a CH_3OH synthesis catalyst with a solid acid catalyst, which is known as a hybrid catalyst. Like CH_3OH, DME synthesis from CO_2 is favoured at low temperatures and high pressure; DME synthesis from CO_2 is also advantageous compared to CH_3OH because of higher DME equilibrium selectivity. Moreover, DME is non-toxic; non-carcinogenic; can be employed as fuel in diesel engines because of its higher cetane number and lower auto-ignition temperature compared to diesel fuel (55-60 compared to 40-50, and 235 °C compared to 250 °C, respectively); and can be easily liquified at low pressure, hence it can be used as a liquified petroleum gas (LPG) substitute.[3, 4]

For the CH_3OH dehydration to dimethyl ether (DME), ZSM-5 zeolites are preferred as acid catalysts because ZSM-5 zeolites contain Lewis and Brønsted acid sites, exhibit high resistance to water, and have excellent chemical and thermal stability.[27] For instance, Aguayo *et al*. compared $Cu\text{-}ZnO\text{-}Al_2O_3/\gamma\text{-}Al_2O_3$ and $Cu\text{-}ZnO\text{-}Al_2O_3$/NaZSM-5 hybrid catalysts for CH_3OH synthesis from the hydrogenation of CO and CO_2, and observed competitive adsorption between H_2O and CH_3OH for acid sites on $\gamma\text{-}Al_2O_3$, leading to lower CO/CO_2 conversion and DME selectivity compared to ZSM-5. Moreover, catalyst

deactivation after regeneration was observed for ɣ-Al_2O_3-containing hybrid catalyst, whilst good regeneration was observed for Cu-ZnO-Al_2O_3/ZSM-5 hybrid catalysts; [5] Similar conclusions were reported by Naik *et al*.[6] Bonura and co-workers studied the effect of water in the CH_3OH dehydration activity over ZSM-5 zeolites; at low temperatures a decrease in CH_3OH conversion was observed due to competition of H_2O with the acid sites and at higher temperatures deactivation is observed, with increasing zeolite acidity. No appreciable decrease in CH_3OH dehydration was observed above 180 °C.[7]

Frusteri *et al*. compared the activity of CuZnZr/ZSM-5 hybrid catalysts with CuZnZr supported over ZSM-5 by co-precipitation. Catalysts where the CH_3OH synthesis catalyst is supported over the solid acid catalyst are known as integrated catalysts. Slightly higher CO_2 conversion and DME productivity was observed over the integrated catalyst, which was attributed to the spatial proximity between the two active functionalities. Other studies compare the hybrid and integrated catalyst configuration for the synthesis of DME from syngas,[8] but scarce literature comparing hybrid and integrated catalysts can be found for DME synthesis from CO_2.

Typically, C_{2+} products can be generated from CO_2 hydrogenation *via* two intermediate routes: CO intermediate route and CH_3OH intermediate route (Figure 5.1a). In the CO intermediate route, CO_2 is first transformed into CO *via* the reverse water–gas shift (RWGS) reaction. As a result, the more reactive CO is subsequently hydrogenated to hydrocarbons (or oxygenates). For the latter route, the CH_3OH intermediate can be obtained using a catalyst for methanol synthesis, which is further converted to hydrocarbons by methanol-to-hydrocarbon (MTH) catalysts.

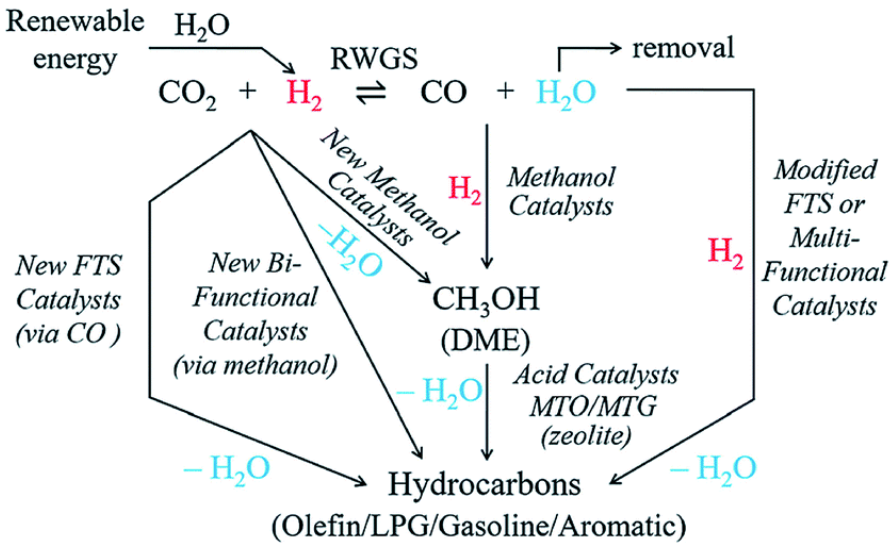

Figure 5.1a – Schematic illustration of CO_2 hydrogenation to C_{2+} products *via* the CO intermediate route and CH_3OH intermediate route.[9]

Various mechanisms have been proposed for the formation of C_{2+} products in the MTH processes, including the oxonium ylide mechanism, carbine mechanism, carbocationic mechanism, free radical mechanism and hydrocarbon pool mechanism. Among the mechanisms, the hydrocarbon pool mechanism in which aromatics and alkenes are important hydrocarbon pool compounds has been widely accepted. Larger hydrocarbons are formed after alkenes and aromatics are methylated with methanol (or dimethyl ether), and then crack or dealkylate to produce light alkenes and regenerate the starting compounds. The division between two classes of intermediates is usually referred to as the dual-cycle concept (Figure 5.1b). In such a mechanism, higher alkenes may be transformed into aromatics and alkanes through cyclisation and hydride transfer reactions, while light alkenes generated from aromatics may enter into the alkene cycle.

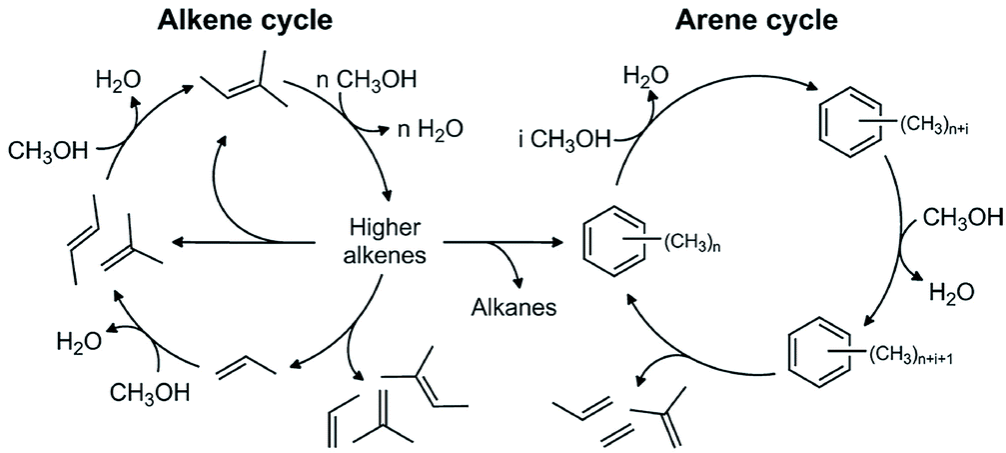

Figure 5.1b – Schematic illustration of the dual-cycle mechanism during the MTH process.[244]

The aim of this chapter is to compare MeOH, DME and higher chain hydrocarbon productivities between various CuZn- or CuZr-Zeolite integrated catalysts, where the zeolite is either commercially available H-ZSM-5 (Si:Al 23; 30; 50 and 80), mordenite (20:1) or zeolite Y, prepared *via* chemical vapour impregnation (CVI) and oxalate gel precipitation. Physical mixtures of the catalysts as well as changes to the catalyst bed are also explored in order to compare the catalyst activity. Cu-ZnO-based catalysts have been extensively studied for CO_2 hydrogenation to methanol, [11,12] variations of these catalysts by the addition of promotors/carrier oxides such as ZrO_2 and the combination of zeolites have allowed for the direct hydrogenation of CO_2 to methanol;[96] by starting with the Cu-ZnO based catalysts we can compare the existing data available in literature to gain a better understanding of the role of each of the catalyst components before introducing additional oxides to the catalyst.

5.2 – Results and Discussion

5.2.1 – Cu/Zn Zeolite Catalysts Prepared by Chemical Vapour Impregnation (CVI)

A series of 20 wt.% CuZn (1:1) catalysts were prepared via Chemical Vapour Impregnation (CVI) on commercial ZSM-5 zeolites (Si:Al 23; 30; 50 and 80), the zeolites in their (NH_4^+) form were activated to H-ZSM-5 via calcination (static air, 550 °C, 5 °C min^{-1}, 4 h). Additional zeolites used include mordenite (20:1) and zeolite Y, theses were investigated to determine if the variations in zeolite structures, particularly with pore sizes and acidity, had an impact on the methanol and DME productivities and hydrocarbon distributions. These catalysts were tested over a temperature range of 230 – 310°C; the higher temperatures for Cu/ZrO_2 were necessary for the production of any higher chain hydrocarbons. Hydrocarbons were identified after calibrating with an Agilent gas mixture and analysed via GC (Agilent 7890) fitted with an FID and TCD detectors; products eluted through a Agilent PoraPLOT Q-HTcolumn. The results are shown in Figures 5.2 and 5.3.

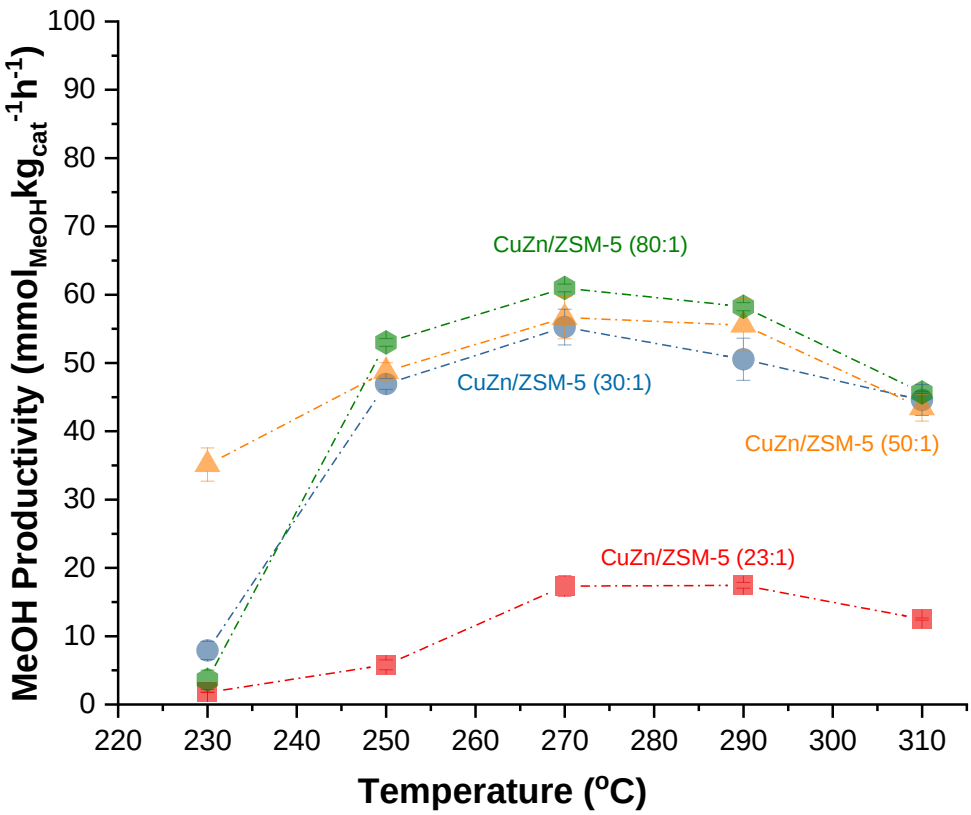

Figure 5.2 – Methanol productivity of CuZn/ZSM-5 catalyst series with Si:Al range (23, 30, 50 and 80) prepared via CVI, **reduced *in-situ***: 1 h at 220 °C in H_2 (2 °C min^{-1}, 1 bar, 30 ml min^{-1} STP). **Reaction conditions:** 230 - 310 °C, 6 h dwells (total = 30 h), 30 ml min^{-1} (STP) of CO_2 : N_2 : H_2 (1:1:3), P(total) = 20 bar.

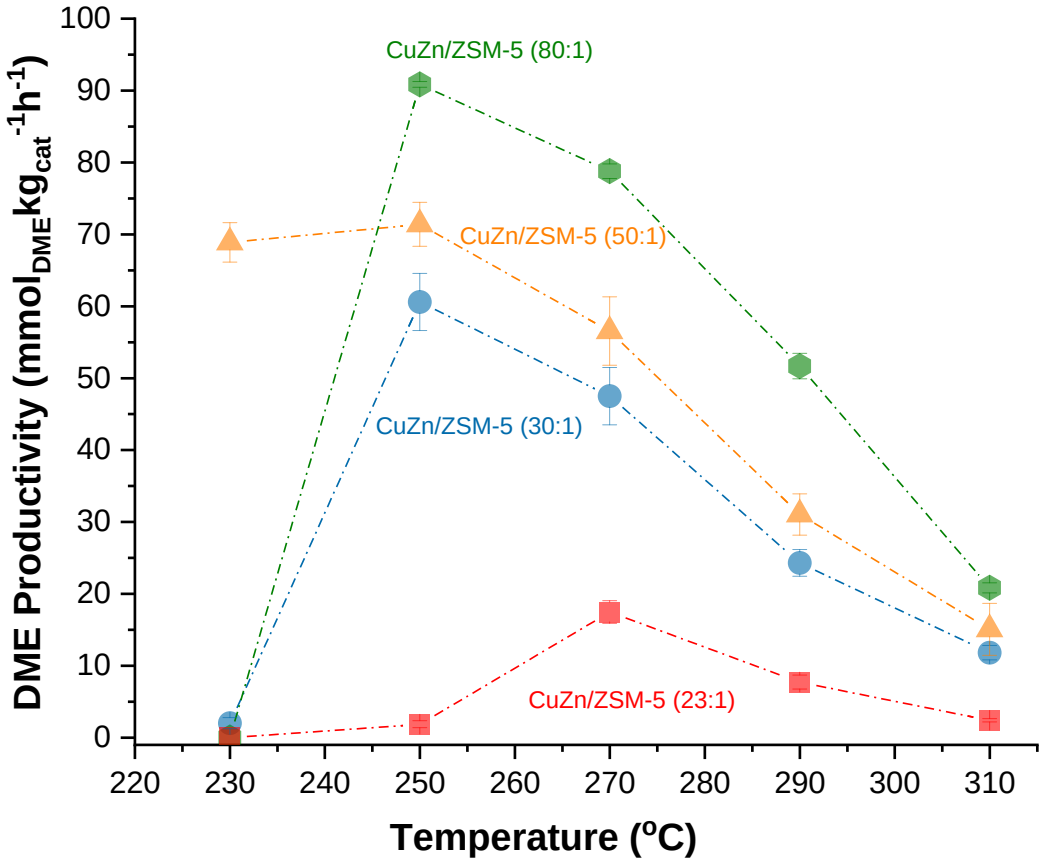

Figure 5.3 – DME productivity of CuZn/ZSM-5 catalyst series with Si:Al range (23, 30, 50 and 80) prepared via CVI, **reduced *in-situ***: 1 h at 220 °C in H_2 (2 °C min^{-1}, 1 bar, 30 ml min^{-1} STP). **Reaction conditions:** 230 - 310 °C, 6 h dwells (total = 30 h), 30 ml min^{-1} (STP) of CO_2 : N_2 : H_2 (1:1:3), P(total) = 20 bar.

A clear trend can be observed where a higher Si:Al ratio results in an increase in both methanol and DME productivity across the temperature range studied. From 250°C upwards a 4x increase in methanol productivity is observed, with the exception of CuZn/ZSM-5 (50:1) with a methanol productivity of 35 mmol$_{MeOH}$kg$_{cat}^{-1}$h^{-1} at 230°C. Beyond 250°C, a drop in methanol productivity is observed; however, the catalysts, apart from CuZn/ZSM-5 (23:1), all fall within the same range. The maximum methanol productivity for the CuZn/ZSM-5 CVI series is 61 mmol$_{MeOH}$kg$_{cat}^{-1}$h^{-1} at 270°C for (80:1).

The differences in catalyst performance are more apparent in the DME productivities; the greatest DME productivity is 91 mmol$_{DME}$kg$_{cat}^{-1}$h^{-1} at 250°C for CuZn/ZSM-5 (80:1). The major difference between the catalysts in the series is the CuZn/ZSM-5 (23:1) catalyst; although the same trend of an initial increase in productivity and then decrease with increased temperature is seen, the values are much lower than other systems, giving MeOH and DME productivities of 17 mmol$_{MeOH}$kg$_{cat}^{-1}$h^{-1} and 18 mmol$_{DME}$kg$_{cat}^{-1}$h^{-1}, respectively. The change is attributed to the increased acidity of the catalyst, resulting in the formation

of other hydrocarbon products with increased temperature; additional products formed include: ethane and propane.

In addition to the ZSM-5 series of catalysts, CuZn catalysts on mordenite (20:1) and zeolite Y were also prepared via the CVI method and tested for methanol and DME productivity under the same conditions above. The results are given in Figure 5.4.

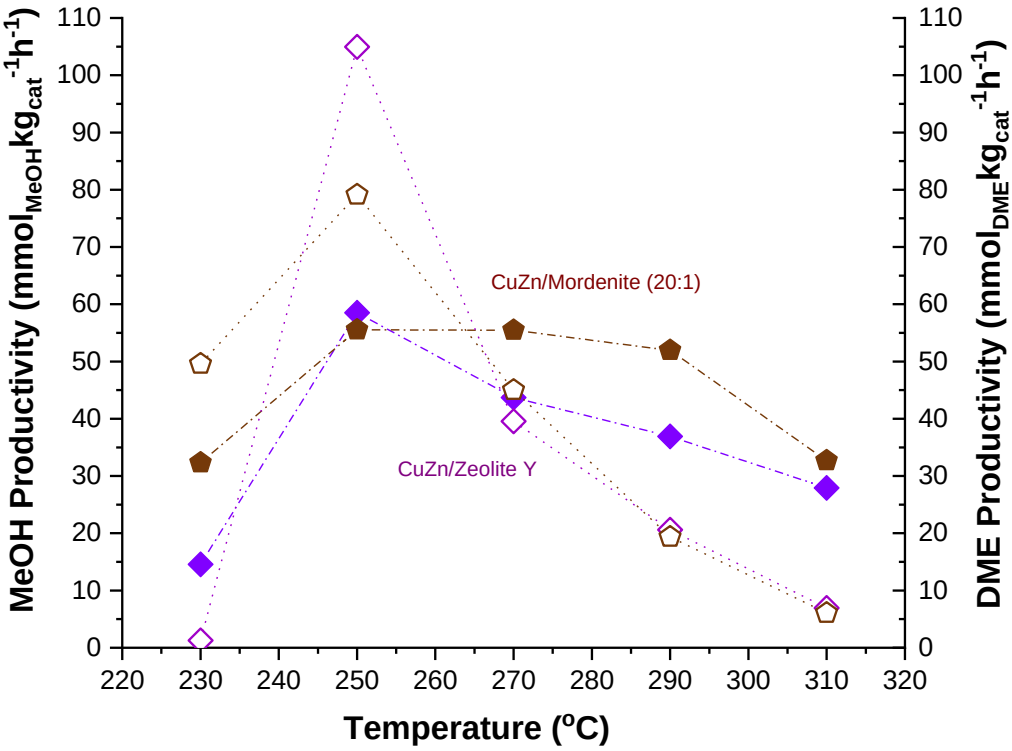

Figure 5.4 – MeOH (filled symbols) and DME productivity (open symbols) of CuZn/mordenite (20:1) and CuZn/Zeolite Y prepared via CVI, **reduced *in-situ***: 1 h at 220 °C in H_2 (2 °C min^{-1}, 1 bar, 30 ml min^{-1} STP). **Reaction conditions:** 230 - 310 °C, 6 h dwells (total = 30 h), 30 ml min^{-1} (STP) of CO_2 : N_2 : H_2 (1:1:3), P(total) = 20 bar.

From the results shown, both catalysts follow a similar trend as for the ZSM-5 series with regards to the MeOH productivity; an increase in productivity is observed up to 250°C before decreasing with increased temperature. The decrease in productivity is more rapid for the zeolite Y catalyst compared to the mordenite catalyst. The highest methanol productivity of 59 mmol$_{MeOH}$kg$_{cat}^{-1}$h^{-1} is achieved for the CuZn/zeolite Y catalyst, which is a slightly higher from the most active ZSM-5 catalyst (80:1), observed at 250°C. For the DME productivities, a substantial increase occurs at 250°C, with the CuZn/Zeolite Y achieving the highest DME productivity of 105 mmol$_{DME}$kg$_{cat}^{-1}$h^{-1} compared to 79 mmol$_{DME}$kg$_{cat}^{-1}$h^{-1} for mordenite. Again, comparing against the most active of the ZSM-5 series (80:1), there is a small increase. Increasing the temperature further results in a large drop in DME productivity

at a much faster rate than the ZSM-5 catalysts, with the exception of CuZn/ZSM-5 (23:1) which performs consistently poorly.

Table 5.1: *Conversion and selectivity data for CuZn/Zeolite catalysts at 250°C*

Catalyst	Temperature (°C)	X CO_2 (%)	S MeOH (%)	S DME (%)	S CO (%)
CuZn/ZSM-5 (23:1)	250	3.3	0.8	0.5	98.7
CuZn/ZSM-5 (30:1)	250	3.2	5.8	14.9	79.3
CuZn/ZSM-5 (50:1)	250	2.8	6.0	17.6	76.4
CuZn/ZSM-5 (80:1)	250	3.4	6.4	22.1	71.0
CuZn/Zeolite Y	250	1.4	10.1	36.0	53.9
CuZn/Mordenite (20:1)	250	2.7	6.4	18.2	75.4

Comparing the data in Table 5.1 the ZSM-5 catalysts show an increase in selectivity towards MeOH and DME at 250°C as the Si:Al ratio increases, and a low CO_2 conversion of 3%. As explained previously, the selectivity data for CuZn/ZSM-5 (23:1) is lower than the other catalysts in the series due to the formation of additional hydrocarbons.

Although the additional zeolite catalysts achieve lower CO_2 conversions, the selectivities for CuZn/Zeolite Y are far greater than ZSM-5, with a MeOH selectivity of 10% and DME selectivity of 36% when compared with the ZSM-5 series; the CuZn/mordenite catalyst also performs similar to the most active of the ZSM-5 series (80:1). As the reaction proceeds, a decrease in selectivity is observed in all the catalysts as the temperature increases.

In order to understand the activity of the catalysts described here, characterisation using XRD and surface area analysis was conducted. The results are shown in Figure 5.5 and Table 5.2. From the XRD patterns, there are two distinct peaks at 2θ = 43.3° and 50.4° assigned to metallic Cu (cubic) and correspond to the (111) and (200) planes respectively (PDF ref. 01-071-4609). Additional peaks observed at 31.8, 34.4, 36.2, 47.5 and 56.5° are associated with ZnO (hexagonal) and these correspond to the (100), (002), (101), (102) and (110) planes respectively (PDF ref. 01-074-9940). The sharpness and high intensity of the Cu peaks with an increase in Si:Al suggest larger particle sizes, as shown in Table 5.2 where the particle size was calculated using the Scherrer equation at 2θ = 43.3°. The overall

surface areas and pore sizes are fairly similar amongst the ZSM-5 series, these were determined from the N_2 adsorption isotherms (- 196°C), and the Cu particle sizes are all large, particularly for the more active catalyst, suggesting additional factors, in addition to the Si:Al ratio, are influencing the activity of the catalysts.

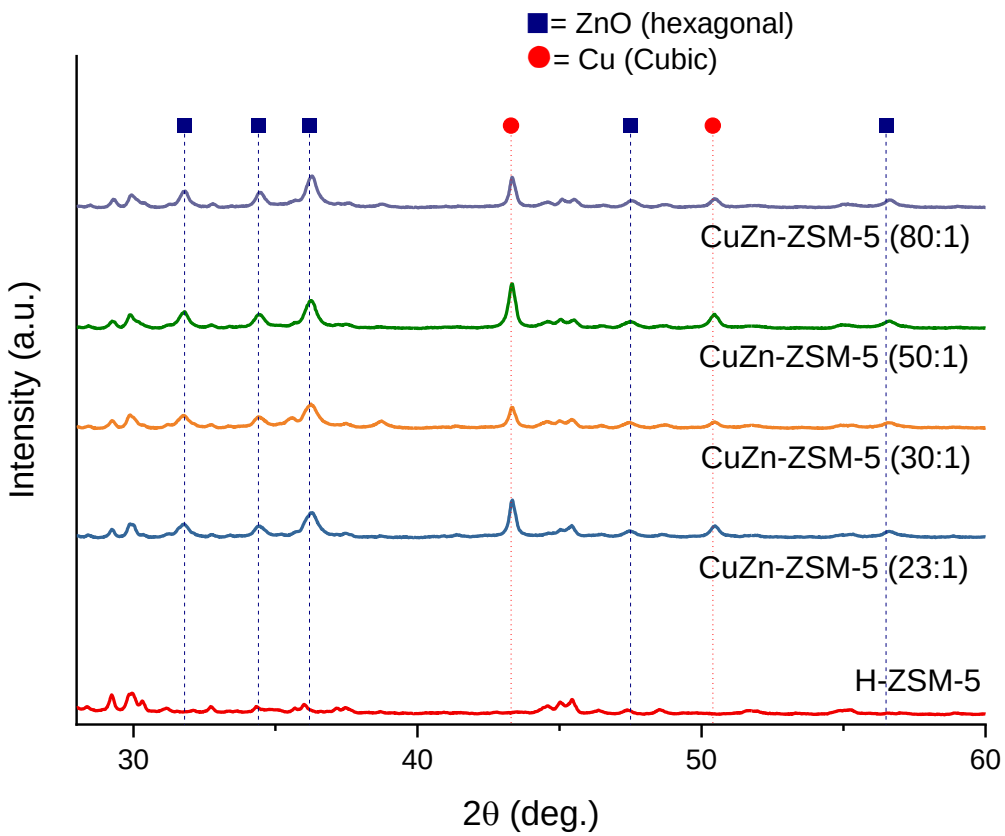

Figure 5.5 – XRD Patterns for reduced CuZn/ZSM-5 CVI series. Cu (○) and ZnO (□) regions have been highlighted.

Table 5.2: *Physiochemical properties of CuZn/zeolite CVI catalysts.*

Catalyst	Cu Particle Size (nm)*	BET Surface area (m^2/g)	Pore Width (Å)
CuZn/ZSM-5 (23:1)	51	258	4.8
CuZn/ZSM-5 (30:1)	71	279	4.9
CuZn/ZSM-5 (50:1)	54	273	4.9
CuZn/ZSM-5 (80:1)	76	297	4.8
CuZn/Mordenite	50	326	5.2 and 4.4
CuZn/Zeolite Y	55	467	5.0, 6.4 and 8.2

**Calculated via Scherrer Equation for Cu (111) at 43.3°*

5.2.2 – Cu/Zn and Cu/Zr Zeolite Catalysts Prepared by Oxalate Gel Precipitation

As established in Section 5.2.1, the preparation of CuZn/Zeolite catalysts via the chemical vapour impregnation method results in the formation of large Cu particles along the surface of the zeolite catalyst, rendering them relatively inactive. In order to improve, an alternative methodology must be adopted to reduce the particle size. Here, the oxalate gel method described in Section 2.2.3 is used as this is an effective and reproducible catalyst preparation technique in producing Cu/ZrO_2 catalysts with Cu particles around 11 nm. A series of 20 wt.% CuZn (1:1) catalysts were prepared on commercial ZSM-5 zeolites (Si:Al 23; 50 and 80) and on mordenite (20:1) and zeolite Y. These catalysts were tested for MeOH, DME and additional hydrocarbon synthesis over a temperature range of 230 – 310°C. The results for the ZSM-5 zeolites are shown in Figures 5.6 and 5.7, the Figures are scaled for ease of comparison.

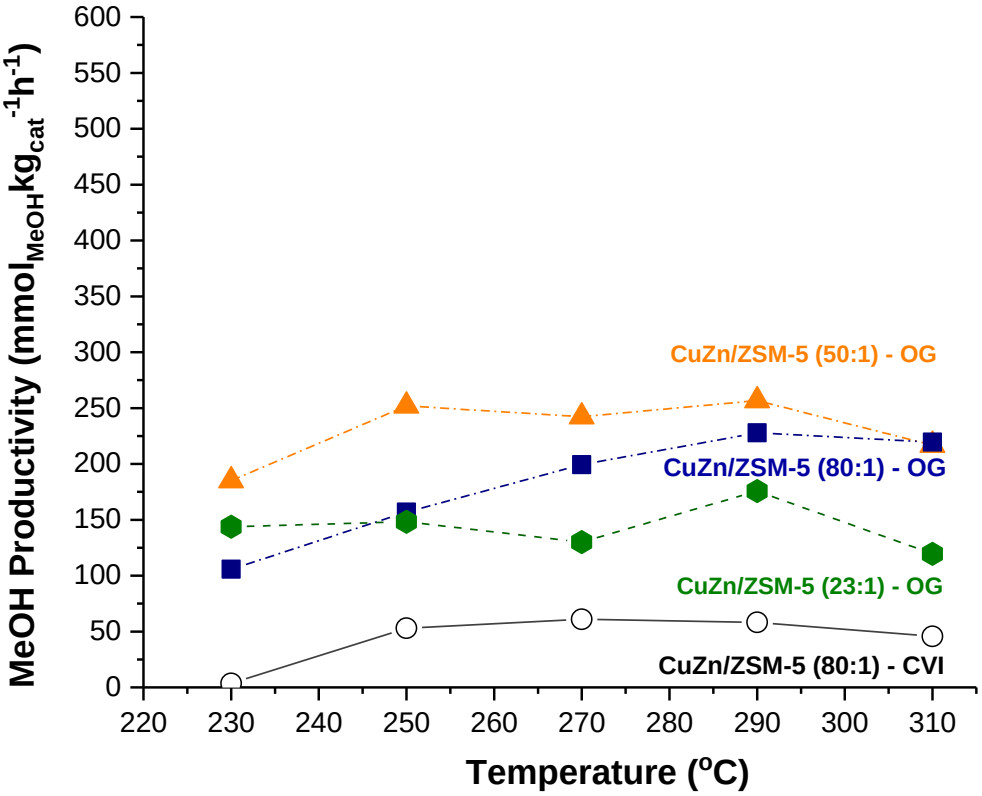

Figure 5.6 – Methanol productivity of CuZn/ZSM-5 catalyst series with Si:Al range (23, 30, 50 and 80) prepared via oxalate gel, **reduced *in-situ***: 1 h at 220 °C in H_2 (2 °C min^{-1}, 1 bar, 30 ml min^{-1} STP). CuZn/ZSM-5 (80:1)-CVI is also plotted for comparison. **Reaction conditions:** 230 - 310 °C, 6 h dwells (total = 30 h), 30 ml min^{-1} (STP) of CO_2 : N_2 : H_2 (1:1:3), P(total) = 20 bar.

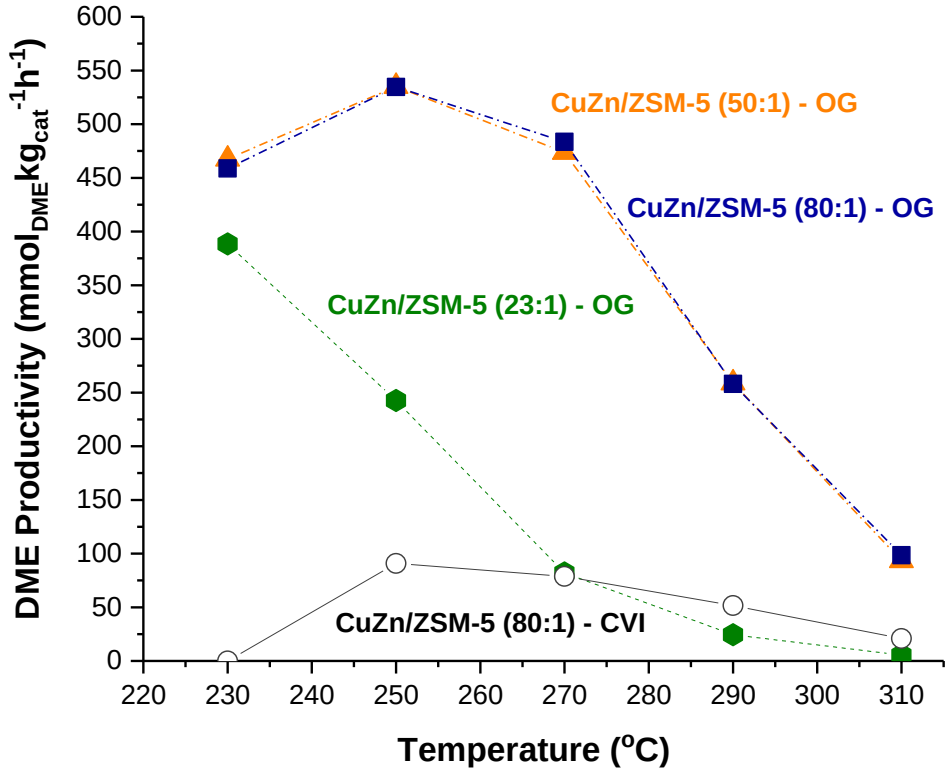

Figure 5.7 – DME productivity of CuZn/ZSM-5 catalyst series with Si:Al range (23, 30, 50 and 80) prepared via oxalate gel, **reduced *in-situ***: 1 h at 220 °C in H_2 (2 °C min^{-1}, 1 bar, 30 ml min^{-1} STP). CuZn/ZSM-5 (80:1)-CVI is also plotted for comparison. **Reaction conditions:** 230 - 310 °C, 6 h dwells (total = 30 h), 30 ml min^{-1} (STP) of CO_2 : N_2 : H_2 (1:1:3), P(total) = 20 bar.

Comparing the results of the CuZn/ZSM-5 oxalate gel (OG) series against the most active of the CuZn/ZSM-5 CVI series (80:1), the catalysts produced via the oxalate gel method show almost 5x higher methanol and DME productivity, achieving a methanol productivity of 242 mmol$_{MeOH}$kg$_{cat}^{-1}$h^{-1} (against 61 mmol$_{MeOH}$kg$_{cat}^{-1}$h^{-1}) at 270°C and DME productivity of 535 mmol$_{DME}$kg$_{cat}^{-1}$h^{-1} (against 71 mmol$_{DME}$kg$_{cat}^{-1}$h^{-1}) at 250°C, respectively. Comparing the productivity profiles of the oxalate gel series against the CVI series, after a small drop in the methanol productivity at 270°C there is an increase at 290°C, for both CuZn/ZSM-5 (23:1) and (50:1), which is likely due to competing reactions as you approach equilibrium, and a continuous increase in methanol productivity with increased temperature for CuZn/ZSM-5 (80:1). These fluctuations are not observed in the CVI catalyst series.

The MeOH and DME productivities, unlike the CVI series, for the 50:1 and 80:1 catalysts are fairly similar; substantial differences are observed for the 23:1 catalyst, as reflected previously in the CVI series. Again, this is due to the formation of additional hydrocarbons (analysed using a GC where additional hydrocarbons were identified using an Agilent gas mix) as the reaction temperature increases, whereby the increase in acidity of the ZSM-5 support aids in the formation of longer chain hydrocarbons. Hydrocarbon products formed include ethane, propane, butane and Cis/trans-2-butene and 1-pentene.

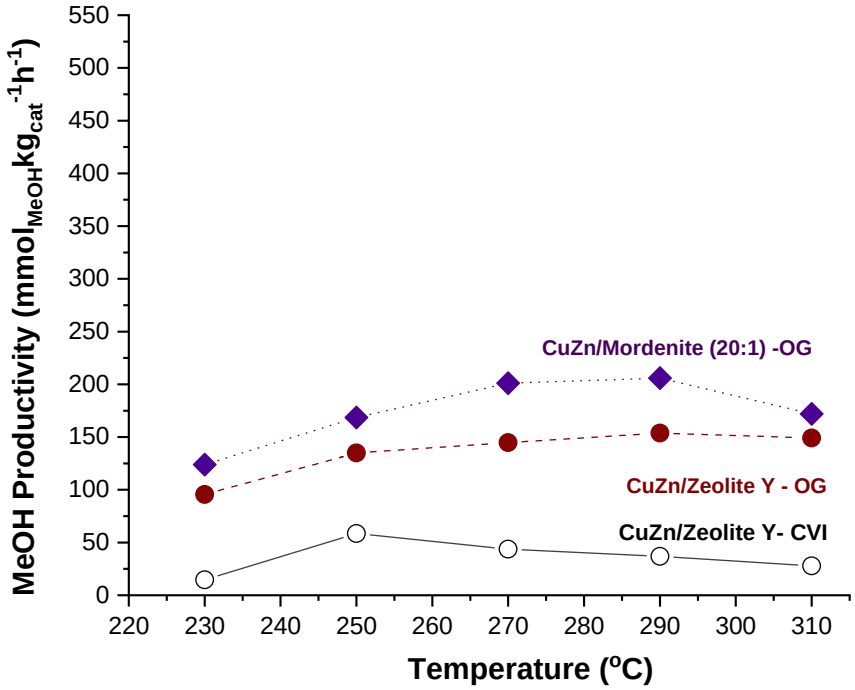

Figure 5.8 – MeOH productivity of CuZn/mordenite (20:1) and CuZn/Zeolite Y prepared via oxalate gel, **reduced *in-situ***: 1 h at 220 °C in H_2 (2 °C min^{-1}, 1 bar, 30 ml min^{-1} STP). CuZn/Zeolite Y-CVI is also plotted for comparison. **Reaction conditions:** 230 - 310 °C, 6 h dwells (total = 30 h), 30 ml min^{-1} (STP) of CO_2 : N_2 : H_2 (1:1:3), P(total) = 20 bar.

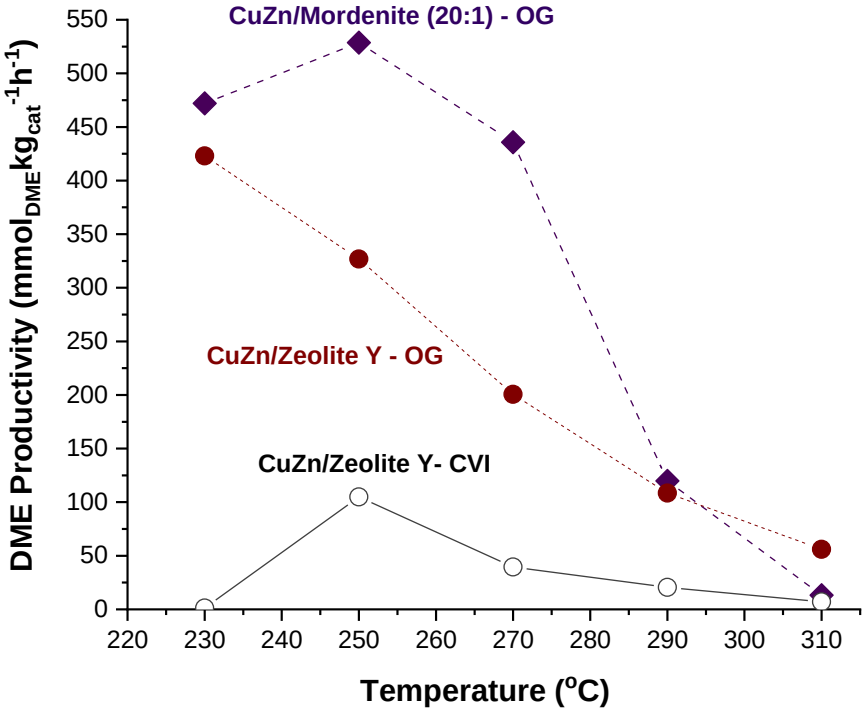

Figure 5.9 – DME productivity of CuZn/mordenite (20:1) and CuZn/Zeolite Y prepared via oxalate gel, **reduced *in-situ***: 1 h at 220 °C in H_2 (2 °C min^{-1}, 1 bar, 30 ml min^{-1} STP). CuZn/Zeolite Y-CVI is also plotted for comparison. **Reaction conditions:** 230 - 310 °C, 6 h dwells (total = 30 h), 30 ml min^{-1} (STP) of CO_2 : N_2 : H_2 (1:1:3), P(total) = 20 bar.

In addition to the ZSM-5 series of catalysts, CuZn catalysts on mordenite (20:1) and zeolite Y were also prepared via the oxalate gel method and tested for methanol and DME productivity under the same conditions. The results are shown above in Figures 5.8 and 5.9.

Comparing the methanol productivity profiles of the CuZn/mordenite (20:1) and zeolite Y catalysts prepared by oxalate gel and CVI, the catalysts prepared via the oxalate gel method are almost 3x more active; the highest methanol productivity of 206 $mmol_{MeOH}kg_{cat}^{-1}h^{-1}$ is achieved by CuZn/mordenite (20:1) at 290°C. The productivity falls slightly short of the CuZn/ZSM-5 (50:1) catalyst at the same temperature, with 257 $mmol_{MeOH}kg_{cat}^{-1}h^{-1}$. The oxalate gel catalysts show a more steady decline in methanol productivity in comparison to the CVI catalyst, as the temperature increases as was also seen for the CuZn/ZSM-5-OG series, suggesting the oxalate gel catalysts are less unstable.

Looking at the DME productivity data, a slightly different trend is seen; the CuZn/Zeolite Y catalyst starts with a DME productivity of 423 $mmol_{DME}kg_{cat}^{-1}h^{-1}$ at 230°C, but this falls as the temperature is increased, which is the opposite to the equivalent CVI catalyst, which follows a similar trend to the mordenite catalyst. The result may be linked to a change in the zeolite or CuZn particles as the reaction proceeds. The CuZn/mordenite (20:1) catalyst achieves the highest DME productivity of 528 $mmol_{DME}kg_{cat}^{-1}h^{-1}$ at 250°C, which is 5x higher than the CuZn/Zeolite Y catalyst prepared by CVI.

The results described above are in contrast to the CVI data shown in Figure 5.4, where the zeolite Y catalyst was more active. Comparing the methanol and DME productivities of the CuZn/mordenite (20:1) catalyst prepared by oxalate gel with the ZSM-5 series of catalysts prepared by the same method, it can be said that the mordenite catalyst performs very similarly to the CuZn/ZSM-5 (80:1) catalyst. The results suggest that changes in the catalyst are introduced when depositing the Cu and Zn onto the zeolites using the different preparation methods.

When comparing the CuZn/ZSM-5 series prepared by the oxalate gel method, the CuZn/ZSM-5 (50:1) is the most active catalyst, this is also true when compared to the mordenite and zeolite Y catalysts prepared by oxalate gel, and this may be linked to the individual structures of the zeolites used in the reaction.

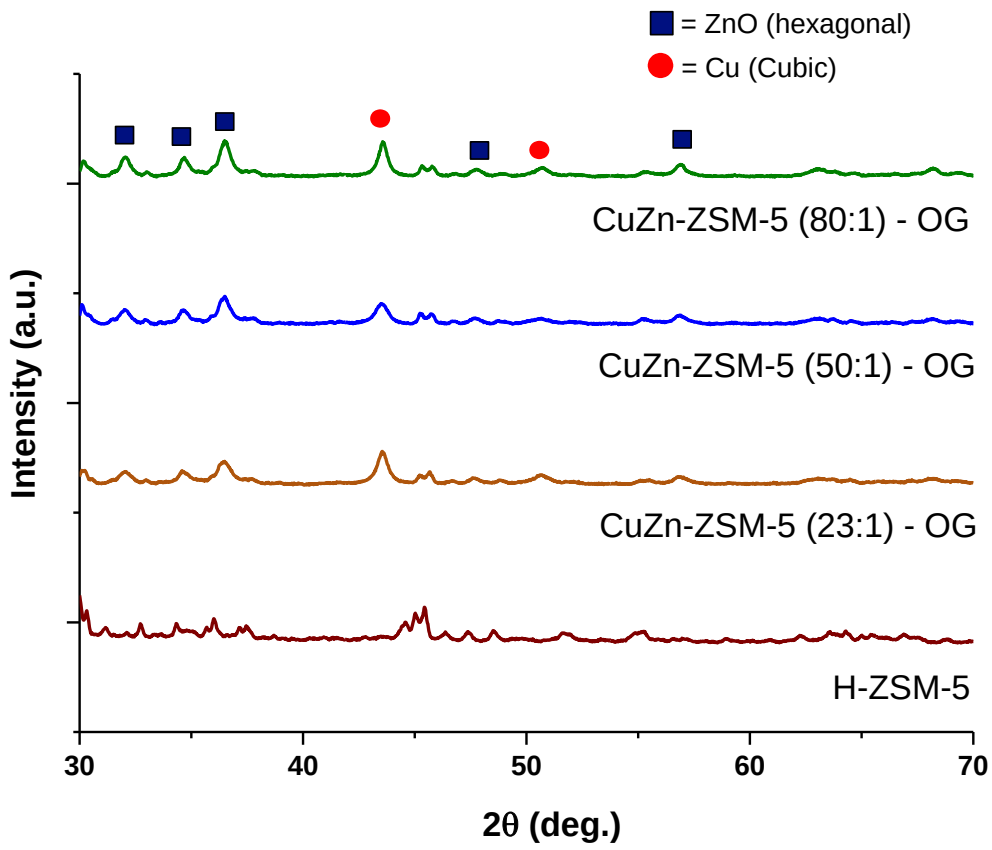

Figure 5.10 – XRD Patterns for reduced CuZn/ZSM-5 oxalate gel series. Cu (○) and ZnO (□) regions have been highlighted.

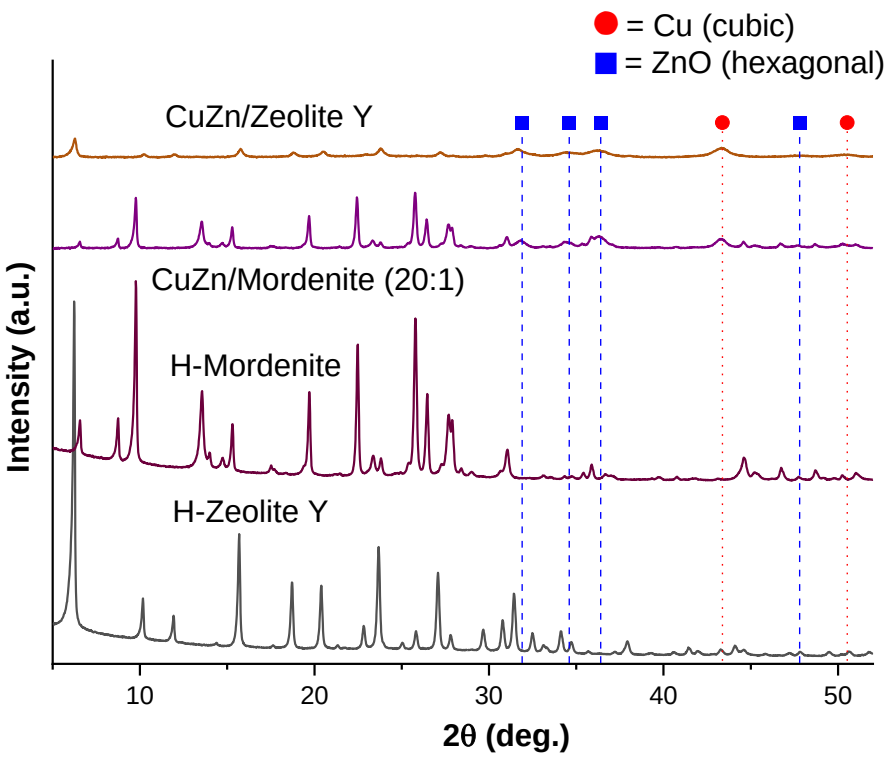

Figure 5.11 – XRD Patterns for reduced CuZn/Zeolite Y and mordenite (20:1) oxalate gel catalysts. Cu (○) and ZnO (□) regions have been highlighted.

Table 5.3: *Physiochemical properties of CuZn/zeolite oxalate gel catalysts.*

Catalyst	Cu Particle Size (nm) reduced and post-reaction*	BET Surface area (m^2/g)	Pore Width (Å)
CuZn/ZSM-5 (23:1)	13 (23)	277	4.9
CuZn/ZSM-5 (50:1)	13 (14)	211	5.0
CuZn/ZSM-5 (80:1)	15 (20)	303	5.0
CuZn/Mordenite	9 (11)	253	4.0 & 5.1
CuZn/Zeolite Y	14 (17)	336	5.0, 6.4 & 7.9

**Calculated via Scherrer Equation for Cu (111) at 43.3°, post-reaction particle size highlighted in red.*

The catalysts were characterised using XRD and the Scherrer equation used to determine the Cu particle size before and after reaction using the Cu (111) at 2θ = 43.3°, BET surface area measurements were made to monitor the changes from the fresh support to the support after the addition of Cu and Zn. The results are shown above in Figures 5.10 and 5.11, and Table 5.3. Comparing the XRD patterns for the oxalate gel series to those prepared via CVI in Figure 5.4, the distinct peaks at 2θ = 43.3° and 50.4° assigned to metallic Cu (cubic) and corresponding to the (111) and (200) planes respectively (PDF ref. 01-071-4609) appear less intense and more broad; upon further analysis the particle sizes are reduced by up to 5x, and even after reaction there is a very small increase in particle size, which is unexpected due to the higher temperatures used during the reaction. Additional peaks observed at 31.8, 34.4, 36.2, 47.5 and 56.5° associated with ZnO (hexagonal) remain the same in both sets of catalysts, and these correspond to the (100), (002), (101), (102) and (110) planes respectively. (PDF ref. 01-074-9940).

The peaks expected for metallic Cu and ZnO are also observed for the CuZn/zeolite Y and mordenite (20:1) catalysts; here, the metallic Cu peaks are less intense and broader, suggesting even smaller Cu particles, particularly for the mordenite (Table 5.3.) Interestingly only a small growth in Cu particle size is observed across all the catalysts post reaction.

Comparing the pore widths, the sizes remain the same, around 5 Å for the ZSM-5 catalysts, and for the mordenite and zeolite Y catalysts it differs slightly; although they are both large pore zeolites, zeolite Y displays a larger pore diameter of 7.9 for its main channel compared to 5.1 Å recorded for mordenite, the other pore sizes however, are of similar size suggesting the method of Cu and Zn deposition used

does not greatly impact the internal structure of the zeolites. However, the surface areas do change according to the type of preparation method used, with a decrease in the surface area observed for the oxalate gel series, which suggests that there are more Cu and Zn particles incorporated onto the zeolite and available for reaction.

Combining the information above it can be said that the choice of preparation method used to deposit the Cu and Zn onto the zeolite greatly influences the size of the resulting particles; here, the oxalate gel method is shown to produce smaller particles compared to CVI. In addition, the selection of zeolite, with regards to the Si:Al ratio, also impacts the activity, with a less acidic support (higher Si:Al) resulting in a more selective catalyst towards DME and MeOH.

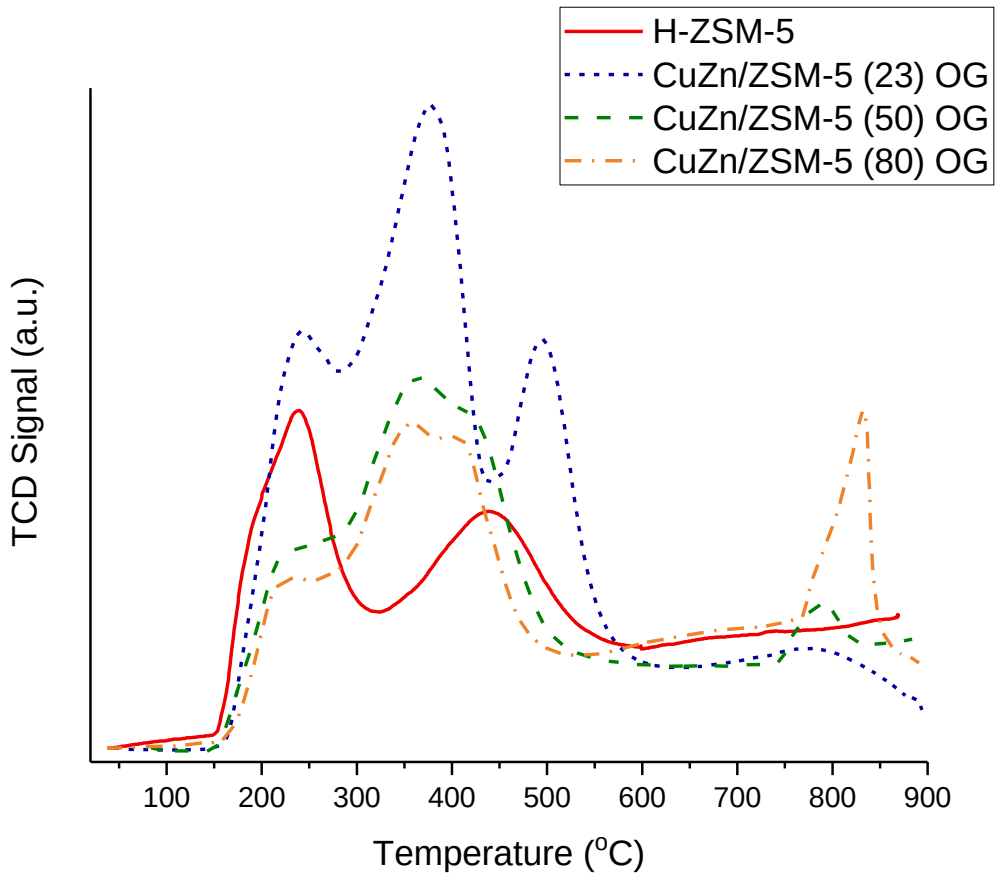

Figure 5.12– NH_3 -TPD Patterns for CuZn/ZSM-5 series prepared via oxalate gel.

NH_3-TPD measurements were taken for the CuZn/ZSM-5 catalysts prepared by the oxalate gel method and compared against the pure H-ZSM-5 zeolite in order to determine the acidity of the catalysts. From the figure, two major peaks are observed for H-ZSM-5: a lower temperature peak at 240°C, associated with the desorption of NH_3 from weak acid site (Lewis acid); and a higher temperature peak at 440°C, associated with the desorption of NH_3 from strong acid sites.[10] Additional peaks are also observed at lower temperatures between 355 and 410°C in the CuZn catalysts, and these are due to the formation of new medium-strength acid sites that arise from the Cu species interacting with the strong acid sites of the zeolite, making their acid strength weaker. As the Si:Al ratio increases, both the high and low temperature peaks shift to lower temperatures, indicating a decrease in the acid strength, this signifies the Al generates acidity; due to its valency, there is an overall negative charge (due to oxygen) on the zeolite which is balanced by a cation, for the ZSM-5 catalysts this charge is balanced by a proton to give a Brønsted acid.

To gain a deeper understanding of the acid sites on these catalysts, the acid sites were quantified via deconvolution of the peaks, by using individual peak areas of the NH_3-TPD profiles and a reference

factor (10554) from NH_3 calibration on the Quantachrome ChemBET TPR/TPD, the µmol NH_3 could be calculated. Dividing the µmol NH_3 by the mass of each catalyst and dividing further to convert to mmol gave the final acidities for each catalyst in mmol/g. This information is shown in Table 5.4.

Table 5.4: *Total number of acid sites for the CuZn/Zeolite catalysts prepared by oxalate gel.*

Catalyst	Total Acid Sites (mmol/g)	Weak Acid Sites (mmol/g)	Medium Acid Sites (mmol/g)	Strong Acid Sites (mmol/g)
CuZn/ZSM-5 (23:1) - OG	0.04	0.01	0.02	0.01
CuZn/ZSM-5 (50:1) - OG	0.02	0.004	0.008	0.005
CuZn/ZSM-5 (80:1) - OG	0.01	0.002	0.007	0.005
CuZn/Zeolite Y - OG	0.05	0.02	0.02	0.005
CuZn/Mordenite (20:1) - OG	0.04	0.01	0.015	0.015

As reflected in the NH_3-TPD profiles, an increase in the Si:Al ratio results in a decrease in the number of total acid sites available. CuZn/ZSM-5 (23) contains the highest amount of strong sites, compared to the other catalysts, as well as medium acid sites, suggesting these are essential towards the formation of higher hydrocarbons, likely through the stabilisation of key reaction intermediates over these sites, thus preventing them from further oxidation into CO and other undesired products. This can also relate back to the reactivity data shown in Figures 5.5 and 5.6, where the lower methanol and DME productivity can be correlated with a higher concentration of total acid sites, as well as the size of the particles. Comparing the zeolite Y and mordenite catalysts, it is clear that zeolite Y offers a greater number of acid sites but the mordenite catalyst contains more of the stronger acid sites, and this may be a factor towards the lower methanol and DME productivity observed in Figures 5.6 and 5.7.

Brønsted acid sites of zeolites act as catalytic sites for CH_3OH conversion via HCP mechanisms. Sufficient Brønsted acid sites ensure successive and efficient reactions. However, an of excess Brønsted acid sites coupled with a high acid strength can cause deactivation by fast coke deposition. In addition, both aromatic and alkene-based mechanisms can occur simultaneously in ZSM-5 zeolites, with the density of the acid sites determining which mechanism is more dominant. Stronger Brønsted acid sites have been linked to the formation of aromatics.[13, 14] Recent work by Gao and co-workers have shown that using a bifunctional catalyst consisting of a zeolite (SAPO-34) and metal oxide (In_2O_3-$ZnZrO_x$) are

effective for the direct hydrogenation of CO_2 to light olefins; the decreased quantity of Brønsted acid sites led to an increased selectivity in lower olefins, in addition, a reduced crystal size of the zeolite was shown to shorten the diffusion length from the surface to the acid sites inside the zeolite pores, thus favouring the mass transfer of intermediate species for efficient C–C coupling to generate lower olefins.[15] Work by Gascon et al. also supports this, interestingly they demonstrated that the incorporation of the alkaline earth metal Ca led to a higher selectivity of lighter olefins, this was attributed to a decrease in Brønsted acidity and formation of Lewis acidic sites. The decreased Brønsted acidity also inhibited the H-transfer reaction producing additional light olefins at the expense of longer chain hydrocarbons.[16]

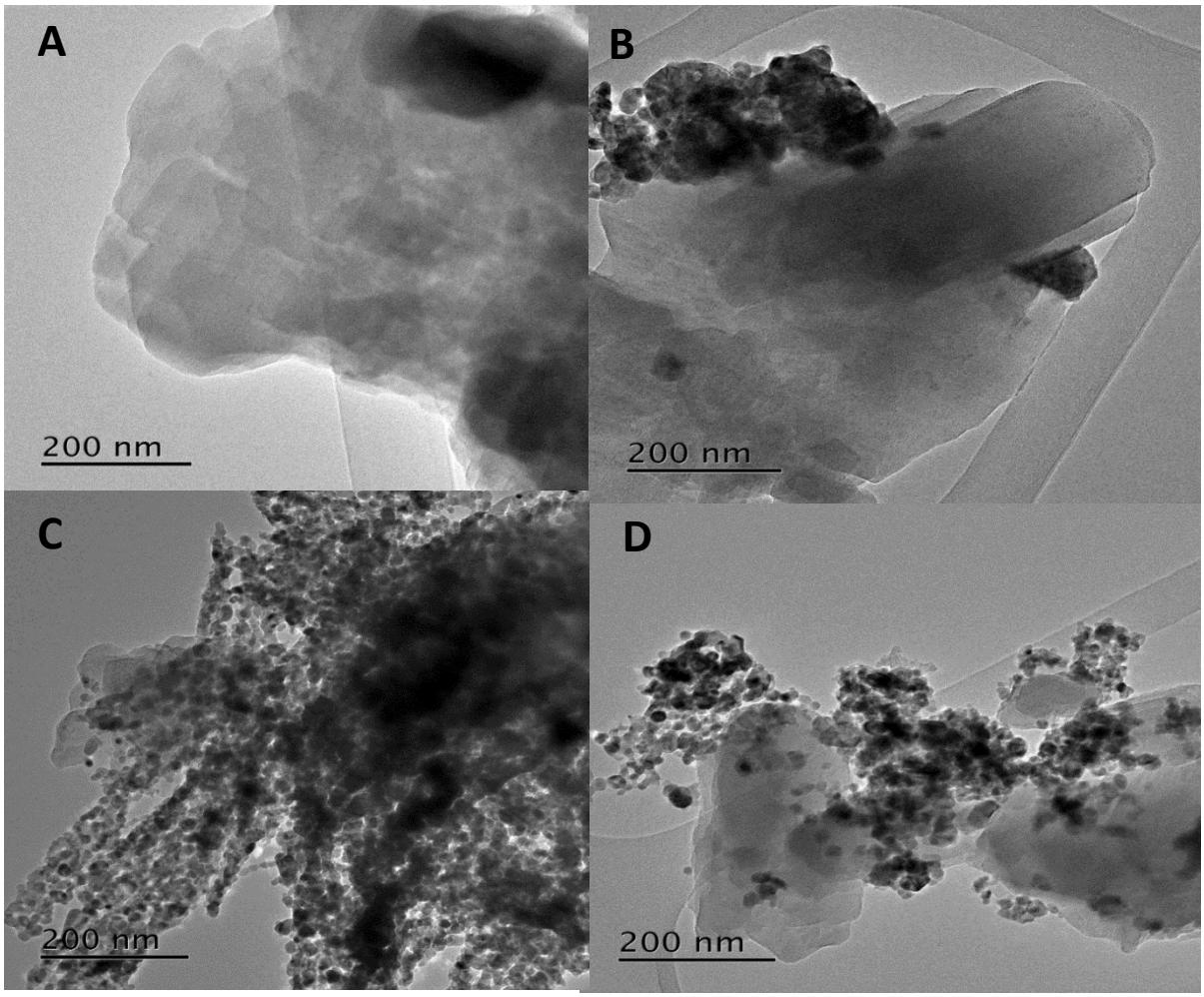

Figure 5.13 – TEM images of CuZn/ZSM-5 (23:1) – CVI and oxalate gel catalysts. **A** = CuZn/ZSM-5 (23:1) CVI – Reduced **B** = CuZn/ZSM-5 (23:1) CVI after reaction **C** = CuZn/ZSM-5 (23:1) OG – Reduced **D** = CuZn/ZSM-5 (23) OG after reaction.

TEM images of the CuZn/ZSM-5 (23:1) catalysts prepared via CVI and oxalate gel were compared after reduction and post reaction (Figure 5.8). In image **A**, the surface is very smooth as CuZn is present as an epitaxial layer and when left under the beam the particle growth can be observed i.e. it is beam

sensitive. After reaction (**B**), the particles begin to emerge on the surface as large agglomerates, and which is due to sintering during the reaction where the surface Cu is exposed to high temperatures. In contrast, the image for the CuZn/ZSM-5 catalyst prepared via oxalate gel after reduction (**C**) displays needles/strings of phase separated CuZn that are detached from the ZSM-5 support; after reaction (**D**), these are largely broken down and seen to accumulate as large clumps across various points on the ZSM-5 surface. Despite the lack of homogeneity and dispersion of the active metals on the surface of the zeolite, the oxalate gel catalyst still maintains its activity through the limited contact, suggesting the key intermediates formed have access to the channels of the zeolite necessary for the hydrocarbon formation. The large particles seen for the CVI catalyst, as supported by the XRD patterns, agglomerate to prevent access to the pores and result in poorly active nanoparticles.

As established in the previous experiments, the CuZn/ZSM-5 (23:1) catalyst was the most acidic of the ZSM-5 series, containing strong sites, and medium acid sites that are essential towards the formation of higher hydrocarbons. In an attempt to increase the hydrocarbon formation, the quantity of zeolite used during the preparation was doubled, whilst maintaining the loadings of Cu and Zn. The results are shown in Figure 5.14.

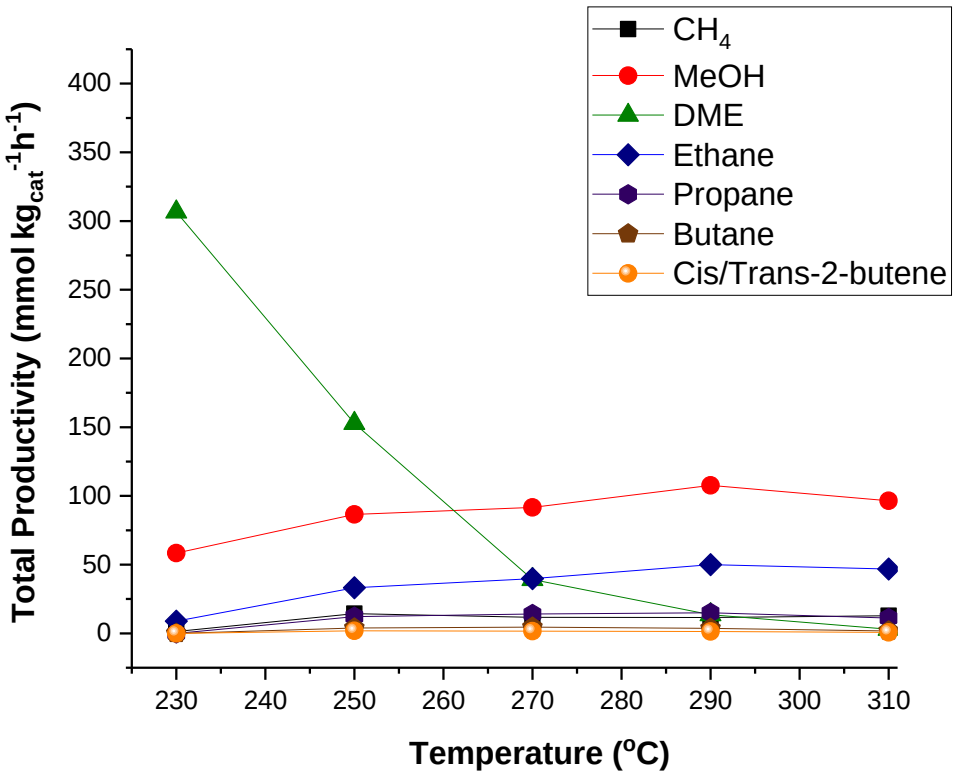

Figure 5.14 – Total productivity of CuZn/ZSM-5 (23:1) prepared via oxalate gel with double mass of zeolite (1 g), **reduced *in-situ***: 1 h at 220 °C in H_2 (2 °C min^{-1}, 1 bar, 30 ml min^{-1} STP). **Reaction conditions:** 230 - 310 °C, 8 h dwells (total = 40 h), 30 ml min^{-1} (STP) of CO_2 : N_2 : H_2 (1:1:3), P(total) = 20 bar.

Looking at the data above, the productivity profiles for all the products follow a similar trend, with the exception of DME, which starts at 307 $mmol_{DME}kg_{cat}^{-1}h^{-1}$ but drops significantly up to 270°C as the higher chain hydrocarbons start to form. Comparing with the previous CuZn/ZSM-5 (23:1) catalyst, the highest methanol productivity of 178 $mmol_{MeOH}kg_{cat}^{-1}h^{-1}$ was achieved at 290°C and DME productivity of 388 $mmol_{DME}kg_{cat}^{-1}h^{-1}$ at 230°C; in comparison, the methanol productivity for the catalyst with double the mass of zeolite was 108 $mmol_{MeOH}kg_{cat}^{-1}h^{-1}$ at 290°C. Although a drop in productivity is observed for MeOH and DME, small amounts of additional products up to C_4 are produced, suggesting a greater concentration of the essential acid sites of the zeolite for hydrocarbon formation.

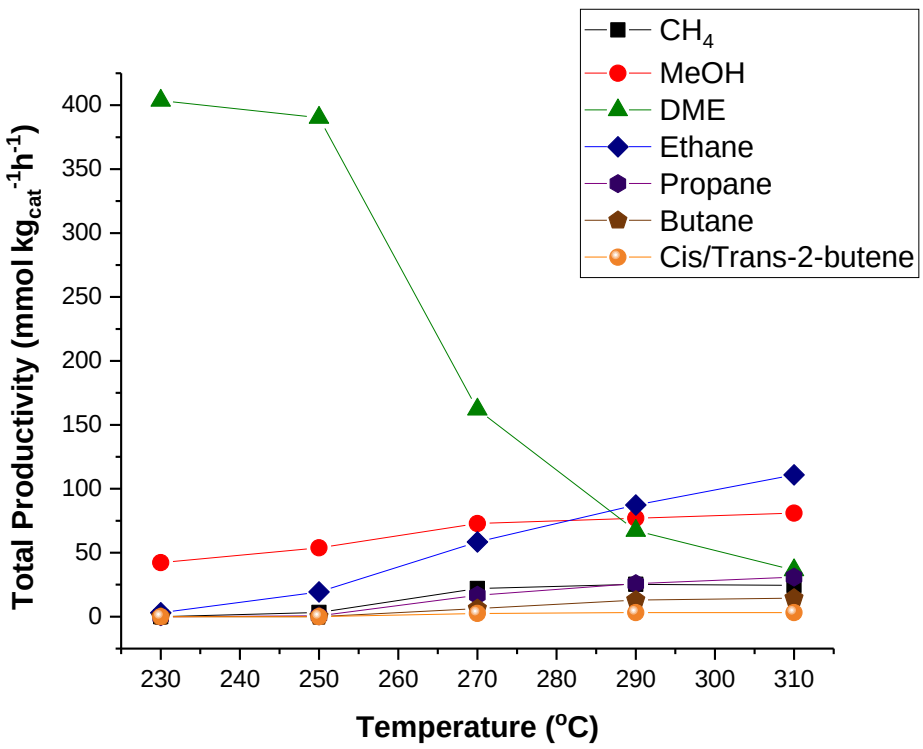

Figure 5.15 – Total productivity of CuZr/ZSM-5 catalyst with Si:Al (23:1) prepared via oxalate gel, **reduced *in-situ***: 1 h at 220 °C in H_2 (2 °C min^{-1}, 1 bar, 30 ml min^{-1} STP). **Reaction conditions:** 230 - 310 °C, 8 h dwells (total = 40 h), 30 ml min^{-1} (STP) of CO_2 : N_2 : H_2 (1:1:3), P(total) = 20 bar.

Although the combination of CuZn with a series of ZSM-5 zeolites was active towards the production of methanol, DME and higher hydrocarbons, a combination of several other copper-based catalysts could be used for the same reaction; indeed, in the previous chapters Cu/ZrO_2 prepared by the oxalate gel method is an active catalyst. Therefore, using the same method to prepare the CuZn/ZSM-5 (23:1) catalyst, an equivalent CuZr catalyst was made.

At the start of the reaction, results are shown in Figure 5.15, the DME productivity is at 408 $mmol_{DME}kg_{cat}^{-1}h^{-1}$; this then rapidly drops from 270°C as the additional hydrocarbons are formed. In comparison to the CuZn/ZSM-5 (23:1) catalyst, the DME productivity is much higher across the temperature range and the MeOH productivity is much lower, which shows that any methanol produced is quickly consumed to generate DME and this is then used in the formation of the higher hydrocarbons. From the data shown, the ethane productivity continuously increases from 250°C onwards and this is slowly followed by the generation of additional hydrocarbons up to C_4.

Recent work by Gascon et al. investigated CO_2 hydrogenation to methanol and its conversion to hydrocarbons using $ZrZnO_x$ catalysts, prepared by co-precipitation, combined with H-ZSM-5 and H-SAPO-34 through mechanical mixing. The best performance was observed for the $ZrZnO_X$ sample with 30% Zn, combined with ZSM-5 at 350 °C, 30 bar and $H_2/CO_2/N_2$ = 6/2/1. Under these conditions, the equilibrium methanol yield was observed after 0.4 s g^{-1} ml^{-1} over $ZrZnO_X$ alone. Mixing with ZSM-5 in a 1:1 weight ratio, methanol was rapidly converted to hydrocarbons, with an optimum C_3 productivity of 1.5 mol kg^{-1} h^{-1} at 24 000 ml h^{-1} g^{-1}.[17] Wang and coworkers developed a bifunctional catalyst composed of $ZnGa_2O_4$ and SAPO-34 which achieved 86% selectivity for C_2–C_4 olefins at 13% conversion of CO_2 (370°C, H_2/CO_2 = 3:1, 30 bar, 45 ml min^{-1}). The oxygen vacancies on the surface of $ZnGa_2O_4$ were responsible for CO_2 activation;[18] this is supported by Sun et al., where for the In_2O_3/H-ZSM-5 bifunctional catalyst, CO_2 was chemisorbed at the oxygen-vacancy sites on the surface of the reducible In_2O_3 and hydrogenated to CH_3OH through several intermediates. The CH_3OH intermediate entered the HZSM-5 zeolite and was further converted to hydrocarbon products at the surface acidic sites of the zeolite via a hydrocarbon-pool mechanism. The proximity of the two components was important in supressing the RWGS and to give a high selectivity for gasoline-range hydrocarbons.[19]

5.2.3 – Physically Mixed Catalysts

The preparation of 20 wt.% CuZn (1:1) catalysts on commercial ZSM-5 zeolites was successful previously by the oxalate gel method; however, from the TEM images not all of the Cu and Zn was homogenously distributed across the zeolite surface. Instead, large phase segregated Cu and Zn detached from the surface; despite this, the catalysts still remained active and the more acidic CuZn/ZSM-5 (23:1) was able to produce high chain hydrocarbons. In order to examine the degree of contact between the active metals and zeolite support, a physical mixture of 10% Cu/ZnO, prepared by the oxalate gel method, and commercial H-ZSM-5 (23:1) was made. Two methods of physical mixture were employed: the first involved shaking the two catalyst components; and the second involved grinding the components together to give the final catalyst. The results for both catalysts are given below in Figures 5.16 and 5.17.

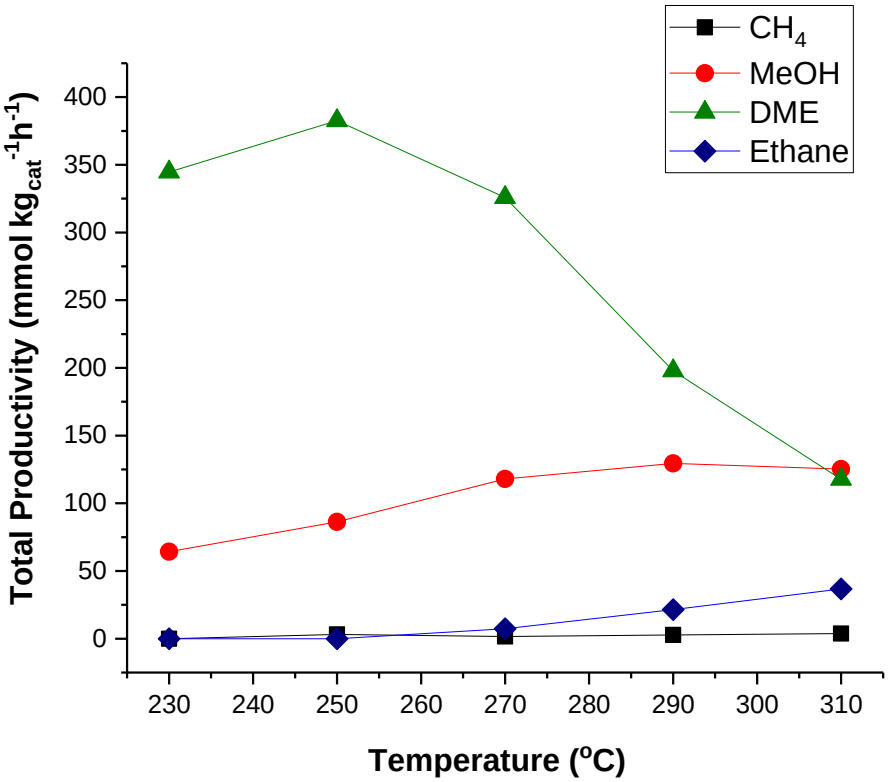

Figure 5.16 – Total productivity of 10% Cu/ZnO + ZSM-5 (23:1) physically mixed catalyst (shaken), **reduced *in-situ***: 1 h at 220 °C in H_2 (2 °C min^{-1}, 1 bar, 30 ml min^{-1} STP). **Reaction conditions:** 230 - 310 °C, 8 h dwells (total = 40 h), 30 ml min^{-1} (STP) of CO_2 : N_2 : H_2 (1:1:3), P(total) = 20 bar.

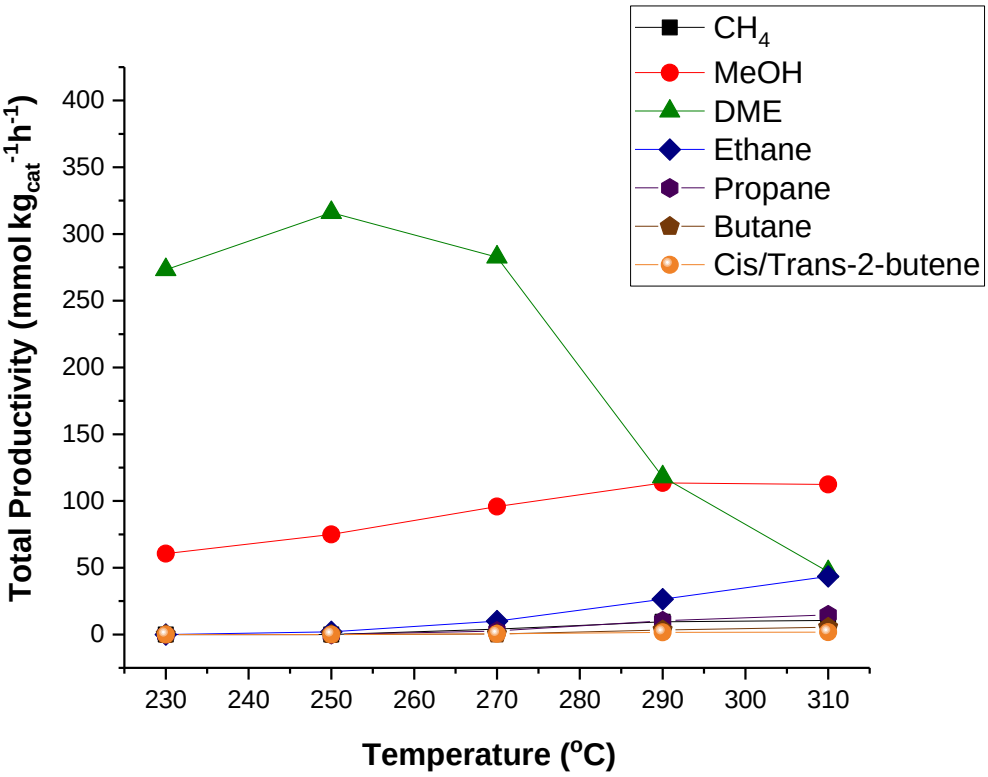

Figure 5.17 – Total productivity of 10% Cu/ZnO + ZSM-5 (23:1) physically mixed catalyst (*254*), **reduced *in-situ***: 1 h at 220 °C in H_2 (2 °C min^{-1}, 1 bar, 30 ml min^{-1} STP). **Reaction conditions:** 230 - 310 °C, 8 h dwells (total = 40 h), 30 ml min^{-1} (STP) of CO_2 : N_2 : H_2 (1:1:3), P(total) = 20 bar.

As expected, the DME productivity decreases after 250°C; the shaken catalyst achieved the highest DME productivity of 383 $mmol_{DME}kg_{cat}^{-1}h^{-1}$ at 250°C, and the ground catalyst achieved a DME productivity of 316 $mmol_{DME}kg_{cat}^{-1}h^{-1}$ at the same temperature. The methanol productivity remains fairly level across the temperature range, starting below 65 $mmol_{MeOH}kg_{cat}^{-1}h^{-1}$ at 230°C and ending at below 126 $mmol_{DME}kg_{cat}^{-1}h^{-1}$ at 310°C, as there is very little hydrocarbon formation.

Comparing the graphs above, it can be seen that the method where the two components of the catalyst were shaken resulted in only the formation of ethane as an additional product, although at very low productivity; the ground 10% Cu/ZnO + ZSM-5 (23:1) catalyst is able to produce higher chain hydrocarbons up to C_4. Although these productivities are low, the importance of the contact required between the strong acid sites of the zeolite and the active metals is demonstrated by revealing the changes in product distribution from the different physical preparation methods employed; also in contrast to previous results in this section, the methanol and DME productivities are lower, this shows the significance of the active metal sites in addition to the acid sites of the zeolite.

A recent study by Gohsh et. al proposed a kinetic model for the direct CO_2 hydrogenation to different hydrocarbon products over an In_2O_3/HZSM-5 bifunctional catalytic bed. The individual components were physically mixed in a mass ratio In_2O_3:HZSM-5 = 2:1 at a total of 1 g. The reaction was conducted at 20-40 bar, 250 - 400°C, H_2:CO_2 – 1:1 to 4:1. Interestingly no DME was detected under any conditions in the effluent gas stream suggesting any DME formed is consumed quickly to form hydrocarbons. Compared with the singular indium catalyst the mixed bed catalyst resulted in lower CO selectivity through the suppression of the undesired RWGS and a higher methanol yield which was mostly converted to hydrocarbons. At a pressure of 40 bar and H_2:CO_2 = 3:1 the mole fraction of methanol increases from 250°C to 350°C and then declines. The concentration of alkanes C_2-C_4 increases above 250°C and at higher temperatures of 350°C there is a rapid increase in alkanes, particularly propane. As seen in the results above however, at much lower concentrations. The presence of alkenes is also observed initially, but this reduces at higher temperatures (> 350°C). The differences observed in this study show that under particular conditions (high partial pressure of H_2, high temperatures, and catalyst mass ratio) the consumption of intermediates and hydrogenation of alkenes can result in higher hydrocarbon formation.[20]

From the information above, we have found that contact between the zeolite and active metals is important. The focus of the experiments conducted is to encourage the formation of DME through methanol dehydration and subsequent higher chain hydrocarbons at elevated temperatures. In order to maximise the efficiency of these reactions, changes to the catalyst bed were investigated. The changes involved either the pellets of the 10%Cu/ZnO and H-ZSM-5 (23:1) placed into separate beds, with the 10% Cu/ZnO placed at the end closest to the initial reaction feed followed by pellets of H-ZSM-5, or the pellets of both 10% Cu/ZnO and H-ZSM-5 were mixed and tested. The results are shown below in Figures 5.18 and 5.19.

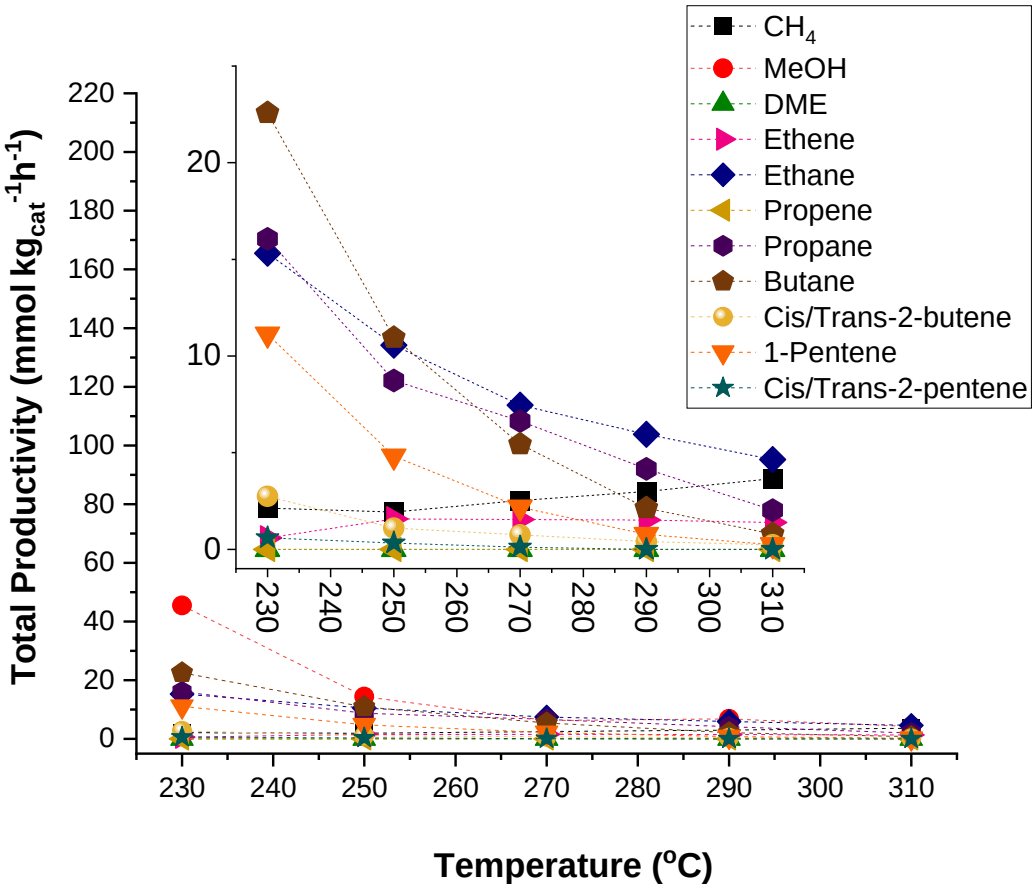

Figure 5.18 – Total productivity of 10% Cu/ZnO + H-ZSM-5 (23:1) pellets in separate beds, **reduced *in-situ***: 1 h at 220 °C in H_2 (2 °C min^{-1}, 1 bar, 30 ml min^{-1} STP). Insert shows product distribution at an enlarged scale for clarity. **Reaction conditions:** 230 - 310 °C, 8 h dwells (total = 40 h), 30 ml min^{-1} (STP) of CO_2 : N_2 : H_2 (1:1:3), P(total) = 20 bar.

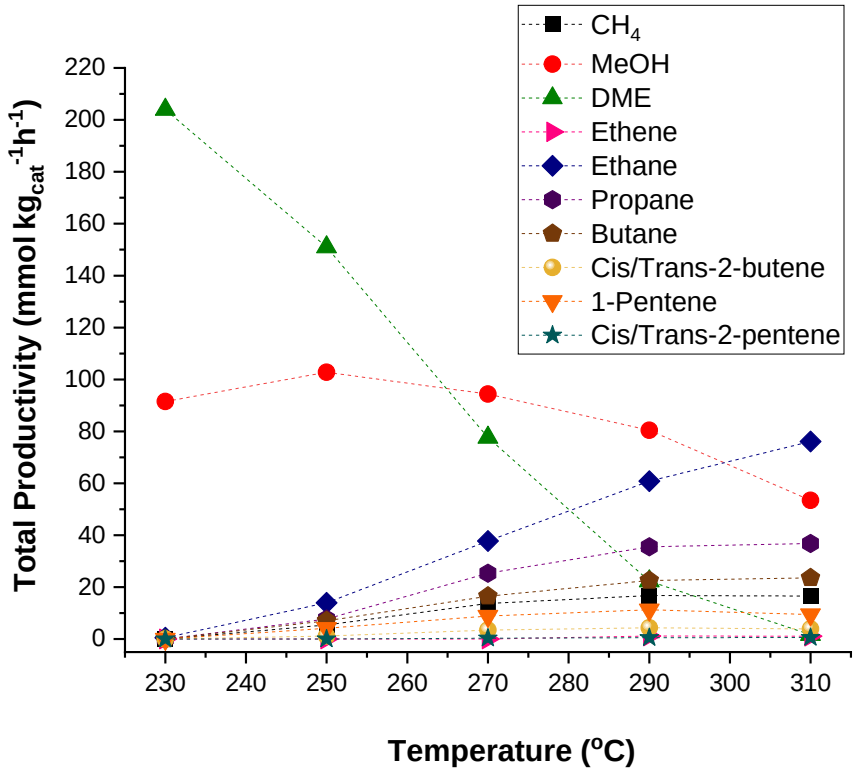

Figure 5.19 – Total productivity of 10% Cu/ZnO + H-ZSM-5 (23:1) pellets in mixed bed, **reduced *in-situ***: 1 h at 220 °C in H_2 (2 °C min^{-1}, 1 bar, 30 ml min^{-1} STP). **Reaction conditions:** 230 - 310 °C, 8 h dwells (total = 40 h), 30 ml min^{-1} (STP) of CO_2 : N_2 : H_2 (1:1:3), P(total) = 20 bar.

From the graphs, the mixed bed has a fourfold increase in total productivity compared to the separate bed. No DME is observed in the separate bed, suggesting that it is either instantly consumed on formation or not formed at all, even at the lower temperatures, as presence of additional hydrocarbons up to C_5 are observed from 230 °C. The total productivity falls below 25 mmol $kg_{cat}^{-1}h^{-1}$ for the separate bed and as the temperature is increased the total productivity decreases, most likely due to the decomposition of methanol to CO which is more favourable at higher temperatures.

Comparing with the results from the mixed bed, we can see there is a complete contrast in the profiles. The product distributions are fairly similar; however, the addition of propene is seen in the separate bed, at a very low productivity. In the case of the mixed bed, the DME is produced at the start and is then slowly consumed with increased temperature, as shown in the catalysts tested previously; compared to the CuZn/ZSM-5 (23:1)-OG catalyst, both the methanol and DME productivities are lower. However, the product distribution is much broader; of the additional products, the highest productivity of 76 $mmol_{C2H6}$ $kg_{cat}^{-1}h^{-1}$ was achieved for ethane at 310 °C.

The results between the catalyst beds and data in Table 5.5 can be linked to the direct exposure of Cu/ZnO catalyst and the contact time between the formed products and zeolite. For the separate bed, the methanol and DME formed have a direct contact with the H-ZSM-5 zeolite across the bed; however, the increasing temperature is likely to impact the exposed Cu/ZnO required for the methanol formation. For the mixed bed the zeolite is more distributed and in good proximity to the Cu/ZnO pellets within the catalyst bed, allowing the rate of DME formation to increase at lower temperatures. As the temperature increases (> 250 °C), the conversion to hydrocarbons increases and DME decreases, which could be associated with the strong acid sites beginning to deactivate (increased water production).

Excessive water has been shown to deactivate surface acidic sites on zeolites, inhibiting C–C bond formation and leading to a low production of C_{2+} products. Fujiwara et al. developed a composite catalyst consisting of a Cu–Zn–Al oxide and modified HB zeolite (addition of 1,4-bis(hydroxydimethylsilyl)benzene to the zeolite surface for hydrophobicity.), this significantly improved the yield of C_{2+} hydrocarbons by suppressing the deactivation of strong acidic sites.[21]

Table 5.5: *Conversion and selectivity data for 10% Cu/ZnO + H-ZSM-5 (23) mixed and separate bed*

10% Cu/ZnO + H-ZSM-5 (23)	Temperature (°C)	*X* CO_2 (%)	*S* MeOH (%)	*S* DME (%)	*S* CH_4 (%)	*S* CO (%)	*S* Ethane (%)	*S* Propane (%)	*S* Butane (%)	*S* 1-Pentene (%)
separate bed										
	230	**20.4**	1.4	1.1	0.1	90.0	0.1	1.6	2.6	1.7
	250	**24.0**	0.4	0	0.06	95.8	0.6	0.8	1.3	0.7
	270	**26.5**	0.2	0	0.06	97.8	0.4	0.5	0.6	0.3
	290	**29.7**	0.1	0	0.06	98.9	0.3	0.3	0.2	0.1
	310	**33.0**	0.1	0	0.08	99.3	0.2	0.1	0.1	0
mixed bed										
	230	**8.8**	6.7	30.0	0	63.2	0.1	0	0	0
	250	**15.6**	4.7	13.3	0.3	76.2	1.5	1.3	1.5	1.1
	270	**18.5**	3.6	6.0	0.5	79.2	2.9	2.9	2.5	1.7
	290	**20.5**	2.8	2.0	0.6	79.4	4.6	4.1	3.4	2.1
	310	**23.0**	1.5	0.1	0.5	85.5	4.5	3.2	2.8	1.4

The table above compares the CO_2 conversion and product selectivity data for the separate bed and mixed bed. For the separate bed, as the temperature and CO_2 conversion increase the selectivity to MeOH and DME decreases, and selectivity to higher chain hydrocarbons increases, particularly for butane up to 270 °C; however, CO remains the major product of the reaction. For the mixed bed, the CO_2 conversions are slightly smaller in comparison but the selectivity towards the higher chain hydrocarbons increases greatly after 270 °C, achieving up to 5% selectivity to ethane at 290 °C, 15x higher than the separate bed.

Pérez and co-workers proposed an eleven-*lump* kinetic model for the reaction of DME to olefins over a HZSM-5 catalyst, considering as *lumps*: methanol, water, DME, ethylene, propylene, butenes, C_2–C_4 paraffins, C_{5+} aliphatic hydrocarbons, BTX, methane and CO. It was shown that slightly above atmospheric pressure DME reacts at a lower temperature to olefins compared to methanol (350°C vs 450°C), and at the same temperature DME reacts 20 times faster than methanol. This is reflected in the results above, in particularly for the mixed bed, where the DME is consumed much quicker as the reaction temperature increases when compared to methanol. [22]

The previous experiment involving the variation in the catalyst bed has shown very interesting results, this is attributed to the contact between the active metal sites and key acid sites of the zeolite, and this can be used in order to influence the product distribution. By preparing a mixed bed catalyst consisting of 31% Cu/ZrO_2 catalyst and commercial H-ZSM-5 (23:1), it was hoped that the catalyst would be more active than those tested previously. As the CuZr/ZSM-5 (23:1) catalyst prepared via the oxalate gel was able to show reasonable productivities towards the desired products (Figure 5.13), the introduction of the ZSM-5 (23:1) zeolite via a mixed bed, with the addition of a higher Cu loading was expected to aid in an increase in methanol productivity and DME productivity, and subsequently the productivities of the higher chain hydrocarbons. The results for this are shown in Figure 5.20.

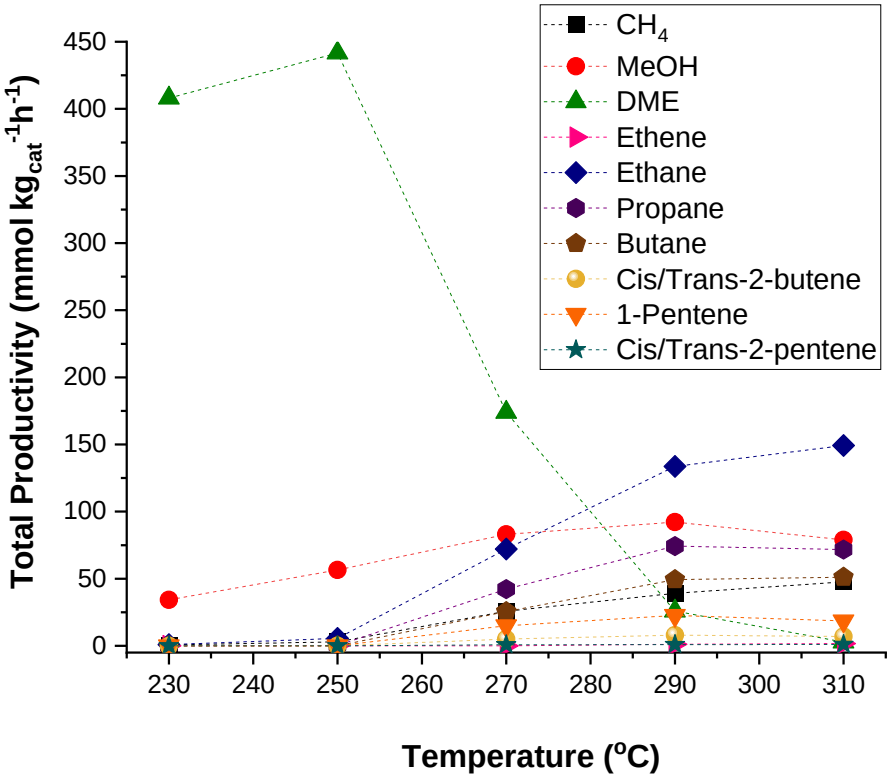

Figure 5.20 – Total productivity of 31% Cu/ZrO_2 + H-ZSM-5 (23:1) pellets in mixed bed, **reduced *in-situ***: 1 h at 220 °C in H_2 (2 °C min^{-1}, 1 bar, 30 ml min^{-1} STP). **Reaction conditions:** 230 - 310 °C, 8 h dwells (total = 40 h), 30 ml min^{-1} (STP) of CO_2 : N_2 : H_2 (1:1:3), P(total) = 20 bar.

The DME productivity is high at the start of the reaction, and in this instance, rises to 442 mmol$_{DME}$kg$_{cat}^{-1}$h^{-1} for 250 °C, and falls as the temperature increases. The MeOH productivity on the other hand remains level across the temperature range. As anticipated, an increase in the higher chain hydrocarbon productivities is observed; the highest productivity is seen for ethane at 310 °C with 149 mmol$_{C2H6}$ kg$_{cat}^{-1}$h^{-1}, which is almost twice as much as that for the 10%CuZn + H-ZSM-5 mixed bed catalyst, suggesting increasing the metal loading of the catalyst in the mixed bed increases the DME productivity and resulting hydrocarbons.

5.3 – Conclusions

A series of 20 wt.% CuZn (1:1) catalysts were prepared via Chemical Vapour Impregnation (CVI) and oxalate gel method (OG) on commercial ZSM-5 zeolites (Si:Al 23; 30; 50 and 80). Additional zeolites used include mordenite (20:1) and zeolite Y. These catalysts were tested over a temperature range of 230 – 310 °C. The activity of the oxalate gel catalysts were far greater than those produced via CVI, with the CuZn/ZSM-5 (50:1) being most active, which is due to the choice of zeolite used and smaller size of the metal particles of the catalyst. From the TEM analysis, the presence of needles/strings of phase separated CuZn detached from the ZSM-5 support were detected; despite this lack of homogeneity and dispersion of the active metals on the surface of the zeolite, the oxalate gel catalyst still maintains its activity through the limited contact and hence access to the channels of the zeolite necessary for the hydrocarbon formation. The equivalent OG catalyst containing CuZr was also tested and found to be slightly more active than the CuZn.

Of the series of H-ZSM-5 catalysts tested, the lowest Si:Al was most acidic, as reflected in the NH_3-TPD profiles where an increase in the Si:Al ratio resulted in a decrease in the number of total acid sites available. CuZn/ZSM-5 (23:1) contains the highest amount of strong sites, compared to the other catalysts, as well as medium acid sites. As higher chain hydrocarbon formation was seen only for the 23:1 catalyst, it is suggested that the acid sites described are essential towards the formation of higher hydrocarbons. Relating back to the reactivity data the lower methanol and DME productivity can be correlated with a higher concentration of total acid sites, as well as the decreased size of the Cu particles, as shown in the XRD patterns.

Physical mixtures of 10% Cu/ZnO, prepared by the oxalate gel method, and commercial H-ZSM-5 (23:1) were made. Two methods of physical mixture were employed: shaking and grinding, where the shaken resulted in only the formation of ethane as an additional product, although at very low productivity; and the ground 10% Cu/ZnO + ZSM-5 (23:1) catalyst, which was able to produce higher chain hydrocarbons up to C_4. Although the productivities are low, it demonstrates the importance of the contact required between the strong acid sites of the zeolite and the active metals.

Pellets of the 10%Cu/ZnO and H-ZSM-5 (23:1) were placed into either a separate bed or mixed bed and tested. Differences in activity can be linked to the direct exposure of Cu/ZnO catalyst and the contact time between the formed products and zeolite. For the separate bed, the methanol and DME formed have a direct contact with the H-ZSM-5 zeolite across the bed; however, the increasing temperature is likely to impact the exposed Cu/ZnO required for the methanol formation. For the mixed bed, the zeolite is more distributed and in good proximity to the Cu/ZnO pellets within the catalyst bed, allowing

the rate of DME formation to increase at lower temperatures. As the temperature increases (> 250 °C) the conversion to hydrocarbons increases and DME decreases, which could be associated with the strong acid sites beginning to deactivate (increased water production).

A mixed bed catalyst consisting of 31% Cu/ZrO_2 catalyst and commercial H-ZSM-5 (23:1) was also prepared, and an increase in the higher chain hydrocarbon productivities observed. The highest productivity is seen for ethane at 310 °C with 149 $mmol_{C2H6}\ kg_{cat}^{-1}h^{-1}$, which is almost twice as much as that for the 10%CuZn + H-ZSM-5 mixed bed catalyst, suggesting that increasing the metal loading of the catalyst in the mixed bed increases the DME productivity and resulting hydrocarbons.

Future work recommended for this section includes the testing of the zeolites themselves and zeolites with the addition of only Cu to determine their potential activity towards the production of methanol, DME and hydrocarbons and compare to the results discussed in this section. Running experiments with an initial feed of DME, as opposed to CO_2, for the conversion to hydrocarbons. This would allow a greater insight into the interaction of key intermediates with the zeolites. In addition, various experimental parameters such as total reaction pressure and H_2/CO_2 ratio can be increased to enhance CO_2 conversion and reduce CO selectivity, thereby increasing the net yield of hydrocarbons over the bifunctional catalytic bed.

5.4 – References

1. J. Ruiz Esquius, H. Bahruji, S. H. Taylor, M. Bowker, G. J. Hutchings, CO_2 Hydrogenation to CH_3OH over PdZn Catalysts, with Reduced CH4 Production. *ChemCatChem* **12**, 6024-6032 (2020).
2. C. Arcoumanis, C. Bae, R. Crookes, E. Kinoshita, The Ootential of di-methyl Ether (DME) as an Alternative Fuel for Compression-ignition Engines: A review. *Fuel* **87**, 1014 (2008).
3. M. Xu, J. H. Lunsford, D. W. Goodman, A. Bhattacharyya, Synthesis of Dimethyl Ether (DME) from Methanol over Solid-acid Catalysts. *Applied Catalysis, A* **149**, 289 (1997).
4. A. T. Aguayo, J. Ereña, I. Sierra, M. Olazar, J. Bilbao, Deactivation and Regeneration of Hybrid Catalysts in the Single-step Synthesis of Dimethyl Ether from Syngas and CO_2. *Catalysis Today* **106**, 265 (2005).
5. S. P. Naik, Synthesis of DME from CO_2/H_2 gas mixture. *Chemical Engineering Journal* **167**, 362-368 (2011).
6. F. Frusteri., Stepwise tuning of metal-oxide and acid sites of CuZnZr-MFI hybrid catalysts for the direct DME synthesis by CO_2 hydrogenation. *Applied Catalysis B: Environmental* **176-177**, 522-531 (2015).
7. S. P. Naik., A Comparative Study of $ZnO-CuO-Al_2O_3/SiO_2-Al_2O_3$ Composite and Hybrid Catalysts for Direct Synthesis of Dimethyl Ether from Syngas. *Industrial & Engineering Chemistry Research* **47**, 9791-9794 (2008).
8. H. Yang, A review of the catalytic hydrogenation of carbon dioxide into value-added hydrocarbons. *Catalysis Science & Technology* **7**, 4580-4598 (2017).
9. M. Westgård Erichsen, S. Svelle, U. Olsbye, The influence of catalyst acid strength on the methanol to hydrocarbons (MTH) reaction. *Catalysis Today* **215**, 216-223 (2013).
10. J. Schumann, A. Tarasov, N. Thomas, R. Schlögl, M. Behrens, Cu,Zn-based catalysts for methanol synthesis: On the effect of calcination conditions and the part of residual carbonates. *Applied Catalysis A: General* **516**, 117-126 (2016).
11. S. G. Jadhav, P. D. Vaidya, B. M. Bhanage, J. B. Joshi, Catalytic carbon dioxide hydrogenation to methanol: A review of recent studies. *Chemical Engineering Research and Design* **92**, 2557-2567 (2014).
12. J. Zhang, Hydrogen transfer versus olefins methylation: On the formation trend of propene in the methanol-to-hydrocarbons reaction over Beta zeolites. *Journal of Catalysis* **368**, 248-260 (2018).
13. Y. Liu, Critical role of formaldehyde during methanol conversion to hydrocarbons. *Nature Communications* **10**, 1462 (2019).
14. S. Dang *et al.*, Selective Transformation of CO_2 and H_2 into Lower Olefins over In_2O_3-$ZnZrO_x$/SAPO-34 Bifunctional Catalysts. *ChemSusChem* **12**, 3582-3591 (2019).
15. A. Dokania *et al.*, Acidity modification of ZSM-5 for enhanced production of light olefins from CO_2. *Journal of Catalysis* **381**, 347-354 (2020).
16. P. Ticali, CO_2 hydrogenation to methanol and hydrocarbons over bifunctional Zn-doped ZrO_2/zeolite catalysts. *Catalysis Science & Technology* **11**, 1249-1268 (2021).
17. X. Liu, Selective transformation of carbon dioxide into lower olefins with a bifunctional catalyst composed of $ZnGa_2O_4$ and SAPO-34. *Chemical Communications* **54**, 140-143 (2018).
18. P. Gao, Direct conversion of CO_2 into liquid fuels with high selectivity over a bifunctional catalyst. *Nature Chemistry* **9**, 1019-1024 (2017).
19. W. Li, P. Lu, D. Xu, K. Tao, CO_2 hydrogenation to methanol over Cu/ZnO catalysts synthesized via a facile solid-phase grinding process using oxalic acid. *Korean Journal of Chemical Engineering*, (2017).

20. S. Ghosh, L. Olsson, D. Creaser, Methanol mediated direct CO2 hydrogenation to hydrocarbons: Experimental and kinetic modeling study. *Chemical Engineering Journal* **435**, 135090 (2022).
21. M. Fujiwara, T. Satake, K. Shiokawa, H. Sakurai, CO2 hydrogenation for C2+ hydrocarbon synthesis over composite catalyst using surface modified HB zeolite. *Applied Catalysis B: Environmental* **179**, 37-43 (2015)
22. P. Perez-Uriarte, A. Ateka, A. T. Aguayo, A. G. Gayubo, J. Bilbao, Kinetic model for the reaction of DME to olefins over a HZSM-5 zeolite catalyst. *Chemical Engineering Journal* **302**, 801-810 (2016)

Chapter 6

Conclusions and Future Work.

Amid global warming concerns and skyrocketing CO_2 emissions in the atmosphere, mainly associated with the combustion of fossil fuels to produce energy, the research community has gained a large interest in CO_2 capture and reutilization to produce renewable fuels such as methanol (MeOH), dimethylether (DME) and additional hydrocarbons. By combining an integrated green hydrogen approach, whereby the H_2 is obtained using renewable sources, the synthesis of these fuels can become more sustainable in the light of the carbon cycle.

The main aims of the work for this project were:

- Identify catalysts that can operate under low temperatures (< 250 °C) for MeOH synthesis from CO_2.
- Identify and develop active catalysts composed of earth-abundant materials for the hydrogenation of CO_2 to MeOH and DME.
- Investigate the formation of hydrocarbons via methanol formation using integrated catalysts (MeOH synthesis + zeolite).

The work in Chapter 3 explored the effect of various supported Cu catalysts prepared via the oxalate gel synthesis method, with a particular focus on Cu/ZrO_2, towards the conversion of CO_2 to MeOH. The role of various promoters (Pd, Pt, Ce, Ni and Ag) and the stability of these catalysts was also investigated. It was found that at low temperatures the Cu/ZrO_2 catalyst is both active towards methanol production and stable. The introduction of promotors did not show any improvement to the catalyst performance; for future studies it would be beneficial to investigate further methods to introduce key promotors to the catalyst surface with an investigation into the loading effects.

The work in Chapter 4 explored the impact of varying the calcination temperature and reduction temperature of the Cu/ZrO_2 catalysts prepared via oxalate gel, towards their hydrogenation of carbon dioxide to methanol and DME. The deposition of Cu onto the ZrO_2 polymorphs by oxalate gel and wet impregnation was also investigated to understand the effects of preparation method and support phase on catalytic activity. It was shown that the type of preparation method used, as well as the ZrO_2 phase,

Cu surface area, and Cu dispersion, are all important factors towards the catalyst activity. Future work could involve the investigation of more refined preparation methods to deposit Cu onto the support; by doing this the main factors listed above can be targeted.

Work in chapter 5 looked at the production of MeOH, DME and higher chain hydrocarbon productivities between various CuZn or CuZr Zeolite integrated catalysts, where the zeolite is either commercially available H-ZSM-5 (Si:Al 23; 30; 50 and 80), mordenite (20:1) or zeolite Y, prepared via chemical vapour impregnation (CVI) and oxalate gel precipitation. Physical mixtures of the catalysts as well as changes to the catalyst bed were also explored in order to compare the catalyst activity. It was found that the preparation method used largely impacted the metal particle size, with oxalate gel forming smaller particles over CVI. Interesting results were seen with regards to hydrocarbon formation using the more acidic H-ZSM-5 (23) catalysts, as well as variation in the catalyst bed. Future studies could include the investigation of varying reaction conditions, such as the temperature, pressure, and gas feeds (start with DME), alongside a mixed bed catalyst to help improve on productivities, research into reactor design to investigate catalyst stability, and a look into using different metal loadings.